Abstract and Applied Analysis

Analytical and Numerical Methods for Solving Partial Differential Equations and Integral Equations Arising in Physical Models 2014

Guest Editors: Santanu Saha Ray, Rasajit K. Bera, Adem Kılıçman, Om P. Agrawal, and Yasir Khan

Analytical and Numerical Methods for Solving Partial Differential Equations and Integral Equations Arising in Physical Models 2014

Abstract and Applied Analysis

Analytical and Numerical Methods for Solving Partial Differential Equations and Integral Equations Arising in Physical Models 2014

Guest Editors: Santanu Saha Ray, Rasajit K. Bera, Adem Kılıçman, Om P. Agrawal, and Yasir Khan

Copyright © 2015 Hindawi Publishing Corporation. All rights reserved.

This is a special issue published in "Abstract and Applied Analysis." All articles are open access articles distributed under the Creative Commons Attribution License, which permits unrestricted use, distribution, and reproduction in any medium, provided the original work is properly cited.

Editorial Board

Ravi P. Agarwal, USA
Bashir Ahmad, Saudi Arabia
M. O. Ahmedou, Germany
Nicholas D. Alikakos, Greece
Debora Amadori, Italy
Douglas R. Anderson, USA
Jan Andres, Czech Republic
Giovanni Anello, Italy
Stanislav Antontsev, Portugal
Mohamed K. Aouf, Egypt
Narcisa C. Apreutesei, Romania
Natig M. Atakishiyev, Mexico
Ferhan M. Atici, USA
Ivan Avramidi, USA
Soohyun Bae, Korea
Chuanzhi Bai, China
Zhanbing Bai, China
Dumitru Baleanu, Turkey
Józef Banaś, Poland
Martino Bardi, Italy
Roberto Barrio, Spain
Feyzi Başar, Turkey
Abdelghani Bellouquid, Morocco
Daniele Bertaccini, Italy
Lucio Boccardo, Italy
Igor Boglaev, New Zealand
Martin J. Bohner, USA
Geraldo Botelho, Brazil
Elena Braverman, Canada
Romeo Brunetti, Italy
Janusz Brzdek, Poland
Detlev Buchholz, Germany
Sun-Sig Byun, Korea
Fabio M. Camilli, Italy
Jinde Cao, China
Anna Capietto, Italy
Jianqing Chen, China
Wing-Sum Cheung, Hong Kong
Michel Chipot, Switzerland
Changbum Chun, Korea
Soon-Yeong Chung, Korea
Jaeyoung Chung, Korea
Silvia Cingolani, Italy
Jean M. Combes, France
Monica Conti, Italy
Juan-Carlos Cortés, Spain
Graziano Crasta, Italy
Zhihua Cui, China
Bernard Dacorogna, Switzerland
Vladimir Danilov, Russia
Mohammad T. Darvishi, Iran
L. F. Pinheiro de Castro, Portugal
Toka Diagana, USA
Jesús I. Díaz, Spain
Josef Diblík, Czech Republic
Fasma Diele, Italy
Tomas Dominguez, Spain
Alexander Domoshnitsky, Israel
Marco Donatelli, Italy
BoQing Dong, China
Wei-Shih Du, Taiwan
Luiz Duarte, Brazil
Roman Dwilewicz, USA
Paul W. Eloe, USA
Luca Esposito, Italy
Khalil Ezzinbi, Morocco
Julian F. Bonder, Argentina
Dashan Fan, USA
Angelo Favini, Italy
Márcia Federson, Brazil
Stathis Filippas, Equatorial Guinea
Alberto Fiorenza, Italy
Xianlong Fu, China
Massimo Furi, Italy
Jesús G. Falset, Spain
Giovanni P. Galdi, USA
Isaac Garcia, Spain
J. A. G.a-Rodríguez, Spain
Leszek Gasinski, Poland
György Gát, Hungary
Vladimir Georgiev, Italy
Lorenzo Giacomelli, Italy
Jaume Giné, Spain
Valery Y. Glizer, Israel
Jean P. Gossez, Belgium
Jose L. Gracia, Spain
Maurizio Grasselli, Italy
Luca Guerrini, Italy
Yuxia Guo, China
Qian Guo, China
Chaitan P. Gupta, USA
Uno Hämarik, Estonia
Maoan Han, China
Ferenc Hartung, Hungary
Jiaxin Hu, China
Chengming Huang, China
Zhongyi Huang, China
Gennaro Infante, Italy
Ivan Ivanov, Bulgaria
Hossein Jafari, South Africa
Jaan Janno, Estonia
Aref Jeribi, Tunisia
Uncig Ji, Korea
Zhongxiao Jia, China
Lucas Jódar, Spain
Jong S. Jung, Republic of Korea
Henrik Kalisch, Norway
Chaudry Masood Khalique, South Africa
Satyanad Kichenassamy, France
Tero Kilpeläinen, Finland
Sung G. Kim, Republic of Korea
Ljubisa Kocinac, Serbia
Andrei Korobeinikov, Spain
Pekka Koskela, Finland
Victor Kovtunenko, Austria
Ren-Jieh Kuo, Taiwan
Pavel Kurasov, Sweden
Milton C. L. Filho, Brazil
Miroslaw Lachowicz, Poland
Kunquan Lan, Canada
Ruediger Landes, USA
Irena Lasiecka, USA
Matti Lassas, Finland
Chun-Kong Law, Taiwan
Ming-Yi Lee, Taiwan
Gongbao Li, China
Elena Litsyn, Israel
Yansheng Liu, China
Shengqiang Liu, China
Carlos Lizama, Chile
Guozhen Lu, USA
Jinhu Lü, China
Grzegorz Lukaszewicz, Poland
Wanbiao Ma, China
Nazim I. Mahmudov, Turkey

Eberhard Malkowsky, Turkey
Salvatore A. Marano, Italy
Cristina Marcelli, Italy
Paolo Marcellini, Italy
J. Marín-Solano, Spain
Mieczysław Mastyło, Poland
Ming Mei, Canada
Taras Mel'nyk, Ukraine
Anna Mercaldo, Italy
Stanislaw Migorski, Poland
Mihai Mihăilescu, Romania
Feliz Minhós, Portugal
Dumitru Motreanu, France
Gaston Mandata N'guérékata, USA
Maria Grazia Naso, Italy
Micah Osilike, Nigeria
Mitsuharu Ôtani, Japan
Turgut Öziş, Turkey
Nikolaos S. Papageorgiou, Greece
Sehie Park, Korea
Kailash C. Patidar, South Africa
Kevin R. Payne, Italy
Ademir F. Pazoto, Brazil
Shuangjie Peng, China
Antonio M. Peralta, Spain
Sergei V. Pereverzyev, Austria
Allan Peterson, USA
Andrew Pickering, Spain
Cristina Pignotti, Italy
Somyot Plubtieng, Thailand
Milan Pokorny, Czech Republic
Sergio Polidoro, Italy
Ziemowit Popowicz, Poland
Maria M. Porzio, Italy
Enrico Priola, Italy
Vladimir S. Rabinovich, Mexico
Irena Rachůnková, Czech Republic
Maria A. Ragusa, Italy
Simeon Reich, Israel
Abdelaziz Rhandi, Italy
Hassan Riahi, Malaysia
Juan P. Rincón-Zapatero, Spain
Luigi Rodino, Italy
Yuriy Rogovchenko, Norway
Julio D. Rossi, Argentina
Wolfgang Ruess, Germany
Bernhard Ruf, Italy
Satit Saejung, Thailand
Stefan G. Samko, Portugal
Martin Schechter, USA
Javier Segura, Spain
Valery Serov, Finland
Naseer Shahzad, Saudi Arabia
Andrey Shishkov, Ukraine
Stefan Siegmund, Germany
Abdel-Maksoud A. Soliman, Egypt
Pierpaolo Soravia, Italy
Marco Squassina, Italy
Hari M. Srivastava, Canada
Svatoslav Staněk, Czech Republic
Antonio Suárez, Spain
Wenchang Sun, China
Wenyu Sun, China
Robert Szalai, UK
Sanyi Tang, China
Chun-Lei Tang, China
Gabriella Tarantello, Italy
Nasser-Eddine Tatar, Saudi Arabia
Gerd Teschke, Germany
Sergey Tikhonov, Spain
Claudia Timofte, Romania
Thanh Tran, Australia
Juan J. Trujillo, Spain
Gabriel Turinici, France
Milan Tvrdy, Czech Republic
Mehmet Ünal, Turkey
Csaba Varga, Romania
Carlos Vazquez, Spain
Jesus Vigo-Aguiar, Spain
Qing-Wen Wang, China
Yushun Wang, China
Shawn X. Wang, Canada
Youyu Wang, China
Jing P. Wang, UK
Peixuan Weng, China
Noemi Wolanski, Argentina
Ngai-Ching Wong, Taiwan
Patricia J. Y. Wong, Singapore
Yonghong Wu, Australia
Zili Wu, China
Shi-Liang Wu, China
Shanhe Wu, China
Tiecheng Xia, China
Xu Xian, China
Yanni Xiao, China
Fuding Xie, China
Gongnan Xie, China
Daoyi Xu, China
Zhenya Yan, China
Xiaodong Yan, USA
Norio Yoshida, Japan
Beong In Yun, Korea
Agacik Zafer, Kuwait
Jianming Zhan, China
Weinian Zhang, China
Chengjian Zhang, China
Zengqin Zhao, China
Sining Zheng, China
Yong Zhou, China
Tianshou Zhou, China
Qiji J. Zhu, USA
Chun-Gang Zhu, China
Malisa R. Zizovic, Serbia
Wenming Zou, China

Contents

Analytical and Numerical Methods for Solving Partial Differential Equations and Integral Equations Arising in Physical Models 2014, Santanu Saha Ray, Rasajit K. Bera, Adem Kılıçman, Om P. Agrawal, and Yasir Khan
Volume 2015, Article ID 193030, 2 pages

Temperature Dependent Viscosity of a Third Order Thin Film Fluid Layer on a Lubricating Vertical Belt, T. Gul, S. Islam, R. A. Shah, I. Khan, and L. C. C. Dennis
Volume 2015, Article ID 386759, 13 pages

Classification of Multiply Travelling Wave Solutions for Coupled Burgers, Combined KdV-Modified KdV, and Schrödinger-KdV Equations, A. R. Seadawy and K. El-Rashidy
Volume 2015, Article ID 369294, 7 pages

Exact Solutions for Unsteady Free Convection Flow of Casson Fluid over an Oscillating Vertical Plate with Constant Wall Temperature, Asma Khalid, Ilyas Khan, and Sharidan Shafie
Volume 2015, Article ID 946350, 8 pages

A Strongly A-Stable Time Integration Method for Solving the Nonlinear Reaction-Diffusion Equation, Wenyuan Liao
Volume 2015, Article ID 539652, 12 pages

Traveling Wave Solutions of the Benjamin-Bona-Mahony Water Wave Equations, A. R. Seadawy and A. Sayed
Volume 2014, Article ID 926838, 7 pages

Nonlinear Nanofluid Flow over Heated Vertical Surface with Sinusoidal Wall Temperature Variations, S. S. Motsa, F. G. Awad, and M. Khumalo
Volume 2014, Article ID 408230, 11 pages

Hindawi Publishing Corporation
Abstract and Applied Analysis
Volume 2015, Article ID 193030, 2 pages
http://dx.doi.org/10.1155/2015/193030

Editorial

Analytical and Numerical Methods for Solving Partial Differential Equations and Integral Equations Arising in Physical Models 2014

Santanu Saha Ray,[1] Rasajit K. Bera,[2] Adem Kılıçman,[3] Om P. Agrawal,[4] and Yasir Khan[5]

[1] *Department of Mathematics, National Institute of Technology, Rourkela 769008, India*
[2] *Department of Science, National Institute of Technical Teachers' Training and Research, BK-301, Sector II, Salt Lake City, Kolkata 700091, India*
[3] *Department of Mathematics and Institute for Mathematical Research, Universiti Putra Malaysia (UPM), 43400 Serdang, Selangor, Malaysia*
[4] *Department of Mechanical Engineering and Energy Processes, Southern Illinois University, Carbondale, IL 62901, USA*
[5] *Department of Mathematics, Zhejiang University, Hangzhou 310027, China*

Correspondence should be addressed to Santanu Saha Ray; santanusaharay@yahoo.com

Received 2 March 2015; Accepted 2 March 2015

Copyright © 2015 Santanu Saha Ray et al. This is an open access article distributed under the Creative Commons Attribution License, which permits unrestricted use, distribution, and reproduction in any medium, provided the original work is properly cited.

Nowadays, partial differential equations (PDEs) have become a suitable tool for describing the natural phenomena of science and engineering models. Most of the phenomena arising in mathematical physics and engineering fields can be expressed by PDEs. Many engineering applications are simulated mathematically as PDEs with initial and boundary conditions. Most physical phenomena of fluid dynamics, gravitation, chemical reaction, dispersion, nonlinear optics, plasma physics, quantum mechanics, electricity, acoustics, solid mechanics, and many other models are controlled within their domain of validity by PDEs. Therefore, it becomes increasingly important to be familiar with all traditional and recently developed methods for solving PDEs and the implementations of these methods.

For many years the subject of functional equations has held a prominent place in the attention of mathematicians. In recent years this attention has been focused on a specific kind of functional equations, an integral equation, where the unknown function occurs under the integral sign. Such equations occur widely in diverse fields including continuum mechanics, potential theory, geophysics, electricity and magnetism, kinetic theory of gases, hereditary phenomena in physics and biology, renewal theory, quantum mechanics, radiation, optimization, optimal control systems, communication theory, mathematical economics, population genetics, queuing theory, medicine, mathematical problems of radiative equilibrium, the particle transport problems of astrophysics and reactor theory, acoustics, fluid mechanics, steady state heat conduction, fracture mechanics, and radiative heat transfer problems. They offer a powerful technique for solving a variety of practical problems.

This special issue is devoted to study the recent works in the above fields of partial differential equations and integral equations done by the leading researchers. Accordingly, various papers on partial differential equations and integral equations have been included in this special issue after completing a heedful, rigorous, and peer-review process. The issue contains eight research papers.

The (2 + 1)-dimensional nonlinear Schrödinger equations (NLS) are transformed into the standard (1 + 1)-dimension nonlinear Schrödinger equation by using appropriate transformation and then by using Exp-function method bisolitons and a series of breather solitons (rogue waves) solutions are obtained. Solutions of the (2 + 1)-dimensional nonlinear Schrödinger equations, which contain Akhmediev breather soliton, Ma breather soliton and Peregrine breather soliton

are represented. Also, higher-order rational rogue wave solutions are obtained for (2 + 1)-dimensional NLS equations by using the similarity transformation on the solutions of the (1 + 1)-dimensional NLS equation. Several arbitrary parameters are involved to generate abundant wave structures which greatly enriched the diversity of wave structures for the (2 + 1)-dimensional nonlinear Schrödinger equations.

By using the central difference, upwind, hybrid, power-law, and exponential scheme, the general transport equation has been investigated. In the solution, three different grid systems of 80×100, 160×200, and 320×400 from nodal points were used by the authors. The obtained results indicate that hybrid and power-law yield better results as compared to the other discretization methods.

Some explicit travelling wave solutions are presented to construct the exact solutions of nonlinear partial differential equations of mathematical physics. Applying Frobenius transformation to the coupled Burgers, combined Korteweg-de Vries- (cKdV-) modified KdV (mKdV) and Schrödinger-KdV equations can be written as bilinear ordinary differential equations and two travelling wave solutions are generated. The properties of the multiply travelling wave solutions are shown in figures. The solutions thus obtained are stable and are used to describe nonlinear interaction of travelling waves.

The authors have studied the influence of heat transfer on thin film flow of a reactive third order fluid with variable viscosity and slip boundary condition. The problem is formulated in the form of coupled nonlinear equations governing the flow together with appropriate boundary conditions. Approximate analytical solutions for velocity and temperature are obtained by using optimal homotopy asymptotic method (OHAM) and are compared with Adomian decomposition method (ADM) solutions. Both of these solutions are found identical as demonstrated in graphs and tables. The graphical results for embedded flow parameters are also shown by the authors.

The nonlinear density temperature variations in two-dimensional nanofluid flow over heated vertical surface with a sinusoidal wall temperature are examined in detail. The model includes the effects of Brownian motion and thermophoresis. Two-dimensional momentum, heat, and mass transfer equations are transferred to nonlinear partial differential equations using the boundary layer approximation and solved numerically using spectral local linearization method. The effects of the governing parameters on the fluid properties as well as on the heat and nanomass transfer coefficients are determined and are shown graphically.

An efficient fourth-order numerical algorithm that combines the Padé approximation in space and fourth-order accurate Rosenbrock method in time is proposed to solve a nonlinear parabolic partial differential equation. The semidiscrete ordinary differential equation (ODE) system resulting from compact higher-order finite difference spatial discretization of the reaction-diffusion equation is highly stiff. Therefore, numerical time integration methods with stiff stability such as implicit Runge-Kutta methods and implicit multistep methods are required to solve the large scale stiff ODE system. In this work the authors construct a new fourth-order Rosenbrock method to solve the nonlinear parabolic partial differential equation supplemented with Dirichlet or Neumann boundary condition. Two numerical examples are solved to demonstrate the efficiency, stability, and accuracy of the proposed method.

The modeling of unidirectional propagation of long water waves in dispersive media is considered. The authors have derived the Korteweg-de Vries (KdV) and Benjamin-Bona-Mahony (BBM) equations from water wave models. By implementing the extended direct algebraic and modified sech-tanh methods, the authors have presented new traveling wave solutions of the KdV and BBM equations. The stability of the obtained traveling wave solutions are analyzed and discussed.

Newtonian fluids described by Navier Stokes equations are extensively studied in the literature for the past few decades. The unsteady free flow of a Casson fluid over an oscillating vertical plate with constant wall temperature has been studied. The Casson fluid model is used to distinguish the non-Newtonian fluid behaviour. The governing partial differential equations corresponding to the momentum and energy equations are transformed into linear ordinary differential equations by using nondimensional variables. The dimensionless governing equations are solved by using the Laplace transform technique. Expressions for shear stress in terms of skin-friction and the rate of heat transfer in terms of Nusselt number are also obtained. Numerical results of velocity and temperature profiles with various values of embedded flow parameters are shown graphically and their effects are discussed in detail.

At the present, the use of partial differential equations and integral equations are commonly encountered in the fields of science and engineering. This issue has addressed some efficient computational tools, recent trends, and developments regarding the analytical and numerical methods for the solutions of partial differential equations and integral equations arising in physical models. Eventually, it may be expected that the present special issue would certainly help to explore the researchers with their new arising problems and stimulate the efficiency and accuracy of the solution methods for those problems in use nowadays.

Santanu Saha Ray
Rasajit K. Bera
Adem Kılıçman
Om P. Agrawal
Yasir Khan

Hindawi Publishing Corporation
Abstract and Applied Analysis
Volume 2015, Article ID 386759, 13 pages
http://dx.doi.org/10.1155/2015/386759

Research Article

Temperature Dependent Viscosity of a Third Order Thin Film Fluid Layer on a Lubricating Vertical Belt

T. Gul,[1] S. Islam,[1] R. A. Shah,[2] I. Khan,[3] and L. C. C. Dennis[4]

[1]*Department of Mathematics, Abdul Wali Khan University Mardan, Khyber Pakhtunkhwa, Pakistan*
[2]*Department of Mathematics, UET Peshawar, Khyber Pakhtunkhwa, Pakistan*
[3]*College of Engineering, Majmaah University, Saudi Arabia*
[4]*Department of Fundamental and Applied Sciences, Universiti Teknologi PETRONAS, 31750 Perak, Malaysia*

Correspondence should be addressed to L. C. C. Dennis; dennis.ling@petronas.com.my

Received 23 July 2014; Revised 28 September 2014; Accepted 30 September 2014

Academic Editor: Yasir Khan

Copyright © 2015 T. Gul et al. This is an open access article distributed under the Creative Commons Attribution License, which permits unrestricted use, distribution, and reproduction in any medium, provided the original work is properly cited.

This paper aims to study the influence of heat transfer on thin film flow of a reactive third order fluid with variable viscosity and slip boundary condition. The problem is formulated in the form of coupled nonlinear equations governing the flow together with appropriate boundary conditions. Approximate analytical solutions for velocity and temperature are obtained using Adomian Decomposition Method (ADM). Such solutions are also obtained by using Optimal Homotopy Asymptotic Method (OHAM) and are compared with ADM solutions. Both of these solutions are found identical as shown in graphs and tables. The graphical results for embedded flow parameters are also shown.

1. Introduction

Thin film fluid flows exist in various aspects of daily life. In engineering, we see their usage in condensers, distillation units, and heat exchangers. In geophysical events, we see thin fluid films in the forms of drilling mud, heat pipes, and debris flow. In biological sciences, we can see thin fluid films coating the airways in the lungs and thin tear films covering the eye. These are a few examples of common use of thin fluid films. All these occurrences can be modeled using mathematical principles. The material properties such as viscosity and density change accordingly when a fluid is subjected to a temperature change. This phenomenon mostly occurs in heat exchangers, chemical reactors, or processes where components are cooled.

Properties of isothermal flows (viscosity at constant temperature) are important in many situations. There have also been many studies done on variety of nonisothermal (temperature dependent viscosity) flows of fluids; particularly, Goussis and Kelly [1, 2] and Hwang and Weng [3] investigated the stability of a fluid film with variable viscosity flowing down a heated plan, while Reisfeld and Bankoff [4] and Wu and Hwang [5] independently considered the progression and final substrate of a fluid film with variable viscosity on a heated horizontal substrate subjected to surface tension and van der Waals forces. Sansom et al. [6] considered the scattering of a thin film flow with temperature dependent viscosity on a horizontal substrate for different viscosity models for both heated and cooled substrate without internal heating within the film and for a substrate at the ambient temperature with constant internal heating within the film.

Many researchers have contributed relevant work in this field. Amongst them, Khaled et al. [7] studied heat transfer inside thin film flow with variable pressure whereas Nadeem and Awais [8] investigated the thin film unsteady flow with variable viscosity. The free micropolar convection for the case of a symmetric boundary conditions or asymmetric heating was investigated by Chamkha et al. [9], later on proceeded by Saleh et al. [10]. Few other relevant studies may be found in [11, 12] and the references therein. One of the well-known models amongst non-Newtonian fluids for thin film is a third grade fluid which has its constitutive equations based on

strong theoretical foundations, where the relation between stress and strain is nonlinear. Therefore, in the present work we have chosen third grade fluid to study its thin film flow over a vertical belt.

On the other hand, several numerical and approximate methods are used by many authors to study real world problems, appearing in mathematics, fluid mechanics, and engineering sciences. Few of these methods include Keller-box [13], shooting [14], Homotopy Perturbation Method (HPM) [15], Homotopy Analysis Method (HAM), and Optimal Homotopy Asymptotic Method (OHAM) [16, 17]. Applications of OHAM for solving nonlinear equations arising in heat transfer have been investigated by Marinca and Herisanu [18]. Marinca et al. [19] analysed steady flow of a fourth grade fluid past a porous plate using OHAM. Micropolar flow in a porous channel with high mass transfer has been investigated by Joneidi [20]. These methods deal with the nonlinear problems effectively. The work under various configurations on the thin film flows has been discussed by Siddiqui et al. [21]. In [22], Siddiqui et al. examined the thin film flows of Sisko and Oldroyd-6 constant fluids on a moving belt. Using the same idea, Gul et al. [23, 24] investigated MHD thin film flow of a third grade fluid for lifting and drainage problems. Constant and variable viscosity fluid has been used in all these studies. In [24] they studied variable viscosity with no-slip boundary conditions. However, in the present problem we have chosen Reynolds model (exponential expression) which is based on variable viscosity in the presence of slip boundary conditions. More exactly, we have shown the effect of variable viscosity with heat transfer in a thin film fluid flow such as silicate melts and polymers past a lubricating belt. In these fluids, viscous friction generates a local increase in temperature near the belt with a resultant viscosity decrease and frequent rise of the flow velocity. This velocity increase may produce an additional growth of the local temperature discussed by Costa et al. [25]. Analytical solution for MHD flow in a third grade fluid with variable viscosity has been discussed by Ellahi and Riaz [26]. Approximate analytical solution for flow of a third grade fluid through a parallel plate channel filled with a porous medium has been investigated by Aksoy et al. [27].

Based on the above motivation, the present paper aims to study the effect of heat on viscosity into a thin film flow of a third grade fluid over a vertical belt with slip boundary conditions using ADM and OHAM. In 1992, Adomian [28, 29] introduced the ADM for the approximate solutions for linear and nonlinear problems. Wazwaz [30, 31] used ADM for reliable treatment of Bratu-type and Emden-Fowler equations. Alam et al. investigated the thin film flow of Johnson-Segalman fluids for lifting and drainage problems [32].

2. Basic Equations

Continuity, momentum, and energy equations of an incompressible isothermal third grade fluid are

$$\nabla \cdot \mathbf{v} = \mathbf{0}, \tag{1}$$

$$\rho \frac{D\mathbf{v}}{Dt} = \nabla \cdot \mathbf{T} + \rho \mathbf{g}, \tag{2}$$

$$\rho c_p \frac{D\Theta}{Dt} = \kappa \nabla^2 \Theta + \operatorname{tr}(\mathbf{T} \cdot \mathbf{L}), \tag{3}$$

where $\mathbf{L} = \nabla \mathbf{v}$ and $D/Dt = \partial/\partial t + (\mathbf{v}.\nabla)$ denotes material time derivative.

Cauchy stress tensor $\mathbf{T}$ is given by

$$\mathbf{T} = -p\mathbf{I} + \mathbf{S}, \tag{4}$$

where $-p\mathbf{I}$ denotes spherical stress and shear stress $\mathbf{S}$ is defined as

$$\begin{aligned} \mathbf{S} = {} & \mu \mathbf{A}_1 + \alpha_1 \mathbf{A}_2 + \alpha_2 \mathbf{A}_1^2 + \beta_1 \mathbf{A}_3 + \beta_2 \left(\mathbf{A}_1 \mathbf{A}_2 + \mathbf{A}_2 \mathbf{A}_1\right) \\ & + \beta_3 \left(\operatorname{tr} \mathbf{A}_2^2\right) \mathbf{A}_1. \end{aligned} \tag{5}$$

Here $\mathbf{A}_1$, $\mathbf{A}_2$, and $\mathbf{A}_3$ are the kinematical tensors given by

$$\begin{aligned} \mathbf{A}_0 &= \mathbf{I}, \\ \mathbf{A}_1 &= (\nabla \mathbf{v}) + (\nabla \mathbf{v})^T, \\ \mathbf{A}_n &= \frac{D\mathbf{A}_{n-1}}{Dt} + \mathbf{A}_{n-1} (\nabla \mathbf{v}) + (\nabla \mathbf{v})^T \mathbf{A}_{n-1}, \quad n \geq 2. \end{aligned} \tag{6}$$

3. Formulation of the Lift Problem

Consider a wide flat belt moves vertically upward at constant speed V through a large bath of a third grade liquid. The belt carries with it a layer of liquid of constant thickness δ. Cartesian coordinate system is chosen for analysis in which the y-axis is taken parallel to the belt and x-axis is perpendicular to the belt. Assume that the flow is steady and laminar after a small distance above the liquid surface layer while external pressure is atmospheric everywhere. The geometry of the problems is shown in Figures 1(a) and 1(b).

Velocity and temperature fields are

$$\begin{aligned} \mathbf{v} &= (0, v(x), 0), \\ \Theta &= \Theta(x). \end{aligned} \tag{7}$$

Modeled slip boundary conditions are

$$\begin{aligned} \mathbf{v} &= V - \gamma T_{xy}, \quad \Theta = \Theta_0, \quad \text{at } x = 0, \\ \frac{d\mathbf{v}}{dx} &= 0, \quad \Theta = \Theta_1, \quad \text{at } x = \delta. \end{aligned} \tag{8}$$

Inserting the velocity field from (7) in continuity equation (1) and in Cauchy stress equation (4), the continuity equation (1) satisfies identically while (4) gives the components of stress tensor as

$$T_{yy} = -P + (2\alpha_1 + \alpha_2) \left(\frac{d\mathbf{v}}{dx}\right)^2,$$

$$T_{xy} = \mu \frac{d\mathbf{v}}{dx} + 2(\beta_2 + \beta_3) \left(\frac{d\mathbf{v}}{dx}\right)^3,$$

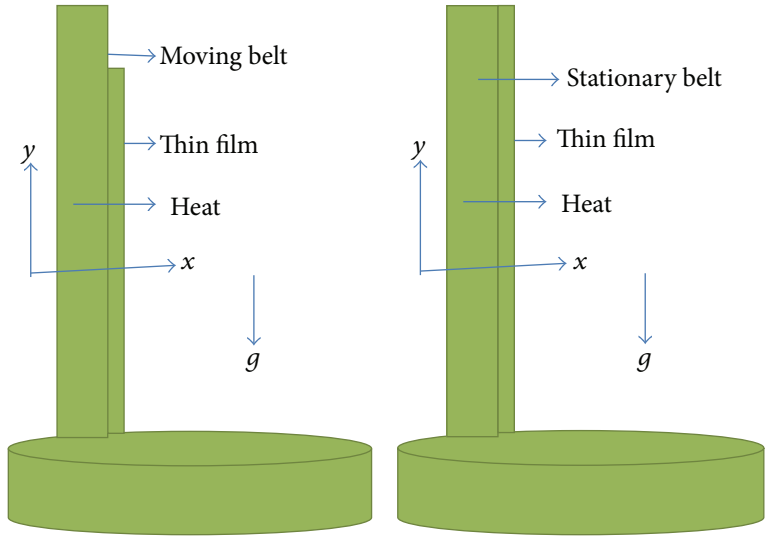

Figure 1: (a) Geometry of lift problem. (b) Geometry of drainage problem.

$$T_{xx} = -P + \alpha_2 \left(\frac{d\mathbf{v}}{dx}\right),$$
$$T_{zz} = -P,$$
$$T_{xz} = T_{yz} = 0. \tag{9}$$

Inserting (9) in (2) and (3), the momentum and energy equations reduce to

$$0 = \mu \frac{d^2\mathbf{v}}{dx^2} + \frac{dv}{dx}\frac{d\mu}{dx} + 6(\beta_2 + \beta_3)\left(\frac{dv}{dx}\right)^2\left(\frac{d^2v}{dx^2}\right) - \rho g, \tag{10}$$
$$0 = \kappa \frac{d^2\boldsymbol{\Theta}}{dx^2} + \mu\left(\frac{d\mathbf{v}}{dx}\right)^2 + 2(\beta_2 + \beta_3)\left(\frac{d\mathbf{v}}{dx}\right)^4.$$

In addition, we introduce the dimensionless parameters

$$\widetilde{v} = \frac{\mathbf{v}}{V},$$
$$\widetilde{x} = \frac{x}{\delta},$$
$$\widetilde{\boldsymbol{\Theta}} = \frac{\boldsymbol{\Theta} - \Theta_0}{\Theta_1 - \boldsymbol{\Theta}_0},$$
$$\widetilde{\mu} = \frac{\mu}{\mu_0},$$
$$\widetilde{\gamma} = \frac{\gamma}{\gamma_0},$$
$$B_r = \frac{\mu_0 V^2}{k(\Theta_1 - \Theta_0)},$$
$$S_t = \frac{\delta^2 \rho g}{\mu_0 V},$$
$$\beta = \frac{(\beta_2 + \beta_3)V^2}{\mu_0 \delta^2},$$
$$\Lambda = \gamma \mu_0. \tag{11}$$

For Reynold's model, the dimensionless viscosity is

$$\mu = \exp(-M\Theta). \tag{12}$$

By making use of Taylor series expansion, one may represent viscosity and its derivative as

$$\mu \cong 1 - M\Theta,$$
$$\frac{d\mu}{dx} \cong -M\frac{d\Theta}{dx}. \tag{13}$$

Inserting dimensionless variables from (11) in modeled boundary conditions (8) and in momentum as well as in energy equations (10) and dropping out the bar notations, we obtain

$$\frac{d^2v}{dx^2} - M\left(\frac{dv}{dx}\frac{d\Theta}{dx} + \Theta(x)\frac{d^2v}{dx^2}\right) + 6\beta\left(\frac{dv}{dx}\right)^2\left(\frac{d^2v}{dx^2}\right) - S_t = 0, \tag{14}$$

$$\frac{d^2\Theta}{dx^2} + B_r\left(\left(\frac{dv}{dx}\right)^2 - M\Theta\left(\frac{dv}{dx}\right)^2 + 2\beta\left(\frac{dv}{dx}\right)^4\right) = 0. \tag{15}$$

According to Gul et al. [24] the boundary conditions for zero component solution are

$$v_n = 1 - \Lambda\left(\frac{dv_n}{dx} - M\Theta\frac{dv_n}{dx} + 2\beta\left(\frac{dv_n}{dx}\right)^3\right), \quad \Theta_n = 0, \quad \text{at } x = 0, \tag{16}$$

$$\frac{dv_n}{dx} = 0, \quad \Theta_n = 1, \quad \text{at } x = 1, \text{ when } n = 0. \tag{17}$$

Similarly the boundary conditions for first, second, and third components solutions are

$$v_n = -\Lambda\left(\frac{dv_n}{dx} - M\Theta\frac{dv_n}{dx} + 2\beta\left(\frac{dv_n}{dx}\right)^3\right), \quad \Theta_n = 0, \quad \text{at } x = 0, \tag{18}$$

$$\frac{dv_n}{dx} = 0, \quad \Theta_n = 0, \quad \text{at } x = 1, \text{ when } n = 1, 2, 3 \ldots. \tag{19}$$

4. Solution of Lifting Problem

4.1. The ADM Solution. The inverse operator $L^{-1} = \iint dv'$ of the Adomian Decomposition Method is used in the second order coupled equations (14) and (15):

$$\begin{aligned} v &= f_1 - 6\beta L^{-1}\left[\left(\frac{dv}{dx}\right)^2\frac{d^2v}{d^2x}\right] + M\left[\frac{dv}{dx}\frac{d\Theta}{dx} + \Theta\frac{d^2v}{dx^2}\right], \\ \Theta &= f_2 - B_r L^{-1}\left(\frac{dv}{dx}\right)^2 + B_r M L^{-1}\Theta\left(\frac{dv}{dx}\right)^2 - 2B_r\beta L^{-1}\left(\frac{dv}{dx}\right)^4, \end{aligned} \tag{20}$$

where f_1, f_2 are the terms, which we get by double integrating source terms S_t, 0 and using the boundary (initial) conditions. As ADM is a series solution method, according to Aksoy et al. [27], the solutions Θ and the nonlinear terms N_1v, N_2v, N_3v, $N_4\Theta$, $N_5\Theta$, and $N_6\Theta$ can be expressed, respectively, in the following series:

$$\begin{aligned} v &= \sum_{n=0}^{\infty} v_n, \\ \Theta &= \sum_{n=0}^{\infty} \Theta_n, \\ N_1 v &= \sum_{n=0}^{\infty} \widehat{A}_n = \left(\frac{dv}{dx}\right)^2\left(\frac{d^2v}{dx^2}\right), \\ N_2 v &= \sum_{n=0}^{\infty} \widehat{B}_n = \left(\frac{dv}{dx}\right)\left(\frac{d\Theta}{dx}\right), \\ N_3 v &= \sum_{n=0}^{\infty} \widehat{C}_n = \Theta\left(\frac{d^2v}{dx^2}\right), \\ N_4\Theta &= \sum_{n=0}^{\infty} \widehat{D}_n = \left(\frac{dv}{dx}\right)^2, \\ N_5\Theta &= \sum_{n=0}^{\infty} \widehat{E}_n = \Theta\left(\frac{dv}{dx}\right)^2, \\ N_6\Theta &= \sum_{n=0}^{\infty} \widehat{F}_n = \left(\frac{dv}{dx}\right)^4, \end{aligned} \tag{21}$$

where $\widehat{A}_n$, $\widehat{B}_n$, $\widehat{C}_n$, $\widehat{D}_n$, $\widehat{E}_n$, and $\widehat{F}_n$ are called the Adomian polynomials. For every nonlinear term these polynomials are obtained from the following formula:

$$\begin{aligned} \widehat{A}_0 &= f_1(v_0), \\ D_0 &= f_2(\Theta_0), \\ \widehat{A}_i = \widehat{B}_i = \widehat{C}_i &= \sum_{\lambda=1}^{i} C(\lambda, n)\, f_1^{(\lambda)}(v_0), \\ \widehat{D}_i = \widehat{E}_i = \widehat{F}_i &= \sum_{\lambda=1}^{i} C(\lambda, n)\, f_2^{(\lambda)}(\Theta_0). \end{aligned} \tag{22}$$

Here $f_1(v)$ and $f_2(\Theta)$ are the nonlinear functions and $f_1^{(\lambda)}$, $f_2^{(\lambda)}$ are the λth derivative of $f_1(v)$ and $f_2(\Theta)$ evaluated at $v = v_0$ and $\Theta = \Theta_0$. The (λ, n) is a well-situated representation of the series coefficients and is formed by forming products or sum of the products of λ components of v whose subscripts add up to i, divided by the factorial of the number of repeated subscripts [26]. The convergence of this method has been discussed in [28–30].

The series solutions of (20) are as follows:

$$\begin{aligned} \sum_{n=0}^{\infty} v_n &= f_1 - 6\beta L^{-1}\left[\sum_{n=0}^{\infty}\widehat{A}_n\right] + ML^{-1}\left[\sum_{n=0}^{\infty}\widehat{B}_n\right] + ML^{-1}\left[\sum_{n=0}^{\infty}\widehat{C}_n\right], \\ \sum_{n=0}^{\infty} \Theta_n &= f_2 - B_r L^{-1}\left[\sum_{n=0}^{\infty}\widehat{D}_n\right] + B_r M L^{-1}\left[\sum_{n=0}^{\infty}\widehat{E}_n\right] - 2B_r\beta L^{-1}\left[\sum_{n=0}^{\infty}\widehat{F}_n\right]. \end{aligned} \tag{23}$$

The first few Adomian polynomials are derived in (24) and (27) when $n \geq 0$:

$$\begin{aligned}
\widehat{A}_0 &= \left(\frac{dv_0}{dx}\right)^2 \frac{d^2v_0}{dx^2},\\
\widehat{B}_0 &= \frac{dv_0}{dx}\frac{d\Theta_0}{dx},\\
\widehat{C}_0 &= \Theta_0(x)\frac{d^2v_0}{dx^2},\\
\widehat{D}_0 &= \left(\frac{dv_0}{dx}\right)^2,\\
\widehat{E}_0 &= \Theta_0(x)\left(\frac{dv_0}{dx}\right)^2,\\
\widehat{F}_0 &= \left(\frac{dv_0}{dx}\right)^4,
\end{aligned} \tag{24}$$

$$\begin{aligned}
\widehat{A}_1 &= \left(\frac{dv_0}{dx}\right)^2 \frac{d^2v_1}{dx^2} + 2\frac{dv_0}{dx}\frac{dv}{dx},\\
\widehat{B}_1 &= \frac{dv_1}{dx}\frac{d\Theta_0}{dx} + \frac{dv_0}{dx}\frac{d\Theta_1}{dx},\\
\widehat{C}_1 &= \Theta_1(x)\frac{d^2v_0}{dx^2} + \Theta_0(x)\frac{d^2v_1}{dx^2},\\
\widehat{D}_1 &= 2\frac{dv_0}{dx}\frac{dv_1}{dx},\\
\widehat{E}_1 &= \Theta_1(x)\left(\frac{dv_0}{dx}\right)^2 + 2\Theta_0(x)\frac{dv_1}{dx}\frac{dv_0}{dx},\\
\widehat{F}_1 &= 4\left(\frac{dv_0}{dx}\right)^3\frac{dv_1}{dx}.
\end{aligned} \tag{26}$$

$$\begin{aligned}
\widehat{A}_1 &= \left(\frac{dv_0}{dx}\right)^2 \frac{d^2v_1}{dx^2} + 2\frac{dv_0}{dx}\frac{dv}{dx},\\
\widehat{B}_1 &= \frac{dv_1}{dx}\frac{d\Theta_0}{dx} + \frac{dv_0}{dx}\frac{d\Theta_1}{dx},\\
\widehat{C}_1 &= \Theta_1(x)\frac{d^2v_0}{dx^2} + \Theta_0(x)\frac{d^2v_1}{dx^2},\\
\widehat{D}_1 &= 2\frac{dv_0}{dx}\frac{dv_1}{dx},\\
\widehat{E}_1 &= \Theta_1(x)\left(\frac{dv_0}{dx}\right)^2 + 2\Theta_0(x)\frac{dv_1}{dx}\frac{dv_0}{dx},\\
\widehat{F}_1 &= 4\left(\frac{dv_0}{dx}\right)^3\frac{dv_1}{dx}.
\end{aligned} \tag{27}$$

Solution of (23) in series form is derived as

$$\begin{aligned}
v_0 + v_1 + \cdots &= f_1 - 6\beta L^{-1}\left[\widehat{A}_0 + \widehat{A}_1 + \cdots\right]\\
&\quad + ML^{-1}\left[\widehat{B}_0 + \widehat{B}_1 + \cdots\right]\\
&\quad + ML^{-1}\left[\widehat{C}_0 + \widehat{C}_1 + \cdots\right],\\
\Theta_0 + \Theta_1 + \cdots &= f_2 - B_rL^{-1}\left[\widehat{D}_0 + \widehat{D}_1 + \cdots\right]\\
&\quad + MB_rL^{-1}\left[\widehat{E}_0 + \widehat{E}_1 + \cdots\right]\\
&\quad - 2B_r\beta L^{-1}\left[\widehat{F}_0 + \widehat{F}_1 + \cdots\right].
\end{aligned} \tag{28}$$

The velocity and heat components up to second component are obtained by comparing both sides of (28).

Components of the lift problem are

$$v_0(x) = f_1, \tag{29}$$

$$\Theta_0(x) = f_2, \tag{30}$$

$$\begin{aligned}
v_1(x) &= -6\beta L^{-1}\left[\widehat{A}_0\right] + ML^{-1}\left[\widehat{B}_0\right]\\
&\quad + ML^{-1}\left[\widehat{C}_0\right],
\end{aligned} \tag{31}$$

$$\begin{aligned}
\Theta_1(x) &= -B_rL^{-1}\left[\widehat{D}_0\right] + MB_rL^{-1}\left[\widehat{E}_0\right]\\
&\quad - 2B_r\beta L^{-1}\left[\widehat{F}_0\right],
\end{aligned} \tag{32}$$

$$\begin{aligned}
v_2(x) &= -6\beta L^{-1}\left[\widehat{A}_1\right] + ML^{-1}\left[\widehat{B}_1\right]\\
&\quad + ML^{-1}\left[\widehat{C}_1\right],
\end{aligned} \tag{33}$$

$$\begin{aligned}
\Theta_2(x) &= -B_rL^{-1}\left[\widehat{D}_1\right] + \Lambda B_rL^{-1}\left[\widehat{E}_1\right]\\
&\quad - 2B_r\beta L^{-1}\left[\widehat{F}_1\right].
\end{aligned} \tag{34}$$

Zero component slip boundary conditions from (16) and (19) are

$$\begin{aligned}
v_0 &= 1 - \Lambda\left(\frac{dv_0}{dx} - M\Theta_0\frac{dv_0}{dx} + 2\beta\left(\frac{dv_0}{dx}\right)^3\right),\\
\Theta_0 &= 0, \quad \text{at } x = 0,
\end{aligned} \tag{35}$$

$$\frac{dv_0}{dx} = 0, \quad \Theta_0 = 1, \quad \text{at } x = 1. \tag{36}$$

First component slip boundary conditions from (17) and (19) are

$$\begin{aligned}
v_1 &= -\Lambda\left(\frac{dv_1}{dx} - M\Theta_0\frac{dv_1}{dx} - M\Theta_1\frac{dv_0}{dx} + 6\beta\left(\frac{dv_0}{dx}\right)^2\frac{dv_1}{dx}\right),\\
\Theta_1 &= 0, \quad \text{at } x = 0,
\end{aligned} \tag{37}$$

$$\frac{dv_1}{dx} = 0, \quad \Theta_1 = 0, \quad \text{at } x = 1. \tag{38}$$

Second component slip boundary conditions from (17) and (19) are

$$\begin{aligned}
v_2 &= -\Lambda\left[\frac{dv_2}{dx} - M\left(\Theta_0\frac{dv_2}{dx} + \Theta_1\frac{dv_1}{dx} + \Theta_2\frac{dv_0}{dx}\right)\right.\\
&\quad \left. + 6\beta\left(\left(\frac{dv_0}{dx}\right)^2\frac{dv_2}{dx} + \left(\frac{dv_1}{dx}\right)^2\frac{dv_0}{dx}\right)\right],\\
\Theta_2 &= 0, \quad \text{at } x = 0,
\end{aligned} \tag{39}$$

$$\frac{dv_2}{dx} = 0, \quad \Theta_2 = 0, \quad \text{at } x = 1. \tag{40}$$

Inserting slip boundary conditions from (35) and (36) into (29) and (30), $v_0(x)$ and $\Theta_0(x)$ are

$$\begin{aligned}
v_0(x) &= \left(1 + \Lambda S_t + 2\beta\Lambda S_t^3\right) - \left(S_t\right)x + \left(\frac{S_t}{2}\right)x^2,\\
\Theta_0(x) &= x.
\end{aligned} \tag{41}$$

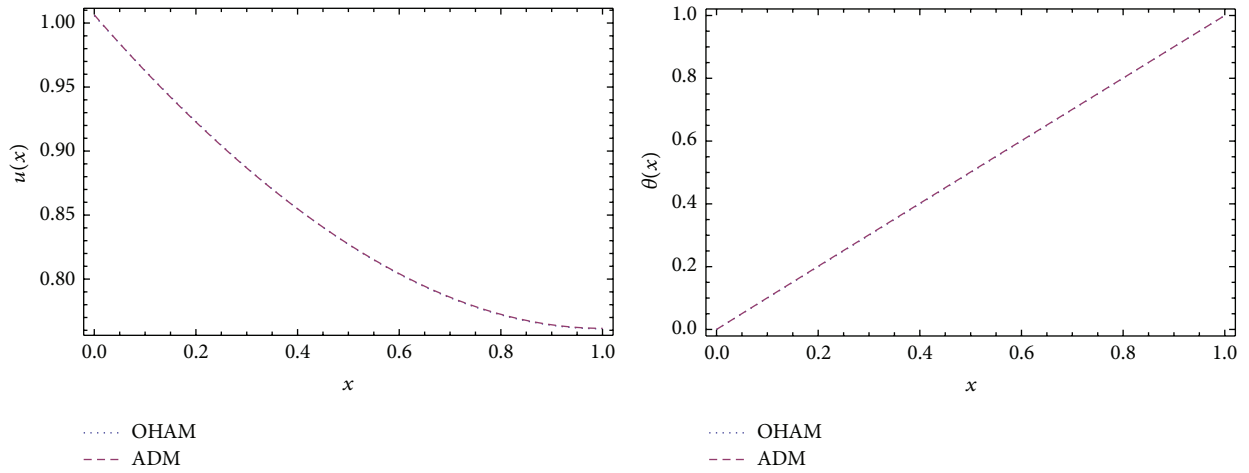

(a) (b)

Figure 2: Comparison of ADM and OHAM methods for lift velocity profile (a) and temperature distribution (b). $S_t = 0.5$, $M = 0.1$, $\beta = 0.3$, $\Lambda = 0.01$, $B_r = 4$, $C_1 = 0.212619$, $S_t = 0.1$, $M = 0.1$, $\beta = 0.3$, $\Lambda = 0.01$, $B_r = 4$, $C_1 = -0.702416$, $C_2 = -0.24397$, $C_3 = 0.01611$, $C_4 = -0.016823$. $C_2 = -0.03461$, $C_3 = -4.49647$, and $C_4 = -16.42906$.

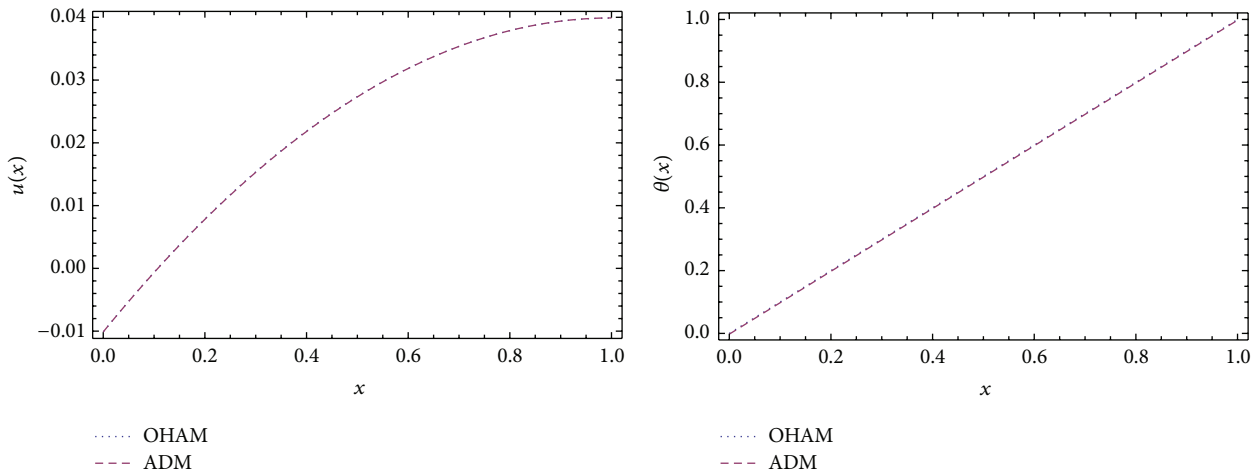

(a) (b)

Figure 3: Comparison of ADM and OHAM methods for drainage velocity profile (a) and temperature distribution (b). $S_t = 0.1$, $M = 0.01$, $\beta = 0.3$, $\Lambda = 0.1$, $B_r = 0.4$, $C_1 = -0.000019$, $S_t = 0.1$, $M = 0.01$, $\beta = 0.3$, $\Lambda = 0.1$, $B_r = 0.4$, $C_1 = -0.073388$, $C_2 = 0.000069$, $C_3 = 1728.447608$, $C_4 = 152.167755$, $C_2 = 0.049829$, $C_3 = -1.123666$, and $C_4 = -0.0230394$.

Inserting slip boundary conditions from (37) and (38) into (31) and (32), $v_1(x)$ and $\Theta_1(x)$ are

$$\begin{aligned} v_1(x) = {} & \left(2\beta\Lambda S_t^3 + 12\beta^2\Lambda S_t^5\right) + \left(2\beta S_t^3\right)x \\ & - \left(\frac{MS_t}{2} + 3\beta S_t^3\right)x^2 + \left(\frac{MS_t}{3} + 2\beta S_t^3\right)x^3 \\ & - \left(\frac{1}{2}\beta S_t^3\right)x^4, \end{aligned} \tag{42}$$

$$\begin{aligned} \Theta_1(x) = {} & \left(\frac{1}{4}B_r S_t^2 - \frac{1}{20}MB_r S_t^2 + \frac{1}{3}\beta B_r S_t^4\right)x \\ & - \left(\frac{1}{2}B_r S_t^2 + \beta B_r S_t^4\right)x^2 \\ & + \left(\frac{1}{3}B_r S_t^2 + \frac{1}{6}MB_r S_t^2 + \frac{4}{3}\beta B_r S_t^4\right)x^3 \\ & - \left(\frac{1}{12}B_r S_t^2 + \frac{1}{6}MB_r S_t^2 + \beta B_r S_t^4\right)x^4 \\ & + \left(\frac{1}{20}MB_r S_t^2 + \frac{2}{5}\beta B_r S_t^4\right)x^5 \\ & - \left(\frac{1}{15}\beta B_r S_t^4\right)x^6. \end{aligned} \tag{43}$$

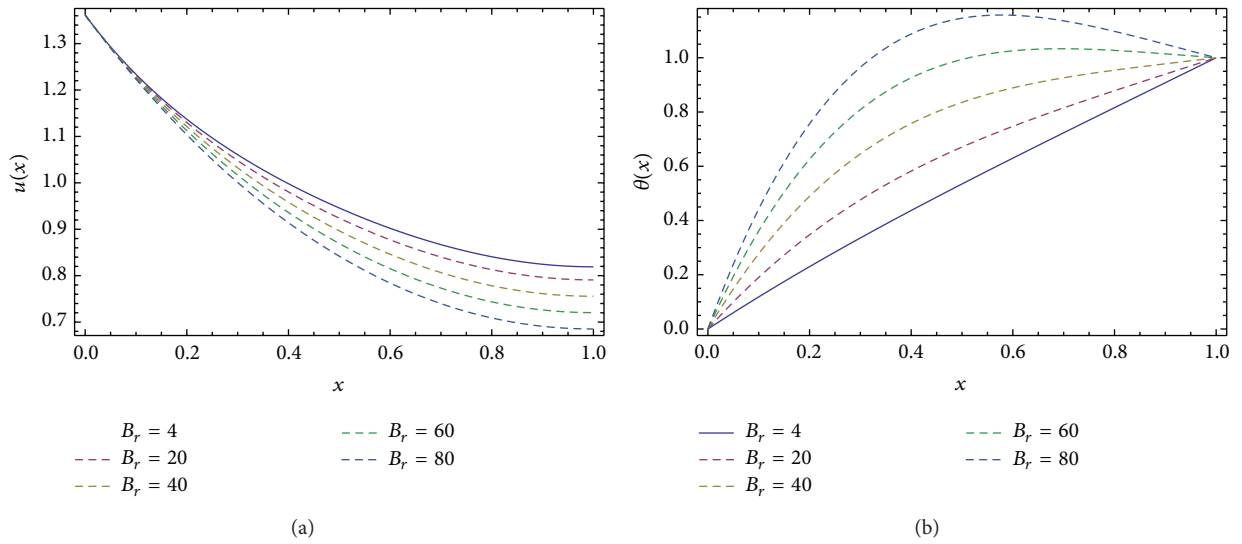

FIGURE 4: Brinkman number on the lift velocity (a) and temperature distribution (b) when $S_t = 1$, $\Lambda = 0.4$, $M = 0.1$, and $\beta = 0.3$ and $S_t = 0.5$, $\Lambda = 0.4$, $M = 0.1$, and $\beta = 0.3$.

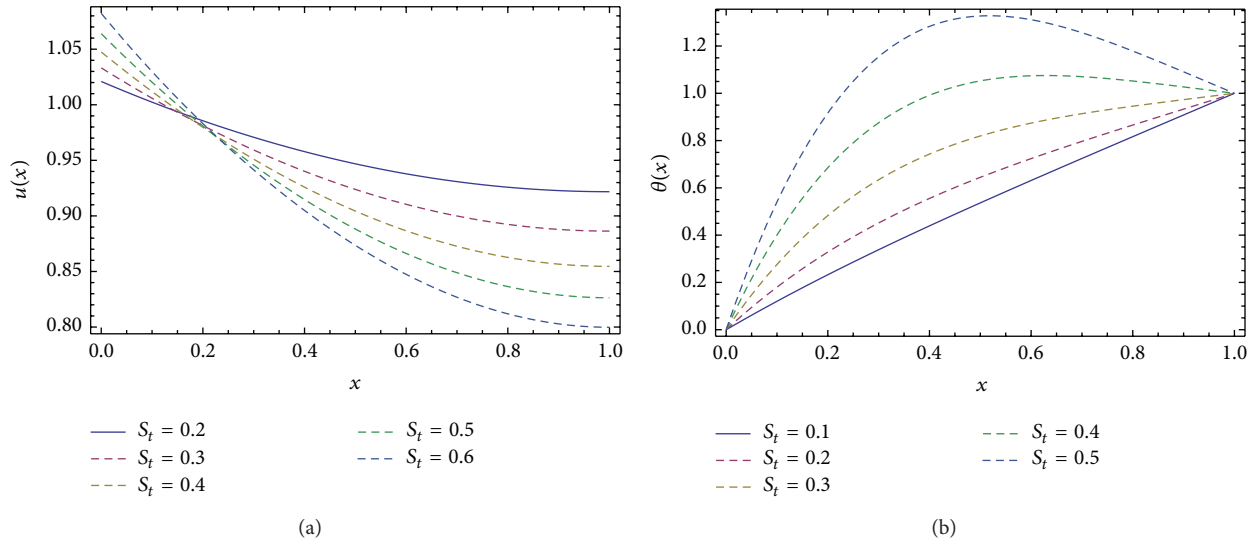

FIGURE 5: Effect of the stock number on lift velocity (a) and temperature distribution (b) when $M = 0.01$, $\beta = 0.3$, $\Lambda = 0.1$, and $B_r = 4$ and $\beta = 0.3$, $M = 0.01$, and $B_r = 100$.

The terms $v_2(x)$ and $\Theta_2(x)$ are too large to be written above; therefore, their expression is mentioned graphically.

5. Formulation of Drainage Problem

The geometry and assumptions of the problem are the same as in previous problem. Consider a film of non-Newtonian liquid draining at volume flow rate Q down the vertical belt. The belt is stationary and the fluid drains down the belt due to gravity. The gravity in this case is opposite to the previous case. Therefore, the stock number is positively mentioned in (14). The coordinate system is selected the same as in previous case. Assume the flow is steady and laminar while external pressure is neglected. Consider fluid shear forces keep the gravity balanced and the film thickness remains constant.

Modeled slip boundary conditions for drainage problem are

$$v = -\gamma T_{xy}, \quad \text{at } x = 0,$$
$$\frac{dv}{dx} = 0, \quad \text{at } x = 1. \tag{44}$$

Making use of nondimensional variables the slip boundary conditions in (42) are

$$v_n = -\Lambda\left(\frac{dv_n}{dx} - M\Theta\frac{dv_n}{dx} + 2\beta\left(\frac{dv_n}{dx}\right)^3\right), \quad \text{at } x = 0,$$
$$\frac{dv_n}{dx} = 0, \quad \text{at } x = 1, \text{ when } n = 0, 1, 2, 3, \ldots. \tag{45}$$

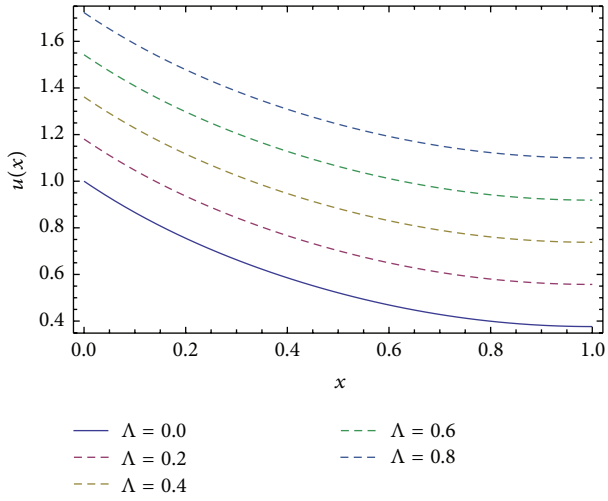

Figure 6: Effect of slip parameter on the lift velocity profile when $S_t = 1$, $M = 0.1$, $\beta = 0.3$, and $B_r = 50$.

For heat, the boundary conditions are identical as given in (36), (38), and (40) regarding both the problems.

6. Solution of Drainage Problem

6.1. The ADM Solution. By making use of ADM in (14) and (15), the Adomian polynomials in (24)–(27) for both problems are the same. The different velocity components are obtained as follows.

Components of Problem. The boundary conditions of first and second components for drainage velocity profile are the same as given in (37). The boundary conditions for temperature distribution are also the same as given in (38), but the solution of these components is different, dependent on the different velocity profile of drainage and lift problems. The terms $v_2(x)$ and $\Theta_2(x)$ are too large to be written above; therefore, their expression is mentioned graphically.

Inserting slip boundary conditions from (45) and from (18) and (19) in (29)–(34) the different components solution is obtained as

$$v_0(x) = \frac{1}{2}\left(2S_t x - S_t x^2\right),$$

$$\Theta_0(x,t) = x,$$

$$v_1(x) = \left(-\frac{1}{3}M^2 S_t - \beta S_t^3\right)x + \left(\frac{\Lambda S_t}{2} + \frac{3\beta S_t^3}{2}\right)x^2 + \left(\frac{M^2 S_t}{6} - \frac{\Lambda S_t}{3} - \beta S_t^3\right)x^3 + \left(-\frac{1}{24}M^2 S_t + \frac{\beta S_t^3}{4}\right)x^4,$$

Table 1: Comparison of present work and existing work [23] for lift velocity profile when $m = S_t = 0.5$, $M = 0$, $\beta = 0.6$, $\Lambda = 0$, $\alpha = 1$.

x	Present work	Existing work	Absolute error
0.0	1	1	0
0.1	0.95485367	0.95485367	0
0.2	0.91553824	0.91553824	0
0.3	0.88114335	0.88114335	0
0.4	0.85118976	0.85118976	0.148×10^{-14}
0.5	0.82550781	0.82550781	0
0.6	0.80413216	0.80413216	1.11×10^{-29}
0.7	0.78721265	0.787212652	0
0.8	0.77494144	0.77494144	-1.11×10^{-29}
0.9	0.76749627	0.767496272	0
1.0	0.765	0.765	-1.11×10^{-29}

$$\Theta_1(x) = \left(\frac{1}{4}B_r S_t^2 - \frac{1}{20}\Lambda B_r S_t^2 + \frac{1}{6}\beta B_r S_t^4\right)x + \left(-\frac{1}{2}B_r S_t^2 - \frac{1}{2}\beta B_r S_t^4\right)x^2 + \left(\frac{1}{3}B_r S_t^2 + \frac{1}{6}\Lambda B_r S_t^2 + \frac{2}{3}\beta B_r S_t^4\right)x^3 + \left(-\frac{1}{12}B_r S_t^2 - \frac{1}{6}\Lambda B_r S_t^2 - \frac{1}{2}\beta B_r S_t^4\right)x^4 + \left(\frac{1}{20}\Lambda B_r S_t^2 + \frac{1}{5}\beta B_r S_t^4\right)x^5 + \left(-\frac{1}{30}\beta B_r S_t^4\right)x^6. \quad (46)$$

In the existence work [23] m is used as gravitational parameter instead of stock number S_t in the present work. Magnetic parameter is defined as M in the existing work and in the present work M is embedding parameter. If we put magnetic parameter = 0, slip parameter $\Lambda = 0$ in the existing work and embedding parameter $M = 0$, slip parameter $\Lambda = 0$ in present work, then comparison of existing and present work is as shown in Table 1.

OHAM solution of the present work has been obtained and used only for comparison through Tables 1, 2, 3, 4, and 5.

7. Results and Discussion

In this study, the heat transfer of a third grade fluid on thin film flow has been examined. The geometry of lift and drainage problems has been shown in Figures 1(a) and 1(b), respectively. The velocity and heat transfer analysis for both lift and drainage problems have been investigated under the influence of stock number S_t, slip parameter Λ, the Brinkman number B_r, non-Newtonian parameter β, and viscosity parameter M. The effects of these physical parameters have been discussed in Figures 2–13. The OHAM solution of the present work has been shown graphically and numerically

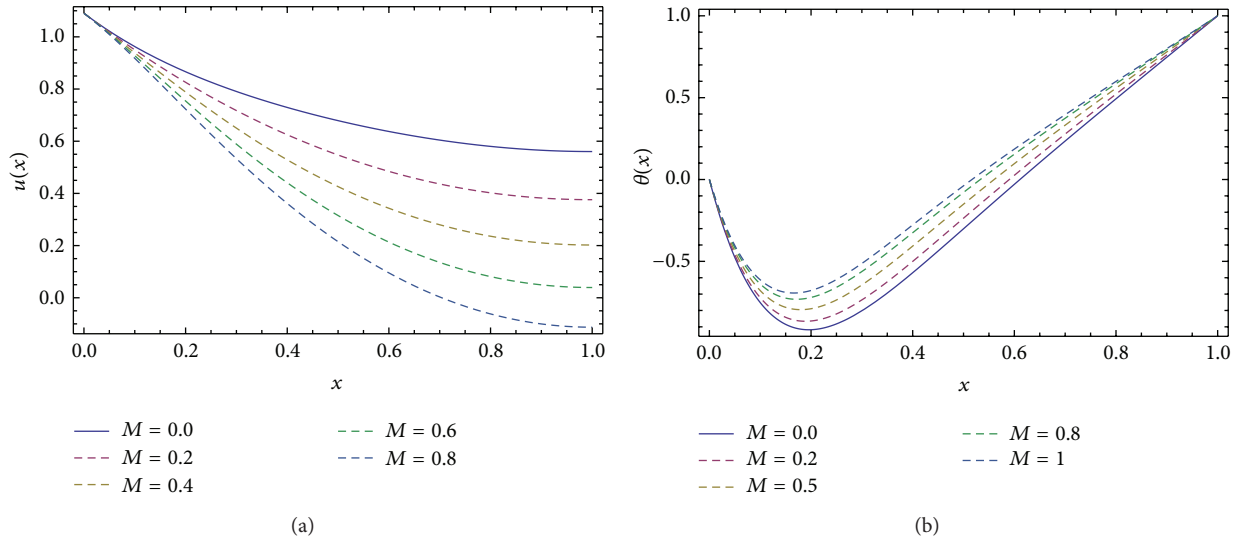

(a) (b)

Figure 7: The effect of viscosity parameter on lift velocity (a) and temperature distribution (b) when $B_r = 40$, $\Lambda = 0.1$, $\beta = 0.3$, and $S_t = 0.5$ and $B_r = 10$, $\beta = 0.6$, and $S_t = 1$.

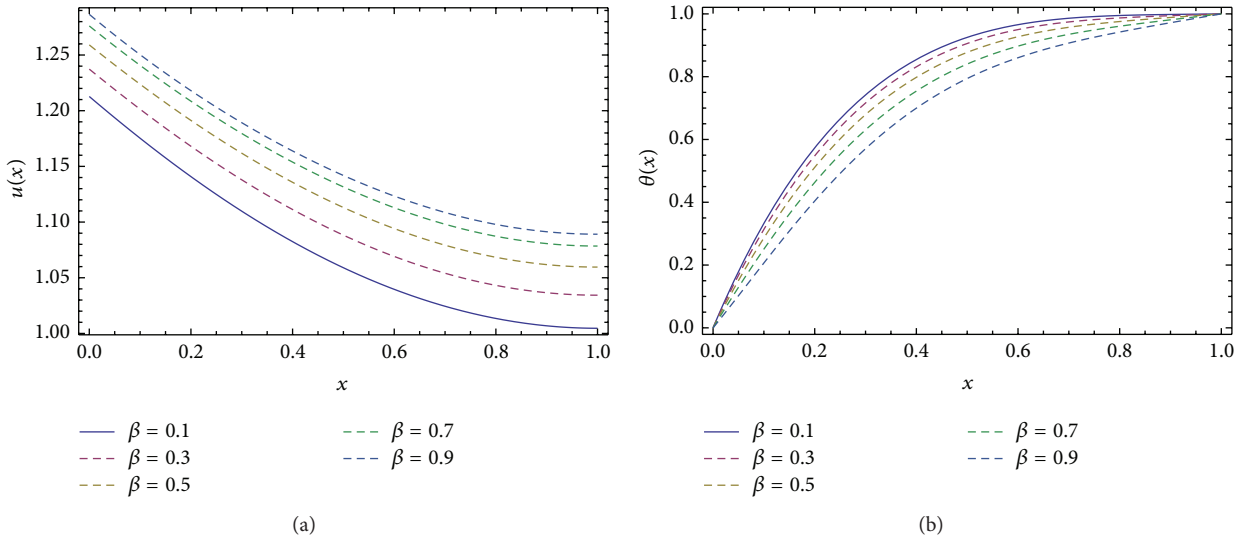

(a) (b)

Figure 8: Effect of β on lift velocity (a) and temperature distribution (b) when $M = 0.1$, $S_t = 0.4$, $\Lambda = 0.5$, and $B_r = 50$.

only for comparison. The comparison of analytical methods ADM and OHAM of the present work for lift velocity and heat transfer analysis is shown in Figures 2(a) and 2(b). Figures 3(a) and 3(b) show the comparison of ADM and OHAM for drainage velocity and temperature distribution. Effect of the Brinkman number B_r, for lift velocity profile, has been shown in Figure 4(a). Behavior of the lift velocity field v can be seen when the velocity of fluid is maximum at the surface of the belt while it is minimum at the surface of the fluid. It has been found out that the velocity of the fluid decreases for large value of B_r as compared to small values of B_r. The observation of Brinkman number B_r associated with heat in lift problem has been countered in Figure 4(b). Since B_r is related with the viscous dissipation term in energy equation, higher values of the B_r should essentially lead to an increase in amount of heat being generated by the shear forces in the fluid leading to increase in the fluid temperature.

In Figure 5(a), we observed that the velocity decreases with an increase in the stock number S_t; due to friction force, the effect of stock number seems to be smaller near the belt. It can be seen that there is a point in the domain, where the velocity of the fluid becomes approximately identical for different values of stock number S_t. The reason is that the friction of the belt becomes negligible at this point. On increasing stock number S_t, after this point in lifting flow, the velocity decreases due to negligible friction. The effect of stock number S_t on temperature distribution has been illustrated in Figure 5(b). It has been observed that the temperature Θ increases steadily by increasing S_t. In Figure 6, it has been noticed that the speed of the fluid near

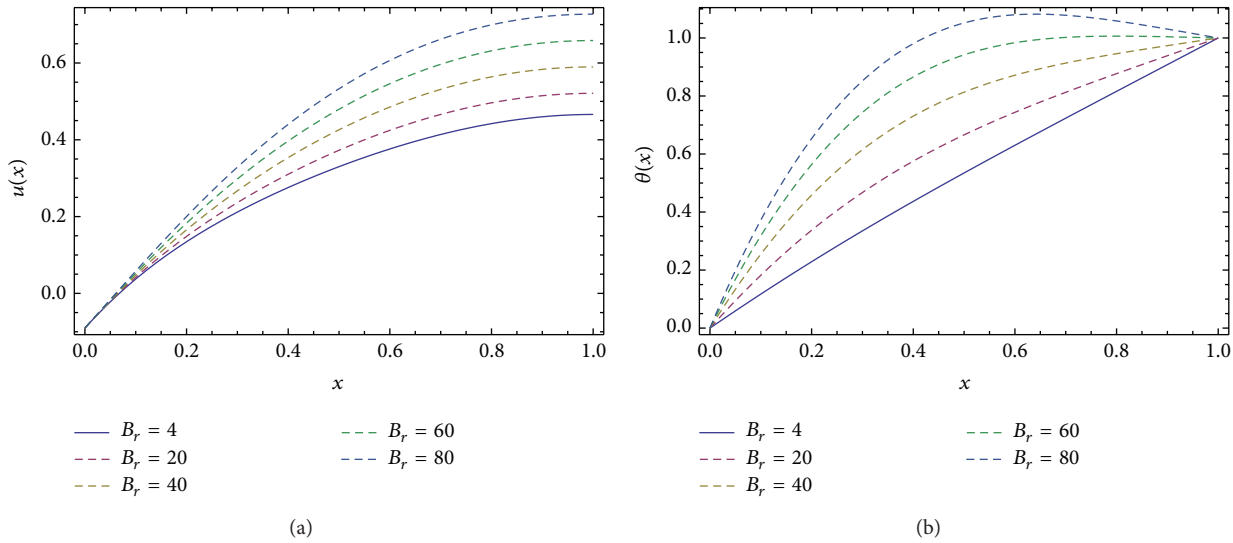

FIGURE 9: Drainage velocity (a) and heat distribution (b) for Brickman number when $S_t = 1$, $\Lambda = 0.1$, $M = 0.2$, and $\beta = 0.3$ and $M = 0.3$, $S_t = 0.5$, $\beta = 0.5$, and $\Lambda = 0.1$.

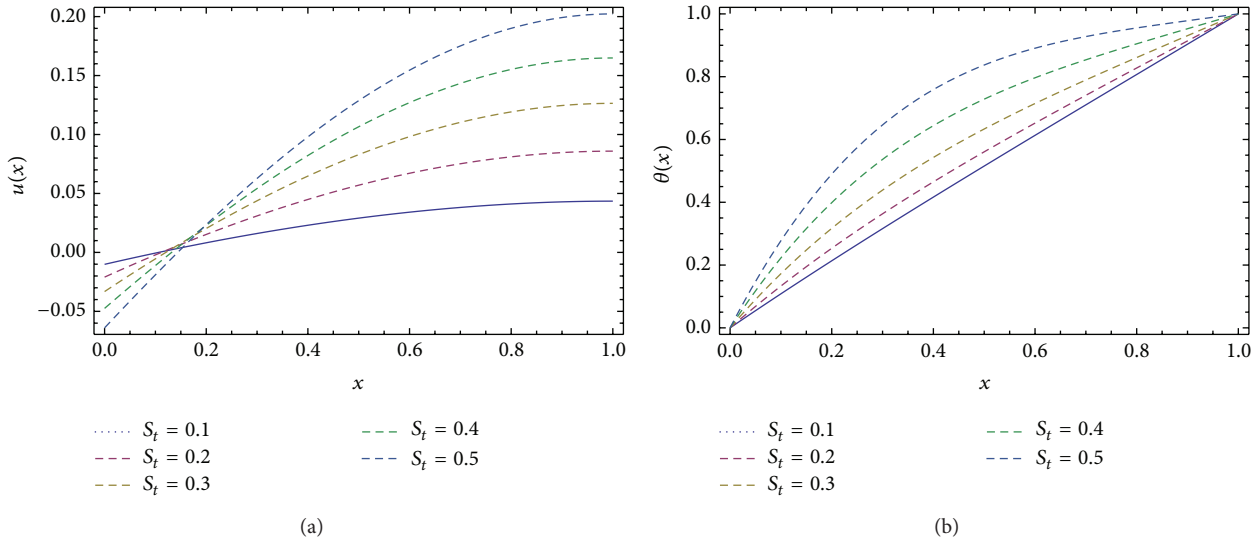

FIGURE 10: Effect of stock number on drainage velocity profile (a) and temperature distribution (b) when $M = 0.2$, $\beta = 0.3$, $\Lambda = 0.1$, and $B_r = 40$.

the belt is greater than the speed at the surface. When we increase the slip parameter, then, due to decrease in friction force, the velocity of the fluid decreases gradually towards the surface of the belt. The effect of viscosity parameter M on lift velocity v has been shown in Figure 7(a). The speed of flow decreases with increasing M. It can also be seen that the thickness of thin film increases in case of dilatant fluids and decreases in pseudoplastic fluids. In Figure 7(b), increase in viscosity parameter M results in increasing temperature distribution steadily. Figure 8(a) indicates the influence of non-Newtonian effect β on lift velocity profile.

For small values of β, the velocity profile differs little from the Newtonian one. However, when β is increased, these profiles become more flatten showing the shear thinning effect. Increase in β results in decreasing temperature distribution as shown in Figure 8(b). The drain velocity increases with increase in Brinkman number as shown in Figure 9(a). Figure 9(b) specifies the effect of B_r for drain temperature distribution. The temperature distribution increases as the B_r increases and becomes more trampled for higher value of B_r. In Figure 10(a), the effect of stock number S_t has been shown for drainage flow. It can be seen that there is a point near the belt, where the velocity of the fluid becomes approximately the same for different values of stock number S_t because friction of the belt becomes negligible at this point. On increasing the stock number S_t, after this point, the curvature of velocity increases due to negligible friction. The effect of stock number S_t on temperature distribution

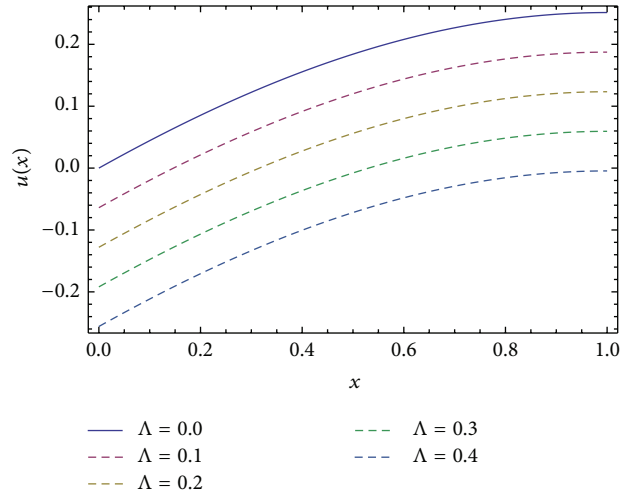

Figure 11: Drain velocity profile for different values of slip parameter when $M = 0.1$, $S_t = 0.5$, $\beta = 0.3$, and $B_r = 40$.

Table 2: Comparison of OHAM and ADM for lift velocity profile when $S_t = 0.5$, $M = 0.1$, $\beta = 0.3$, $\Lambda = 0.01$, $B_r = 4$, $C_1 = 0.212619$, $C_2 = -0.243971$, $C_3 = 0.016110$, $C_4 = -0.0168232$.

x	OHAM	ADM	Absolute error
0.0	1.00586	1.0064	0.543×10^{-3}
0.1	0.962821	0.962544	0.277×10^{-3}
0.2	0.923093	0.922658	0.435×10^{-3}
0.3	0.887013	0.886739	0.274×10^{-3}
0.4	0.854908	0.854893	0.148×10^{-4}
0.5	0.827086	0.827304	0.217×10^{-3}
0.6	0.803834	0.804202	0.367×10^{-3}
0.7	0.785409	0.785838	0.428×10^{-3}
0.8	0.77204	0.772463	0.423×10^{-3}
0.9	0.763914	0.764303	0.389×10^{-3}
1.0	0.76118	0.761549	0.369×10^{-3}

Table 3: Comparison of OHAM and ADM for lift heat distribution when $S_t = 0.1$, $M = 0.1$, $\beta = 0.3$, $\Lambda = 0.01$, $B_r = 4$, $C_1 = -0.70242$, $C_2 = -0.03461$, $C_3 = -4.49647$, $C_4 = -16.42906$.

x	OHAM	ADM	Absolute error
0.0	0	0	0.840×10^{-3}
0.1	0.09998	0.10083	0.135×10^{-2}
0.2	0.19998	0.20133	0.159×10^{-2}
0.3	0.29998	0.30157	0.163×10^{-2}
0.4	0.39998	0.40162	0.152×10^{-2}
0.5	0.49998	0.50151	0.130×10^{-2}
0.6	0.59998	0.60129	0.101×10^{-2}
0.7	0.69998	0.70101	0.693×10^{-3}
0.8	0.79999	0.80068	0.423×10^{-3}
0.9	0.863914	0.90034	0.349×10^{-3}
1.0	1.000000	1.000000	0.294×10^{-19}

Table 4: Comparison of OHAM and ADM for drainage velocity profile when $S_t = 0.1$, $M = 0.01$, $\beta = 0.3$, $\Lambda = 0.1$, $B_r = 0.4$, $C_1 = -0.00002$, $C_2 = 0.00007$, $C_3 = 1728.44761$, $C_4 = 152.16776$.

x	OHAM	ADM	Absolute error
0.0	−0.01012	−0.01012	0.0
0.1	−0.00062	−0.00067	0.461×10^{-4}
0.2	0.00789	0.00781	0.702×10^{-4}
0.3	0.01538	0.01531	0.768×10^{-4}
0.4	0.02188	0.02181	0.708×10^{-4}
0.5	0.02738	0.02733	0.561×10^{-4}
0.6	0.03188	0.03185	0.371×10^{-4}
0.7	0.03538	0.03536	0.168×10^{-4}
0.8	0.03788	0.037881	0.920×10^{-8}
0.9	0.03938	0.03939	0.134×10^{-3}
1.0	0.03988	0.03989	0.182×10^{-3}

Table 5: Comparison of OHAM and ADM for drain heat distribution when $S_t = 0.1$, $M = 0.01$, $\beta = 0.3$, $\Lambda = 0.1$, $B_r = 0.4$, $C_1 = -0.07339$, $C_2 = 0.049829$, $C_3 = -1.12367$, $C_4 = -0.02304$.

x	OHAM	ADM	Absolute error
0.0	0	0	0
0.1	0.100082	0.100081	0.818×10^{-6}
0.2	0.200131	0.20013	0.115×10^{-5}
0.3	0.300154	0.300153	0.118×10^{-5}
0.4	0.400158	0.400157	0.107×10^{-5}
0.5	0.500147	0.500146	0.887×10^{-6}
0.6	0.600126	0.600125	0.689×10^{-6}
0.7	0.700098	0.700097	0.501×10^{-6}
0.8	0.800067	0.800066	0.326×10^{-6}
0.9	0.900034	0.900033	0.161×10^{-6}
1.0	1.000000	1.000000	0.261×10^{-18}

is illustrated in Figure 10(b). In Figure 11, it is noticed that the speed of the fluid near the belt is smaller than the speed at the surface. When we increase the slip parameter, the velocity of the fluid increases because the friction goes on decreasing. It has been observed that the temperature Θ increases monotonically on increasing S_t. Figure 12(a) illustrates the effect of variable viscosity parameter M on the drain velocity profile. For higher values of viscosity parameter M the velocity of fluid increases gradually towards the surface of the fluid. Increase in viscosity parameter M causes increase in temperature field gradually as shown in Figure 12(b). The effect of non-Newtonian parameter β totally depends on the shear thining effect as shown in Figure 13(a). Increase in β results in increasing speed of the drain velocity profile but increase in β decreases temperature profile dependent on the shear thinning and thickening properties of fluid film as shown in Figure 13(b).

8. Conclusion

We have investigated the temperature dependent viscosity of a third grade thin film fluid flow subject to lifting and

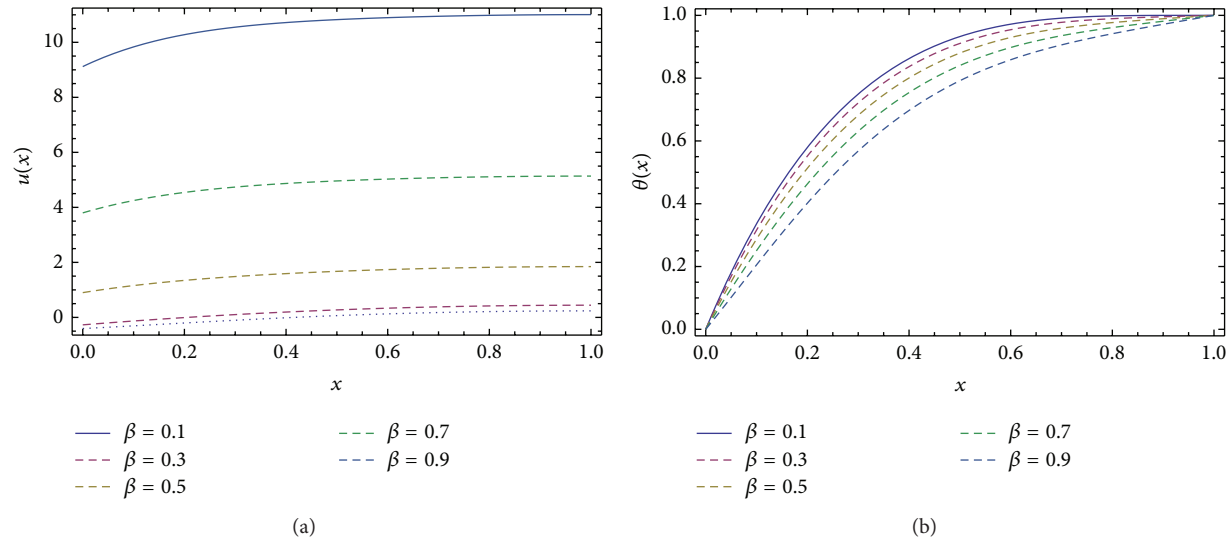

FIGURE 12: The effect of non-Newtonian β on velocity profile (a) and temperature distribution (b) when $M = 0.2$, $S_t = 1$, $\Lambda = 0.3$, and $B_r = 50$ and $M = 0.3$, $S_t = 0.5$, $\Lambda = 0.1$, and $B_r = 50$.

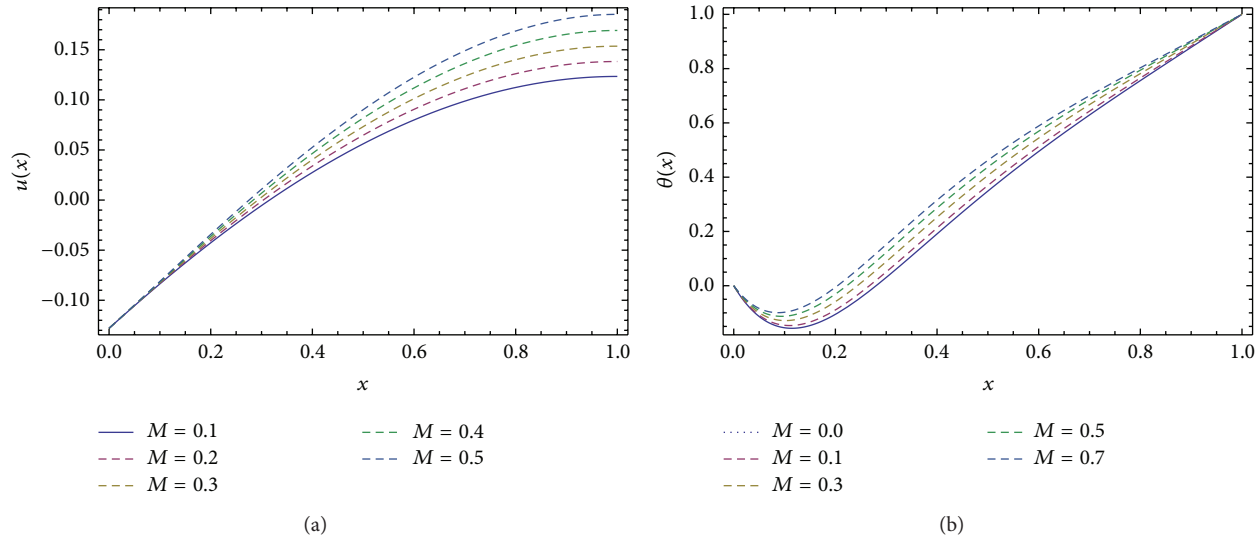

FIGURE 13: Effect of the viscosity parameter M on the drainage velocity (a) and temprature (b) when $S_t = 0.5$, $\beta = 0.3$, $\Lambda = 0.2$, and $B_r = 40$ and $S_t = 1$, $\beta = 0.5$, and $B_r = 10$.

drainage of fluid. Problems have been solved analytically by using Adomian Decomposition Method (ADM). The comparison of ADM and Optimal Homotopy Asymptotic Method (OHAM) has been derived graphically and numerically. Expression for velocity fields and temperature distribution has been presented and sketched. These solutions are valid not only for small but also for large values of emerging parameters. The observation of Brinkman number B_r associated with heat is countered in both lift and drainage problems. Since B_r is related with the viscous dissipation term in heat equation, higher values of the B_r should essentially lead to an increase in the amount of heat being generated by the shear forces in the fluid leading to increase in the fluid temperature. It has been observed that the temperature Θ increases monotonically on increasing S_t. The speed of flow decreases with increasing viscosity parameter M. Increase in M increases the temperature distribution. It can also be seen that the thickness of thin film increases in case of dilatant fluids and decreases in pseudoplastic fluids. According to the best of our knowledge, no research has been carried out yet regarding our study. This is our first attempt to handle this problem with variable viscosity and slip boundary conditions.

Conflict of Interests

The authors declare that there is no conflict of interests regarding the publication of this paper.

Acknowledgment

The authors would like to thank Universiti Teknologi PETRONAS for the financial support.

References

[1] D. Goussis and R. E. Kelly, "Effects of viscosity variation on the stability of film flow down heated or cooled inclined surfaces: long-wavelength analysis," *The Physics of Fluids*, vol. 28, no. 11, pp. 3207–3214, 1985.

[2] D. A. Goussis and R. E. Kelly, "Effects of viscosity variation on the stability of a liquid film flow down heated or cooled inclined surfaces, finite wavelength analysis," *Physics of Fluids*, vol. 30, pp. 974–982, 1987.

[3] C.-C. Hwang and C.-I. Weng, "Non-linear stability analysis of film flow down a heated or cooled inclined plane with viscosity variation," *International Journal of Heat and Mass Transfer*, vol. 31, pp. 1775–1784, 1988.

[4] B. Reisfeld and S. G. Bankoff, "Nonlinear stability of a heated thin liquid film with variable viscosity," *Physics of Fluids A*, vol. 2, pp. 2066–2067, 1990.

[5] M. C. Wu and C. C. Hwang, "Nonlinear theory of film rupture with viscosity variation," *International Communications in Heat and Mass Transfer*, vol. 18, pp. 705–713, 1991.

[6] A. Sansom, J. R. King, and D. S. Riley, "Degenerate-diffusion models for the spreading of thin non-isothermal gravity currents," *Journal of Engineering Mathematics*, vol. 48, no. 1, pp. 43–68, 2004.

[7] A. R. A. Khaled and K. Vafai, "Hydrodynomic Squeezed flow and heat transfer over a sensor surface," *International Journal of Engineering Science*, vol. 42, pp. 509–519, 2004.

[8] S. Nadeem and M. Awais, "Thin film flow of an unsteady shrinking sheet through porous medium with variable viscosity," *Physics Letters A*, vol. 372, pp. 4965–4972, 2008.

[9] A. J. Chamkha, T. Grosan, and I. Pop, "Fully developed free convection of a micro polar fluid in a vertical channel," *International Communications in Heat and Mass Transfer*, vol. 29, pp. 1119–1127, 2002.

[10] H. Saleh and I. Hashim, "Simulation of micropolar fluid flow in a vertical channel using homotopy-perturbation method," in *Proceedings of the Applied Computing Conference*, pp. 1–4, Istanbul, Turkey, 2008.

[11] Y. M. Aiyesimi and G. T. Okedao, "MHD flow of a third grade fluid with heat transfer down an inclined plane," *Mathematical Theory and Modeling*, vol. 2, no. 9, pp. 108–109, 2012.

[12] K. Nrgis and T. Mahmood, "The influence of slip condition on the thin film flow of a third order fluid," *International Journal of Nonlinear Science*, vol. 1, no. 13, pp. 105–116, 2012.

[13] M. I. Anwar, I. Khan, A. Hussnan, M. Z. Salleh, and S. Sharidan, "Stagnation-point flow of a nanofluid over a nonlinear stretching sheet," *World Applied Sciences Journal*, vol. 23, no. 8, pp. 998–1006, 2013.

[14] M. Qasim, I. Khan, and S. Sharidan, "Heat transfer and mass diffusion in nanofluids with convective boundary conditions," *Mathematical Problems in Engineering*, vol. 2013, Article ID 254973, 7 pages, 2013.

[15] A. M. Siddiqui, R. Mahmood, and Q. K. Ghori, "Homotopy perturbation method for thin film flow of a third grade fluid down an inclined plane," *Chaos, Solitons & Fractals*, vol. 35, no. 1, pp. 140–147, 2008.

[16] S. J. Liao, *Beyond Perturbation: Introduction to Homotopy Analysis Method*, Chapman & Hall, Boca Raton, Fla, USA, 2003.

[17] V. Marinca, N. Herisanu, and I. Nemes, "Optimal homotopy asymptotic method with application to thin film flow," *Central European Journal of Physics*, vol. 6, no. 3, pp. 648–653, 2008.

[18] V. Marinca and N. Herisanu, "Application of optimal Homotopy asymptotic method for solving non-linear equations arising in heat transfer," *International Communications in Heat and Mass Transfer*, vol. 35, pp. 710–715, 2008.

[19] V. Marinca, N. Herişanu, C. Bota, and B. Marinca, "An optimal homotopy asymptotic method applied to the steady flow of a fourth-grade fluid past a porous plate," *Applied Mathematics Letters*, vol. 22, no. 2, pp. 245–251, 2009.

[20] A. A. Juneidi, D. D. Gangi, and M. Babaelahi, "Micropolar flow in a porous channel with high mass transfer," *International Communications in Heat and Mass Transfer*, vol. 36, pp. 1082–1088, 2009.

[21] A. M. Siddiqui, M. Ahmed, and Q. K. Ghori, "Thin film flow of non-Newtonian fluids on a moving belt," *Chaos, Solitons & Fractals*, vol. 33, no. 3, pp. 1006–1016, 2007.

[22] A. M. Siddiqui, R. Mahmood, and Q. K. Ghori, "Homotopy perturbation method for thin film flow of a fourth grade fluid down a vertical cylinder," *Physics Letters A*, vol. 352, pp. 404–410, 2006.

[23] T. Gul, R. A. Shah, S. Islam, and M. Arif, "MHD thin film flows of a third grade fluid on a vertical belt with slip boundary conditions," *Journal of Applied Mathematics*, vol. 2013, Article ID 707286, 14 pages, 2013.

[24] T. Gul, S. Islam, R. A. Shah, I. Khan, and S. Shafie, "Thin film flow in MHD third grade fluid on a vertical belt with temperature dependent viscosity," *PLoS ONE*, vol. 9, no. 6, Article ID e97552, 2014.

[25] A. Costa and G. Macedonio, "Viscous heating in fluids with temperature-dependent viscosity: implications for magma flows," *Nonlinear Processes in Geophysics*, vol. 10, no. 6, pp. 545–555, 2003.

[26] R. Ellahi and A. Riaz, "Analytical solutions for MHD flow in a third-grade fluid with variable viscosity," *Mathematical and Computer Modelling*, vol. 52, no. 9-10, pp. 1783–1793, 2010.

[27] Y. Aksoy and M. Pakdemirly, "Approximate analytical solution for flow of a third grade fluid through a parallel-plate channel filled with a porous medium," *Transport in Porous Media*, vol. 83, no. 2, pp. 375–395, 2010.

[28] G. Adomian, *Solving Frontier Problems of Physics: The Decomposition Method*, vol. 60 of *Fundamental Theories of Physics*, Kluwer Academic, Dordrecht, The Netherlands, 1994.

[29] G. Adomian, "A review of the decomposition method and some recent results for nonlinear equations," *Mathematical and Computer Modelling*, vol. 13, no. 7, pp. 17–43, 1990.

[30] A. M. Wazwaz, "Adomian decomposition method for a reliable treatment of the Bratu-type equations," *Applied Mathematics and Computation*, vol. 166, pp. 652–663, 2005.

[31] A. M. Wazwaz, "Adomian decomposition method for a reliable treatment of the Emden-Fowler equation," *Applied Mathematics and Computation*, vol. 161, pp. 543–560, 2005.

[32] M. K. Alam, M. T. Rahim, T. Haroon, S. Islam, and A. M. Siddiqui, "Solution of steady thin film flow of Johnson-Segalman fluid on a vertical moving belt for lifting and drainage problems using Adomian decomposition method," *Applied Mathematics and Computation*, vol. 218, no. 21, pp. 10413–10428, 2012.

Hindawi Publishing Corporation
Abstract and Applied Analysis
Volume 2015, Article ID 369294, 7 pages
http://dx.doi.org/10.1155/2015/369294

Research Article

Classification of Multiply Travelling Wave Solutions for Coupled Burgers, Combined KdV-Modified KdV, and Schrödinger-KdV Equations

A. R. Seadawy[1,2] and K. El-Rashidy[2,3]

[1] *Mathematics Department, Faculty of Science, Taibah University, Al-Ula, Saudi Arabia*
[2] *Mathematics Department, Faculty of Science, Beni-Suef University, Egypt*
[3] *Mathematics Department, College of Arts and Science, Taif University, Ranyah, Saudi Arabia*

Correspondence should be addressed to A. R. Seadawy; aly742001@yahoo.com

Received 24 August 2014; Accepted 1 November 2014

Academic Editor: Yasir Khan

Copyright © 2015 A. R. Seadawy and K. El-Rashidy. This is an open access article distributed under the Creative Commons Attribution License, which permits unrestricted use, distribution, and reproduction in any medium, provided the original work is properly cited.

Some explicit travelling wave solutions to constructing exact solutions of nonlinear partial differential equations of mathematical physics are presented. By applying a theory of Frobenius decompositions and, more precisely, by using a transformation method to the coupled Burgers, combined Korteweg-de Vries- (KdV-) modified KdV and Schrödinger-KdV equation is written as bilinear ordinary differential equations and two solutions to describing nonlinear interaction of travelling waves are generated. The properties of the multiple travelling wave solutions are shown by some figures. All solutions are stable and have applications in physics.

1. Introduction

The investigation of traveling wave solutions of nonlinear evolution equations (NLEEs) plays a vital role in different branches of mathematical physics, engineering sciences, and other technical arenas, such as plasma physics, nonlinear optics, solid state physics, fluid mechanics, chemical physics, and chemistry.

The Burgers' equation has been found to describe various kinds of phenomena such as a mathematical model of turbulence [1] and the approximate theory of flow through a shock wave traveling in viscous fluid [2]. Fletcher using the Hopf-Cole transformation [3] gave an analytic solution for the system of two-dimensional Burgers' equations.

The Korteweg-de Vries (KdV) equation which models shallow-water phenomena has been analyzed extensively using the invariance properties that occur from the Lie point symmetry generator that admits it. In particular, travelling wave solutions arise from the combination of translations in space and time. Also, Galilean invariants and scale-invariant solutions are dependent on first and second Painleve transcendent [4]. Further, the modified KdV (mKdV) has attracted interest in a similar way and its Lie point symmetry generators are known [5]. Recently, the combined KdV (cKdV) and mKdV equation has been studied using various methods with a special reference to soliton-type solutions. For example, simple soliton solutions to cKdV-mKdV used in plasma and fluid physics are obtained in [6]. Here, the particular form uses the fact that the equation admits a scaling symmetry which is nonexistent for the general cKdV [7, 8].

The topic of solitons produced by nonlinear interactions is a very fundamental topic in various fields, including optical solitons in fibers [9]. The one-dimensional soliton can be considered as a localized wave pulse that propagates along one space direction undeformed; that is, dispersion is completely compensated by the nonlinear effects. There is an enormous amount of literature about the integrability of nonlinear equations related to scattering equations, including especially inverse scattering theories, in relation to solitons [10]. In particular, analysis related to NLS and KdV equations has been studied [10–12].

In recent years, various methods have been established to obtain exact traveling solutions of nonlinear partial differential equations, for example, the Jacobi elliptic function expansion method [13], the generalized Riccati equation method [14], the Backlund transformation method [15], the Hirota's bilinear transformation method [16], the variational iteration method [17–20], the tanh-coth method [21, 22], the direct algebraic method [23, 24], the Cole-Hopf transformation method [25, 26], the Exp-function method [27–29], and others [30]. Recently, Wang et al. [31] introduced a method to obtain traveling wave solutions of the nonlinear partial differential equations, called the (G'/G)- expansion method.

This paper is organized as follows. An introduction is given in Section 1. In Section 2, an analysis and theory of method theory of transformation the partial differential equations to a bilinear ordinary differential equations. In Section 3, the multiple travelling wave solutions of coupled Burgers' equations are obtained. Two cases of traveling wave solutions of the combined KdV-modified KdV equation are given in Section 4. In Section 5, multiple travelling wave solutions of the coupled Schrödinger-KdV equations are given.

2. An Analysis of the Method and Applications

Now, we simply describe the generalized extended tanh-function method. Consider a given system of NEEs, say, in two variables, x and t:

$$H\left(u, v, u_t, v_t, u_x, v_x, u_{xt}, v_{xt}, \ldots\right) = 0, \tag{1}$$

$$G\left(u, v, u_t, v_t, u_x, v_x, u_{xt}, v_{xt}, \ldots\right) = 0. \tag{2}$$

We consider the following formal traveling wave solutions $u(x,t) = U(\xi)$, $v(x,t) = V(\xi)$, and $\xi = x - ct$, where c is a constant to be determined later. Then, (1) and (2) become system of nonlinear ordinary differential equations as

$$H\left(U, V, U', V', U'', V'', \ldots\right) = 0, \tag{3}$$

$$G\left(U, V, U', V', U'', V'', \ldots\right) = 0. \tag{4}$$

In order to seek the traveling wave solutions of (3) and (4), we introduce the following new ansätz:

$$U(\xi) = a_{10} + \sum_{j=1}^{m_1} \left\{ a_{1j}\phi^j + b_{1j}\phi^{-j} + c_{1j}\phi^{j-1}\sqrt{b+\phi^2} + d_{1j}\frac{\sqrt{b+\phi^2}}{\phi^j} \right\}, \tag{5}$$

$$V(\xi) = a_{20} + \sum_{j=1}^{m_2} \left\{ a_{2j}\phi^j + b_{2j}\phi^{-j} + c_{2j}\phi^{j-1}\sqrt{b+\phi^2} + d_{2j}\frac{\sqrt{b+\phi^2}}{\phi^j} \right\}, \tag{6}$$

where $a_{i0}, a_{ij}, b_{ij}, c_{ij}, d_{ij}$ $(j = 1, 2, \ldots, m_i; i = 1, 2)$, and b are constants to be determined later. The value of m_i in (5) and (6) can be determined by balancing the highest-order derivative term with the nonlinear term in (5) and (6). The new variable $\phi = \phi(\xi)$ satisfies $\phi' = b + \phi^2$.

There exist the following steps to be considered further.

Step 1. Determine the m_1 and m_2 of (5) and (6) by, respectively, balancing the highest order partial differential terms and the nonlinear terms in (3) and (4).

Step 2. Substituting (5) and (6) into (3) and (4), the corresponding ODEs, then let all coefficients of $\phi^p(\sqrt{b+\phi^2})^q$ $(q = 0, 1;\ p = 0, 1, 2, \ldots)$ be zero to get an overdetermined system of nonlinear algebraic equations with respect to $a_{i0}, a_{ij}, b_{ij}, c_{ij}, d_{ij}, b, c$ $(j = 1, 2, \ldots, m_i;\ i = 1, 2)$.

Step 3. By solving the system, we may determine the above parameters.

Step 4. Substituting the parameters $a_{i0}, a_{ij}, b_{ij}, c_{ij}, d_{ij}, b, c$ $(j = 1, 2, \ldots, m_i;\ i = 1, 2)$ obtained in Step 3 into (2), we can derive the solutions of equation.

3. Example I

The coupled Burgers' equations [32] have applications in the quantum field theory, plasma physics, fluid mechanics, and solid state physics. The usual system of equation is as follows:

$$u_t - u_{xx} + 2uu_x + \alpha(uv)_x = 0, \tag{7}$$

$$v_t - v_{xx} + 2vv_x + \beta(uv)_x = 0. \tag{8}$$

Let us consider the traveling wave solutions $u(x,t) = U(\xi)$, $v(x,t) = V(\xi)$, and $\xi = x - ct$, and then (4) becomes

$$-cU - U' + U^2 + \alpha UV = 0, \tag{9}$$

$$-cV - V' + V^2 + \beta UV = 0. \tag{10}$$

Balancing the nonlinear term U^2 and the highest order derivative U' gives $m = 2$. We suppose the solutions of (5) and (6) are of the forms

$$U(\xi) = a_0 + a_1\varphi + a_2\varphi^{-1} + a_3\sqrt{b+\varphi^2} + a_4\frac{\sqrt{b+\varphi^2}}{\varphi}, \tag{11}$$

$$V(\xi) = b_0 + b_1\varphi + b_2\varphi^{-1} + b_3\sqrt{b+\varphi^2} + b_4\frac{\sqrt{b+\varphi^2}}{\varphi} + b_5\varphi^2 + b_6\varphi^{-2} + b_7\varphi\sqrt{b+\varphi^2} + b_8\frac{\sqrt{b+\varphi^2}}{\varphi^2}. \tag{12}$$

Substituting (11) and (12) into (9) and (10) with $\phi' = b + \phi^2$ yields a set of algebraic equations for a_0, a_1, a_2, a_3, a_4, b_0, b_1, b_2, b_3, b_4, b_5, b_6, b_7, b_8.

By the solution of the above system of equations, we can find

$$a_0 = \frac{2c}{\beta}, \quad a_1 = 0, \quad a_2 = \frac{2c^2}{\beta - 1}, \quad a_3 = -\frac{3c\sqrt{-b - 2c^2 - 2c^2\beta}}{\beta(b + 2c^2 + 2c^2\beta)}, \quad a_4 = 0, \tag{13}$$

$$b_0 = -2c, \quad b_1 = -1, \quad b_2 = \frac{2\beta^2c^2}{1-\beta}, \quad b_3 = \frac{3c\sqrt{-b - 2c^2 - 2c^2\beta}}{b + 2c^2 + 2c^2\beta}, \quad b_4 = \pm\sqrt{-b - 2c^2 - 2c^2\beta}, \quad b_5 = b_6 = b_7 = b_8 = 0. \tag{14}$$

Then, combining (11) and (12) with (13) and (14), we obtain the traveling wave solutions of (7) and (8) as

$$u(x,t) = \frac{2c}{\beta} + \frac{2c^2}{(\beta-1)\sqrt{b}}\cot\sqrt{b}(x+ct) - \frac{3c\sqrt{-b - 2c^2 - 2c^2\beta}}{\beta(b + 2c^2 + 2c^2\beta)}\sqrt{b}\sec\sqrt{b}(x+ct), \tag{15}$$

$$v(x,t) = -2c - \sqrt{b}\tan\sqrt{b}(x+ct) + \frac{2\beta^2c^2}{(1-\beta)\sqrt{b}}\cot\sqrt{b}(x+ct) + \frac{3c\sqrt{-b - 2c^2 - 2c^2\beta}}{b + 2c^2 + 2c^2\beta}\sqrt{b}\sec\sqrt{b}(x+ct) \pm \sqrt{-b - 2c^2 - 2c^2\beta}\csc\sqrt{b}(x+ct). \tag{16}$$

The shape solutions (15) and (16) are shown in Figures 1(a), 1(b), 1(c), and 1(d), with $\beta = -2$, $b = 2$, and $c = \pm 2$.

4. Example II

Consider the combined KdV-modified KdV equation:

$$u_t - \alpha u u_x + \beta u^2 u_x + \delta u_{xxx} = 0, \quad \beta \neq 0, \tag{17}$$

where α, β, and δ are constants. Let us consider the traveling wave solutions $u(x,t) = U(\xi)$ and $\xi = x + ct$, and then (17) becomes

$$cU + \frac{\alpha}{2}U^2 + \frac{\beta}{3}U^3 + U'' = 0. \tag{18}$$

We suppose the solution of (18) is of the form (11) and substituting into (18) yields a set of algebraic equations for a_0, a_1, a_2, a_3, a_4. We have two cases for these equations that are found.

Case 1. By the solution of (11), we can find

$$a_0 = -\frac{\alpha}{2\beta}, \quad a_1 = 0, \quad a_2 = \pm i\sqrt{\frac{3}{2\beta}}b, \quad a_3 = 0, \quad a_4 = \pm i\sqrt{\frac{3b}{2\beta}}. \tag{19}$$

Substituting (11) into (19) we have obtained the following solution of (17):

$$u(x,t) = -\frac{\alpha}{2\beta} \pm i\sqrt{\frac{3b}{2\beta}}\cot\left[\sqrt{b}(x+ct)\right] \pm i\sqrt{\frac{3b}{2\beta}}\csc\left[\sqrt{b}(x+ct)\right]. \tag{20}$$

Case 2. By the solution of (11), we can find

$$a_0 = -130, \quad a_1 = \pm 65\sqrt{\frac{2}{b}}, \quad a_2 = \pm 65\sqrt{2b}, \quad a_3 = a_4 = 0. \tag{21}$$

Substituting from (11) and (21) we have obtained the following solution of (17):

$$u(x,t) = -130 \pm 65\sqrt{2}\tan\left[\sqrt{b}(x+ct)\right] \pm 65\sqrt{2}\cot\left[\sqrt{b}(x+ct)\right]. \tag{22}$$

The shape solution (22) is shown in Figure 2(b), with $b = 2$ and $c = -16$.

5. Example III

Consider the coupled Schrödinger-KdV equations (Davey-Stewartson)

$$iu_t + u_{xx} - u_{yy} - 2|u|^2 u - 2uv = 0, \tag{23}$$

$$v_{xx} - v_{yy} - 2\left(|u|^2\right)_{xx} = 0. \tag{24}$$

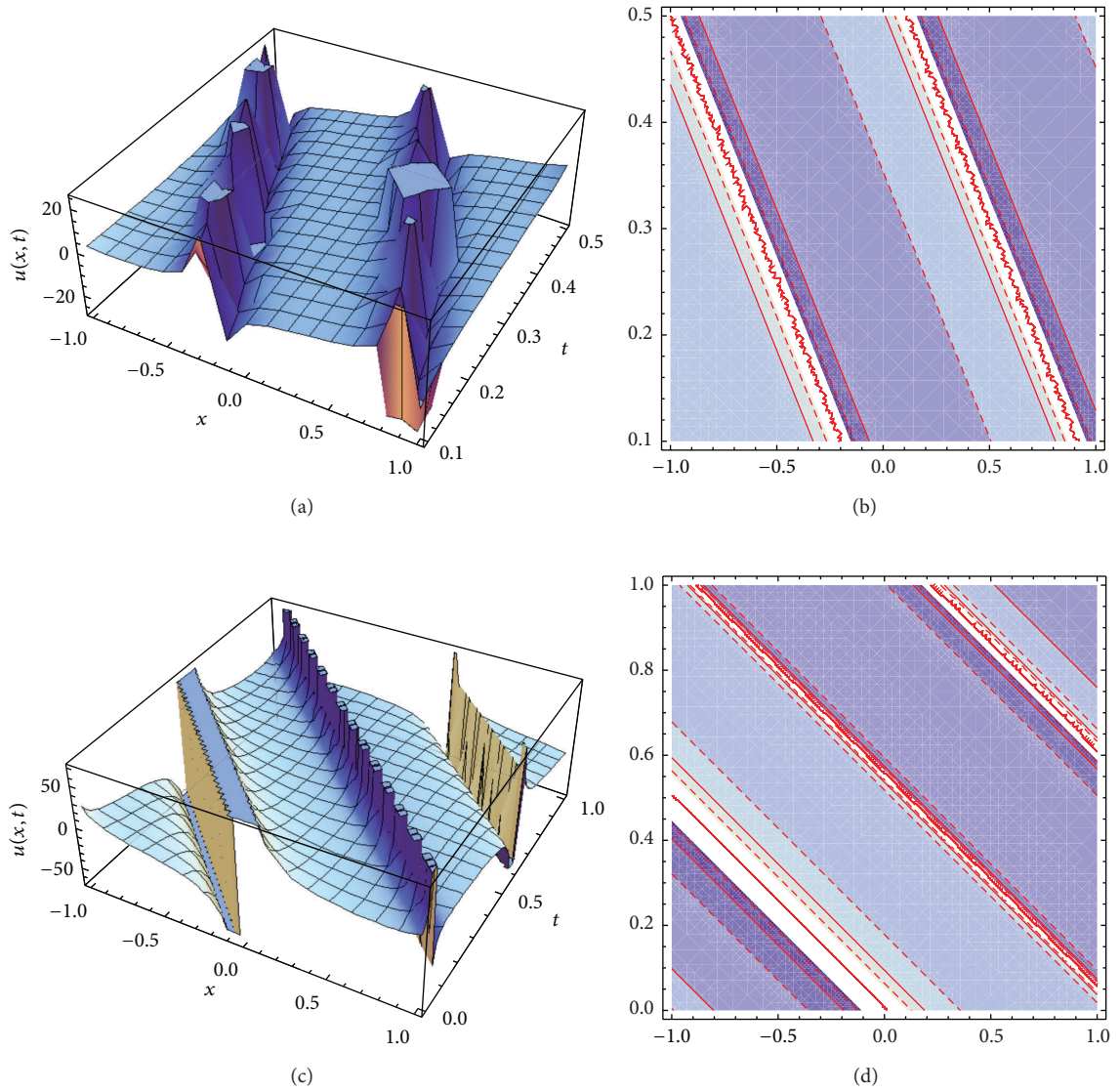

FIGURE 1: Travelling waves solutions (15) with various different shapes are plotted: periodic solitary waves in (a) and contour plot in (b). Travelling waves solutions (16) with various different shapes are plotted: periodic solitary waves in (c) and contour plot in (d).

Let us consider the traveling wave solutions $u(x,t) = U(\xi)$ and $\xi = (kx + cy + dt)/(x + y - dt)$, and then (23) and (24) become

$$\left(q^2 - p^2 - r\right)U + \left(k^2 - c^2\right)U'' + k^3 - 2U^{(3)} - 2UV = 0, \tag{25}$$

$$\left(k^2 + c^2\right)V'' + \left(U^2\right)'' = 0. \tag{26}$$

We suppose the solutions of (25) and (26) are of the forms (11) and (12). Substituting (11) and (12) into (25) and (26) yields a set of algebraic equations for $a_0, a_1, a_2, a_3, a_4, b_0, b_1, b_2, b_3, b_4, b_5, b_6, b_7, b_8$. The solution of the system of equations has two cases.

Case 1. Consider the following: $k^2 = 1/4$, $c^2 = 3/4$, and $b = 5/9$,

$$\begin{aligned} &a_0 = 0, \qquad a_1 = \pm\frac{10\sqrt{2}}{9}, \qquad a_2 = -1, \\ &a_3 = 2, \qquad a_4 = \frac{3}{2}, \\ &b_0 = \frac{1}{36}\left(-17 \pm 80\sqrt{2} - 18p^2 + 18q^2 - 18r\right), \\ &b_1 = -\frac{112}{27}, \qquad b_2 = -\frac{10}{3}, \end{aligned} \tag{27}$$

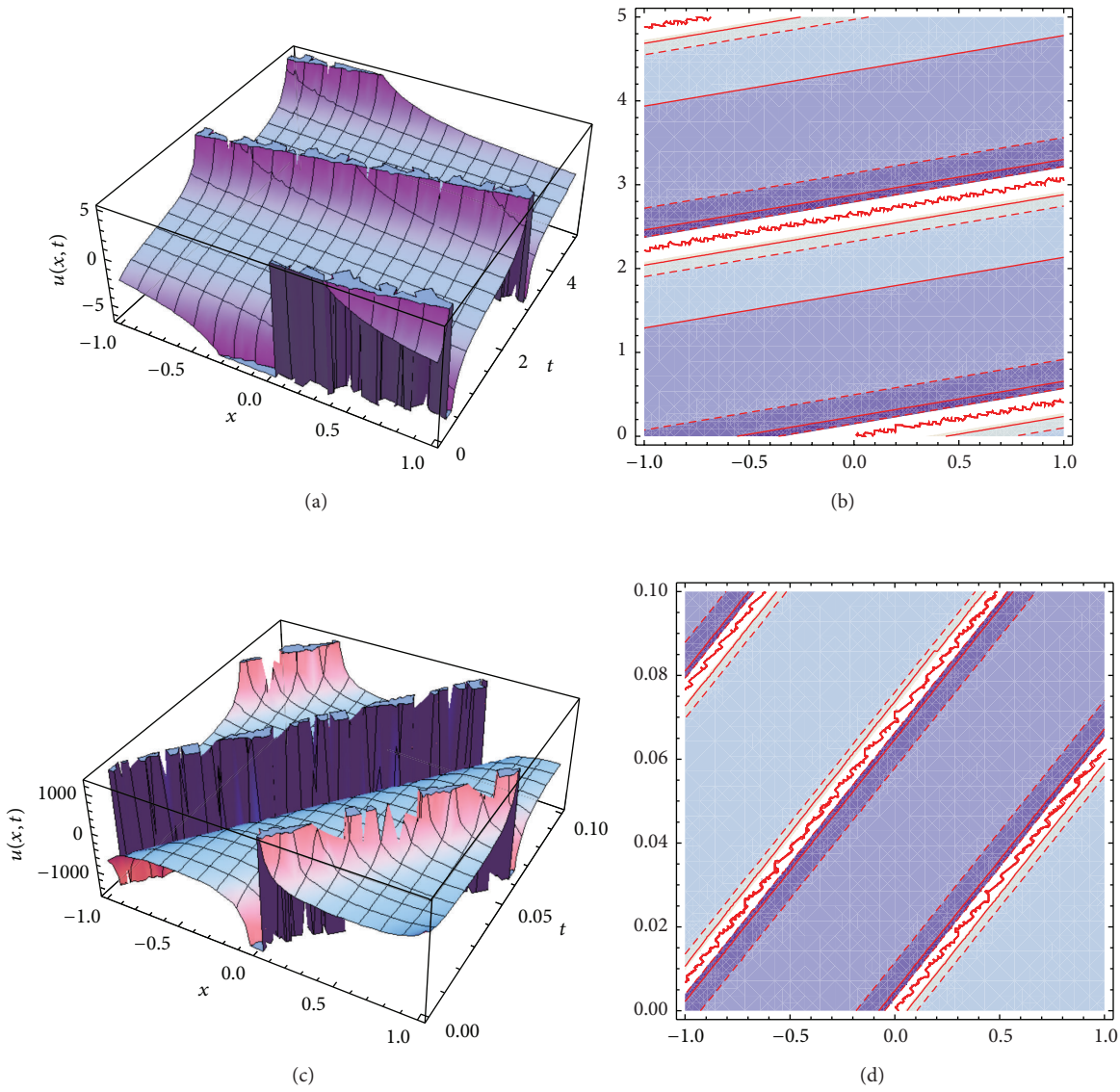

FIGURE 2: Travelling waves solutions (20) with various different shapes are plotted: periodic solitary waves in (a) and contour plot in (b). Travelling waves solutions (22) with various different shapes are plotted: periodic solitary waves in (c) and contour plot in (d).

$$b_3 = \mp\frac{10\sqrt{2}}{3}, \qquad b_4 = 4, \qquad b_5 = -16,$$
$$b_6 = -\frac{9}{4}, \qquad b_7 = \frac{20}{9}\left(1 \pm 2\sqrt{2}\right), \qquad b_8 = 3. \tag{28}$$

Substituting from (25), (26), (27), and (28), we have obtained the following solutions of (23) and (24):

$$u(x,t) = \pm\frac{10\sqrt{2b}}{9}\tan\xi - \frac{1}{\sqrt{b}}\cot\xi + 2\sqrt{b}\sec\xi + \frac{3}{2}\csc\xi, \tag{29}$$

$$\begin{aligned} v(x,t) &= \frac{1}{36}\left(-17 \pm 80\sqrt{2} - 18p^2 + 18q^2 - 18r\right) \\ &\quad - \frac{112\sqrt{b}}{27}\tan\xi - \frac{10}{3\sqrt{b}}\cot\xi \mp \frac{10\sqrt{2b}}{3}\sec\xi + 4\csc\xi \\ &\quad - 16b\tan^2\xi - \frac{9}{4b}\cot^2\xi + \frac{20b}{9}\left(1 \pm 2\sqrt{2}\right)\tan\xi\sec\xi \\ &\quad + \frac{3}{\sqrt{b}}\cot\xi\csc\xi, \end{aligned} \tag{30}$$

with $\xi = \sqrt{b}((x + \sqrt{3}y + \sqrt{4}t)/\sqrt{4}(x + y - t))$.

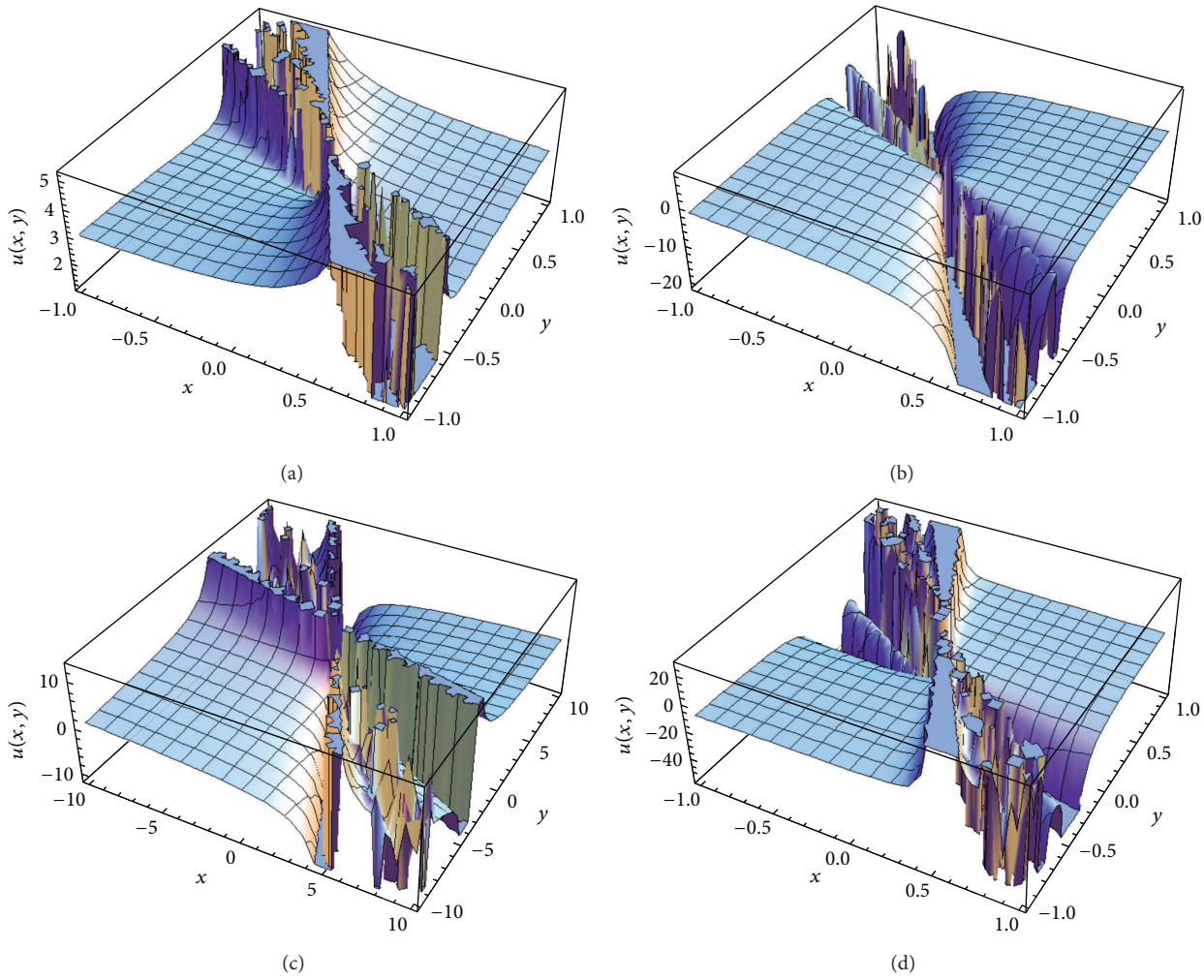

Figure 3: Travelling waves solutions (29) and (30) with various different shapes are plotted: multiple travelling wave solutions (a and b). Travelling waves solutions (33) and (34) with various different shapes are plotted: multiple travelling wave solutions (c and d).

Case 2. Consider the following: $k^2 = 1/9$, $c^2 = 8/9$, and $b = 1$,

$$a_0 = a_4 = 1, \qquad a_1 = a_3 = \mp\frac{\sqrt{14}}{3}, \qquad a_2 = \pm\frac{1}{3}\sqrt{\frac{7}{2}}, \tag{31}$$

$$b_0 = -2, \qquad b_1 = \pm 2\sqrt{\frac{14}{3}}, \qquad b_2 = \pm\frac{\sqrt{14}}{3},$$
$$b_3 = \mp\frac{8\sqrt{14}}{3}, \qquad b_4 = \frac{1}{54}\left(-10 + 9p^2 - 9q^2 + 9r\right),$$
$$b_5 = -\frac{14}{9}, \qquad b_6 = \frac{1}{108}\left(-36 + 9p^2 - 9q^2 + 9r\right), \tag{32}$$
$$b_7 = \frac{28}{9}, \qquad b_8 = \mp\frac{\sqrt{14}}{3}.$$

Substituting (31) and (32) into (25) and (26), we have obtained the following solutions of (23) and (24):

$$u(x,t) = 1 \mp \frac{\sqrt{14b}}{3}\tan\xi \pm \frac{1}{3}\sqrt{\frac{7}{2b}}\cot\xi \mp \frac{\sqrt{14b}}{3}\sec + \csc\xi, \tag{33}$$

$$\begin{aligned} v(x,t) = {} & -2 \pm 2\sqrt{\frac{14b}{3}}\tan\xi \pm \frac{\sqrt{14}}{3b}\cot\xi \mp \frac{8\sqrt{14b}}{3}\sec\xi \\ & + \frac{1}{54}\left(-10 + 9p^2 - 9q^2 + 9r\right)\csc\xi \\ & - \frac{14b}{9}\tan^2\xi \\ & + \frac{1}{108b}\left(-36 + 9p^2 - 9q^2 + 9r\right)\cot^2\xi \\ & + \frac{28b}{9}\tan\xi\sec\xi \mp \frac{\sqrt{14}}{3\sqrt{b}}\cot\xi\csc\xi, \end{aligned} \tag{34}$$

with $\xi = \sqrt{b}((x + \sqrt{8}y + \sqrt{9}t)/\sqrt{9}(x + y - t))$.

The shape solutions (29) and (30) are shown in Figures 3(a)and 3(b), with $p = q = r = 1$ and $t = 0.01$. The shape solutions (33) and (34) are shown in Figures 3(c)and 3(d), with $p = q = r = 1$ and $t = 0.01$.

Conflict of Interests

The authors declare that there is no conflict of interests regarding the publication of this paper.

References

[1] J. M. Burgers, "A mathematical model illustrating the theory of turbulence," in *Advances in Applied Mechanics*, pp. 171–199, Academic Press, New York, NY, USA, 1948.

[2] C. A. J. Fletcher, "Generating exact solutions of the two-dimensional Burgers' equations," *International Journal for Numerical Methods in Fluids*, vol. 3, no. 3, pp. 213–216, 1983.

[3] J. D. Cole, "On a quasi-linear parabolic equation occurring in aerodynamics," *Quarterly of Applied Mathematics*, vol. 9, pp. 225–236, 1951.

[4] P. J. Olver, *Applications of Lie Groups to Differential Equations*, vol. 107, Springer, New York, NY, USA, 1986.

[5] G. Bluman and S. Kumei, *Symmetries and Differenti al Equations*, Springer, New York, NY, USA, 1986.

[6] J. Zhang, F. Wu, and J. Shi, "Simple soliton solution method for the combined KdV and MKdV equation," *International Journal of Theoretical Physics*, vol. 39, no. 6, pp. 1697–1702, 2000.

[7] A. R. Seadawy, "New exact solutions for the KdV equation with higher order nonlinearity by using the variational method," *Computers & Mathematics with Applications*, vol. 62, no. 10, pp. 3741–3755, 2011.

[8] A. R. Seadawy, "Stability analysis for Zakharov-Kuznetsov equation of weakly nonlinear ion-acoustic waves in a plasma," *Computers & Mathematics with Applications*, vol. 67, no. 1, pp. 172–180, 2014.

[9] G. P. Agrawal, *Applications of Nonlinear Fiber Optics*, Elsevier, 2008.

[10] E. Infeld and G. Rowlands, *Nonlinear Waves, Solitons and Chaos*, Cambridge University Press, 2000.

[11] A. H. Khater, M. A. Helal, and A. R. Seadawy, "General soliton solutions of ndimensional nonlinear Schrödinger equation," *IL Nuovo Cimento B*, vol. 115, pp. 1303–1312, 2000.

[12] A. R. Seadawy, "Exact solutions of a two-dimensional nonlinear Schrödinger equation," *Applied Mathematics Letters*, vol. 25, no. 4, pp. 687–691, 2012.

[13] S. Liu, Z. Fu, S. Liu, and Q. Zhao, "Jacobi elliptic function expansion method and periodic wave solutions of nonlinear wave equations," *Physics Letters. A*, vol. 289, no. 1-2, pp. 69–74, 2001.

[14] Z. Yan and H. Zhang, "New explicit solitary wave solutions and periodic wave solutions for Whitham-Broer-Kaup equation in shallow water," *Physics Letters A*, vol. 285, no. 5-6, pp. 355–362, 2001.

[15] C. Rogers and W. F. Shadwick, *Backlund Transformations and Their Applications*, Academic Press, New York, NY, USA, 1982.

[16] R. Hirota, "Exact solution of the korteweg-de vries equation for multiple Collisions of solitons," *Physical Review Letters*, vol. 27, no. 18, pp. 1192–1194, 1971.

[17] J. H. He, "Variational iteration method for delay differential equations," *Communications in Nonlinear Science and Numerical Simulation*, vol. 2, no. 4, pp. 235–236, 1997.

[18] A. S. Arife and A. Yildirim, "New modified variational iteration transform method (MVITM) for solving eighth-order boundary value problems in one step," *World Applied Sciences Journal*, vol. 13, no. 10, pp. 2186–2190, 2011.

[19] M. A. Helal and A. R. Seadawy, "Variational method for the derivative nonlinear Schrödinger equation with computational applications," *Physica Scripta*, vol. 80, no. 3, Article ID 035004, pp. 350–360, 2009.

[20] S. T. Mohyud-Din, "Modified variational iteration method for integro-differential equations and coupled systems," *Zeitschrift für Naturforschung A*, vol. 65, no. 4, pp. 277–284, 2010.

[21] W. Malfliet, "Solitary wave solutions of nonlinear wave equations," *The American Journal of Physics*, vol. 60, no. 7, pp. 650–654, 1992.

[22] A. Bekir and A. C. Cevikel, "Solitary wave solutions of two nonlinear physical models by tanh-coth method," *Communications in Nonlinear Science and Numerical Simulation*, vol. 14, no. 5, pp. 1804–1809, 2009.

[23] A. R. Seadawy and K. El-Rashidy, "Traveling wave solutions for some coupled nonlinear evolution equations," *Mathematical and Computer Modelling*, vol. 57, no. 5-6, pp. 1371–1379, 2013.

[24] A. R. Seadawy, "Traveling wave solutions of the Boussinesq and generalized fifth order KdV equations by using the direct algebraic method," *Applied Mathematical Sciences*, vol. 6, pp. 4081–4090, 2012.

[25] A. H. Salas and C. A. Gomez, "Application of the Cole-Hopf transformation for finding exact solutions to several forms of the seventh-order KdV equation," *Mathematical Problems in Engineering*, vol. 2010, Article ID 194329, 14 pages, 2010.

[26] W. X. Ma and B. Fuchssteiner, "Explicit and exact solutions to a Kolmogorov-Petrovskii-PISkunov equation," *International Journal of Non-Linear Mechanics*, vol. 31, no. 3, pp. 329–338, 1996.

[27] H. Naher, F. A. Abdullah, and M. A. Akbar, "The exp-function method for new exact solutions of the nonlinear partial differential equations," *International Journal of Physical Sciences*, vol. 6, no. 29, pp. 6706–6716, 2011.

[28] I. Aslan and V. Marinakis, "Some remarks on exp-function method and its applications," *Communications in Theoretical Physics*, vol. 56, no. 3, pp. 397–403, 2011.

[29] A. Yıldırım and Z. Pınar, "Application of the exp-function method for solving nonlinear reaction-diffusion equations arising in mathematical biology," *Computers & Mathematics with Applications*, vol. 60, no. 7, pp. 1873–1880, 2010.

[30] A.-M. Wazwaz, "A new (2+1)-dimensional Korteweg-de Vries equation and its extension to a new (3+1)-dimensional Kadomtsev-Petviashvili equation," *Physica Scripta*, vol. 84, no. 3, Article ID 035010, 2011.

[31] M. Wang, X. Li, and J. Zhang, "The (G'/G)-expansion method and travelling wave solutions of nonlinear evolution equations in mathematical physics," *Physics Letters A*, vol. 372, no. 4, pp. 417–423, 2008.

[32] D. Kaya, "An explicit solution of coupled viscous Burgers' equation by the decomposition method," *International Journal of Mathematics and Mathematical Sciences*, vol. 27, no. 11, pp. 675–680, 2001.

Hindawi Publishing Corporation
Abstract and Applied Analysis
Volume 2015, Article ID 946350, 8 pages
http://dx.doi.org/10.1155/2015/946350

Research Article

Exact Solutions for Unsteady Free Convection Flow of Casson Fluid over an Oscillating Vertical Plate with Constant Wall Temperature

Asma Khalid,[1,2] Ilyas Khan,[3] and Sharidan Shafie[1]

[1]*Department of Mathematical Sciences, Faculty of Science, Universiti Teknologi Malaysia (UTM), 81310 Skudai, Malaysia*
[2]*Department of Mathematics, SBK Women's University, Quetta 87300, Pakistan*
[3]*College of Engineering, Majmaah University, Majmaah 11952, Saudi Arabia*

Correspondence should be addressed to Sharidan Shafie; sharidan@utm.my

Received 17 July 2014; Accepted 23 October 2014

Academic Editor: Yasir Khan

Copyright © 2015 Asma Khalid et al. This is an open access article distributed under the Creative Commons Attribution License, which permits unrestricted use, distribution, and reproduction in any medium, provided the original work is properly cited.

The unsteady free flow of a Casson fluid past an oscillating vertical plate with constant wall temperature has been studied. The Casson fluid model is used to distinguish the non-Newtonian fluid behaviour. The governing partial differential equations corresponding to the momentum and energy equations are transformed into linear ordinary differential equations by using nondimensional variables. Laplace transform method is used to find the exact solutions of these equations. Expressions for shear stress in terms of skin friction and the rate of heat transfer in terms of Nusselt number are also obtained. Numerical results of velocity and temperature profiles with various values of embedded flow parameters are shown graphically and their effects are discussed in detail.

1. Introduction

Newtonian fluids described by Navier-Stokes equations are extensively studied in the literature for the past few decades. Largely, this is due to the fact that they are relatively simple and their solutions are convenient [1–10]. However, Newtonian fluids which have a linear relationship between the stress and the rate of strain are limited in view of their applications. They do not explain several phenomena observed for the fluids in industry and other technological applications. For example, many complex fluids such as blood, soap, clay coating, certain oils and greases, elastomers, suspensions, and many emulsions are noteworthy due to their various applications in industry. Unfortunately, Navier-Stokes equations are no more convincing to describe such fluids. In the literature, they are known as non-Newtonian fluids. These fluids are described by a nonlinear relationship between the stress and the rate of strain. The understanding of flow characteristics of non-Newtonian fluids is very important because they play a significant role in industry and engineering. Such interest is motivated because of extensive applications in diverse areas of biorheology, geophysics, and chemical and petroleum industries [11, 12]. In view of these particular applications, the study and understanding of non-Newtonian fluids have now become an increasingly appealing topic of current research in this field.

Rheological properties of non-Newtonian fluids are described by their so-called constitutive equations. Due to complexity of fluids, several non-Newtonian fluid models/constitutive equations based on their empirical observations have been proposed. Amongst the different non-Newtonian fluids there is one known as Casson fluid which was originally introduced by Casson for the prediction of the flow behavior of pigment-oil suspensions [13]. The Casson model is based on a structure model of the interactive behavior of solid and liquid phases of a two-phase suspension. Casson fluid exhibits yield stress. It is a shear thinning liquid which has an infinite viscosity at zero rates of shear, a yield stress below which no flow occurs, and a zero viscosity at an infinite rate of shear [14]. More exactly, if a shear stress less than the yield stress is applied to the fluid, it behaves like a solid, whereas if a shear stress greater than yield

stress is applied, it starts to move. Some famous examples of Casson fluid include jelly, tomato sauce, honey, soup, and concentrated fruit juices. Human blood can also be treated as Casson fluid due to the presence of several substances such as protein, fibrinogen, and globulin in aqueous base plasma and human red blood cells [15, 16].

In the earlier studies on Casson fluid, Fredrickson [17] investigated its steady flow in a tube whereas Boyd et al. [18] described the steady and oscillatory flow of blood flow by taking into account Casson fluid. Mernone et al. [19] discussed the peristaltic flow of a Casson fluid in a two-dimensional channel. Mustafa et al. [20] studied the unsteady boundary layer flow and heat transfer of a Casson fluid over a moving flat plate with a parallel free stream using homotopy analysis method (HAM). Mixed convection stagnation-point flow of Casson fluid with convective boundary conditions is examined by Hayat et al. [21]. Mukhopadhyay [22] described the effects of thermal radiation on Casson fluid flow and heat transfer over an unsteady stretching surface subjected to suction/blowing. Mukhopadhyay et al. [23] also analyzed the Casson fluid flow over an unsteady stretching surface. Bhattacharyya [24] investigated the boundary layer stagnation-point flow of Casson fluid and heat transfer towards a shrinking/stretching sheet and Pramanik [25] studied the Casson fluid flow and heat transfer past an exponentially porous stretching surface in presence of thermal radiation.

In all of the above studies the solutions of Casson fluid are obtained by using either approximate method or any numerical scheme. There are very few cases in which the exact analytical solutions of Casson fluid are obtained. These solutions are even rare when Casson fluid in free convection flow with constant wall temperature is considered. On the other hand, the flow of Casson fluids (such as drilling muds, clay coatings and other suspensions, certain oils and greases, polymer melts, blood, and many emulsions), in the presence of heat transfer, is an important research area due to its relevance to the optimized processing of chocolate, toffee, and other foodstuffs [26].

Motivated by the above investigations, the present analysis is focused on the study of unsteady boundary layer flow of a Casson fluid past an oscillating vertical plate with constant wall temperature. Exact solutions are obtained by using the Laplace transform technique. Analytical as well as numerical results for skin friction and Nusselt number are provided. Graphical results are presented and discussed for various physical parameters. Exact solutions obtained in this paper are important; not only do they correspond to some fundamental flow situations, but also they are useful for explaining the flow physics in detail as well as for being used as a benchmark for validation of other solutions obtained via approximate or numerical schemes.

2. Formulation of the Problem

Let us consider the effect of heat transfer on unsteady boundary layer flow of an incompressible Casson fluid past an infinite vertical flat plate situated at the flow being confined to $y > 0$, where y is the coordinate measured in the normal direction to the surface. It is assumed that, at the initial moment $t = 0$, both the plate and fluid are at rest with constant temperature T_∞. At time $t = 0^+$ the plate begins to oscillate in its plane ($y = 0$) according to

$$\mathbf{V} = UH(t)\cos(\omega t)\,\mathbf{i}; \quad \text{or} \quad \mathbf{V} = U\sin(\omega t)\,\mathbf{i}; \quad t > 0, \tag{1}$$

where the constant U is the amplitude of the plate oscillations, $H(t)$ is the unit step function, $\mathbf{i}$ is the unit vector in the vertical flow direction, and ω is the frequency of oscillation of the plate. At the same time, the plate temperature is raised to T_w which is thereafter maintained constant (Figure 1).

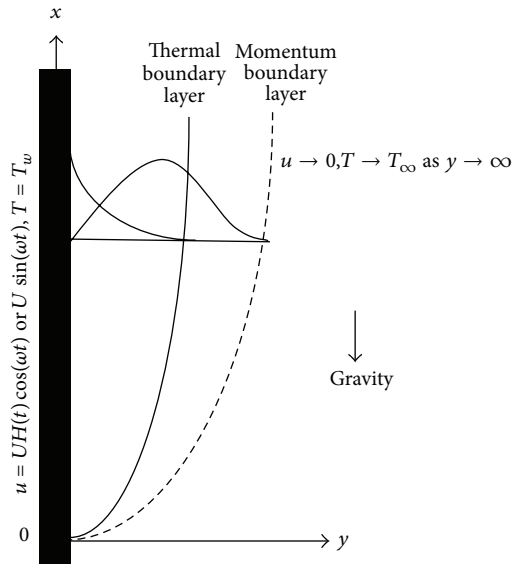

Figure 1: Physical model and coordinate system.

We assume that the rheological equation of state for an isotropic and incompressible flow of a Casson fluid can be written as (see the study by Mukhopadhyay [22])

$$\tau = \tau_0 + \mu\dot{\gamma}, \tag{2}$$

or

$$\tau_{ij} = \begin{cases} 2\left(\mu_B + \dfrac{p_y}{\sqrt{2\pi}}\right)e_{ij}, & \pi > \pi_c \\ 2\left(\mu_B + \dfrac{p_y}{\sqrt{2\pi_c}}\right)e_{ij}, & \pi < \pi_c, \end{cases} \tag{3}$$

where $\pi = e_{ij}e_{ij}$ and e_{ij} is the $(i, j)^{ih}$ component of the deformation rate, π is the product of the component of deformation rate with itself, π_c is a critical value of this product based on the non-Newtonian model, μ_B is plastic dynamic viscosity of the non-Newtonian fluid, and p_y is yield stress of fluid. Under these conditions along with the assumption that the viscous dissipation term in the energy equation is neglected, we get the following set of partial differential equations:

$$\rho\frac{\partial u}{\partial t} = \mu_B\left(1 + \frac{1}{\gamma}\right)\frac{\partial^2 u}{\partial y^2} + \rho g\beta\left(T - T_\infty\right),$$
$$\rho c_p\frac{\partial T}{\partial t} = k\frac{\partial^2 T}{\partial y^2}, \tag{4}$$

together with initial and boundary conditions

$$\begin{gathered} t<0: u=0, \quad T=T_{\infty} \quad \forall y>0, \\ t \geq 0: u=UH(t)\cos(\omega t) \quad \text{or} \quad u=U\sin(\omega t), \\ T=T_{w} \quad \text{at } y=0, \\ u \longrightarrow 0, \qquad T \longrightarrow T_{\infty} \quad \text{as } y \longrightarrow \infty. \end{gathered} \tag{5}$$

We introduce the dimensionless variables

$$\begin{gathered} u^{*}=\frac{u}{U}, \qquad y^{*}=\frac{U}{\nu}y, \qquad t^{*}=\frac{U^{2}}{\nu}t, \\ \theta=\frac{T-T_{\infty}}{T_{w}-T_{\infty}}, \qquad \omega^{*}=\frac{\omega\nu}{U^{2}}, \qquad \tau^{*}=\frac{\tau}{\rho u^{2}} \end{gathered} \tag{6}$$

into (4)-(5), and we get ($*$ symbols are dropped for simplicity)

$$\frac{\partial u}{\partial t}=\left(1+\frac{1}{\gamma}\right)\frac{\partial^{2}u}{\partial y^{2}}+\mathrm{Gr}\theta, \tag{7}$$

$$\mathrm{Pr}\,\frac{\partial \theta}{\partial t}=\frac{\partial^{2}\theta}{\partial y^{2}}, \tag{8}$$

with associated initial and boundary conditions

$$\begin{gathered} t<0: u=0, \qquad \theta=0 \quad \forall y>0, \\ t \geq 0: u=H(t)\cos(\omega t) \quad \text{or} \quad u=\sin(\omega t), \\ \theta=1 \quad \text{at } y=0, \\ u \longrightarrow 0, \qquad \theta \longrightarrow 0 \quad \text{as } y \longrightarrow \infty, \end{gathered} \tag{9}$$

where

$$\mathrm{Pr}=\frac{\mu c_{p}}{k}, \qquad \mathrm{Gr}=\frac{\nu g\beta\left(T_{w}-T_{\infty}\right)}{U^{3}}, \qquad \gamma=\frac{\mu_{B}\sqrt{2\pi_{c}}}{p_{y}} \tag{10}$$

are the Prandtl, Grashof numbers, and the Casson parameter.

3. Solution of the Problem

Applying Laplace transforms to (7) and (8), using initial and boundary conditions (9), we get the following solutions in the transformed (y,q) plane:

$$\overline{\theta}(y,q)=\frac{1}{q}e^{-y\sqrt{\mathrm{Pr}\,q}}, \tag{11}$$

$$\overline{u}(y,q)=\frac{q}{q^{2}+\omega^{2}}e^{-y\sqrt{aq}}+\frac{b}{q^{2}}e^{-y\sqrt{aq}}+\frac{b}{q^{2}}e^{-y\sqrt{\mathrm{Pr}\,q}}. \tag{12}$$

The inverse Laplace transforms of (11) and (12) are obtained as follows:

$$\theta(y,t)=\operatorname{erfc}\left(\frac{y}{2}\sqrt{\frac{\mathrm{Pr}}{t}}\right), \tag{13}$$

$$\begin{aligned} u_{c}(y,t) &= \frac{H(t)}{4}e^{-i\omega t}\left[e^{-y\sqrt{-i\omega a}}\operatorname{erfc}\left(\frac{y}{2}\sqrt{\frac{a}{t}}-\sqrt{-i\omega t}\right)\right. \\ &\quad \left.+e^{y\sqrt{-i\omega a}}\operatorname{erfc}\left(\frac{y}{2}\sqrt{\frac{a}{t}}+\sqrt{-i\omega t}\right)\right] \\ &\quad +\frac{H(t)}{4}e^{i\omega t}\left[e^{-y\sqrt{i\omega a}}\operatorname{erfc}\left(\frac{y}{2}\sqrt{\frac{a}{t}}-\sqrt{i\omega t}\right)\right. \\ &\quad \left.+e^{y\sqrt{i\omega a}}\operatorname{erfc}\left(\frac{y}{2}\sqrt{\frac{a}{t}}+\sqrt{+i\omega t}\right)\right] \\ &\quad +b\left[\left(t+\frac{ay^{2}}{2}\right)\operatorname{erfc}\left(\frac{y}{2}\sqrt{\frac{a}{t}}\right)-y\sqrt{a}\sqrt{\frac{t}{\pi}}e^{-ay^{2}/4t}\right] \\ &\quad -b\left[\left(t+\frac{\mathrm{Pr}\,y^{2}}{2}\right)\operatorname{erfc}\left(\frac{y}{2}\sqrt{\frac{\mathrm{Pr}}{t}}\right)\right. \\ &\quad \left.-y\sqrt{\mathrm{Pr}}\sqrt{\frac{t}{\pi}}e^{-\mathrm{Pr}\,y^{2}/4t}\right]. \end{aligned} \tag{14}$$

The subscript "c" on the left side of (14) stands for the cosine oscillations of the plate. Similarly, the velocity corresponding to the sine oscillations of the plate is given by

$$\begin{aligned} u_{s}(y,t) &= -\frac{1}{4i}e^{-i\omega t} \\ &\quad \times\left[e^{-y\sqrt{-i\omega a}}\operatorname{erfc}\left(\frac{y}{2}\sqrt{\frac{a}{t}}-\sqrt{-i\omega t}\right)\right. \\ &\quad \left.+e^{y\sqrt{-i\omega a}}\operatorname{erfc}\left(\frac{y}{2}\sqrt{\frac{a}{t}}+\sqrt{-i\omega t}\right)\right] \\ &\quad +\frac{1}{4i}e^{i\omega t}\left[e^{-y\sqrt{i\omega a}}\operatorname{erfc}\left(\frac{y}{2}\sqrt{\frac{a}{t}}-\sqrt{i\omega t}\right)\right. \\ &\quad \left.+e^{y\sqrt{i\omega a}}\operatorname{erfc}\left(\frac{y}{2}\sqrt{\frac{a}{t}}+\sqrt{+i\omega t}\right)\right] \\ &\quad +b\left[\left(t+\frac{ay^{2}}{2}\right)\operatorname{erfc}\left(\frac{y}{2}\sqrt{\frac{a}{t}}\right)-y\sqrt{a}\sqrt{\frac{t}{\pi}}e^{-ay^{2}/4t}\right] \\ &\quad -b\left[\left(t+\frac{\mathrm{Pr}\,y^{2}}{2}\right)\operatorname{erfc}\left(\frac{y}{2}\sqrt{\frac{\mathrm{Pr}}{t}}\right)\right. \\ &\quad \left.-y\sqrt{\mathrm{Pr}}\sqrt{\frac{t}{\pi}}e^{-\mathrm{Pr}\,y^{2}/4t}\right], \end{aligned} \tag{15}$$

where

$$a = \frac{\gamma}{1+\gamma}, \qquad b = \frac{a\mathrm{Gr}}{\mathrm{Pr}-1}. \tag{16}$$

Note that the above solutions for velocity are only valid for $\mathrm{Pr} \neq 1$. Moreover the solution for $\mathrm{Pr} = 1$ can be easily obtained by putting $\mathrm{Pr} = 1$ into (8) and can follow a similar procedure as discussed above. The obtained solutions for cosine and sine oscillations of the plate when $\mathrm{Pr} = 1$ are

$$\begin{aligned} u_c(y,t) &= \frac{H(t)}{4} e^{-i\omega t} \\ &\times \left[e^{-y\sqrt{-i\omega a}}\, \mathrm{erf}\, c\left(\frac{y}{2}\sqrt{\frac{a}{t}} - \sqrt{-i\omega t}\right) \right. \\ &\left. + e^{y\sqrt{-i\omega a}}\, \mathrm{erf}\, c\left(\frac{y}{2}\sqrt{\frac{a}{t}} + \sqrt{-i\omega t}\right)\right] \\ &+ \frac{H(t)}{4} e^{i\omega t} \left[e^{-y\sqrt{i\omega a}}\, \mathrm{erf}\, c\left(\frac{y}{2}\sqrt{\frac{a}{t}} - \sqrt{i\omega t}\right) \right. \\ &\left. + e^{y\sqrt{i\omega a}}\, \mathrm{erf}\, c\left(\frac{y}{2}\sqrt{\frac{a}{t}} + \sqrt{+i\omega t}\right)\right] \\ &+ \frac{a\mathrm{Gr}\, y}{2}\left[2\sqrt{\frac{t}{\pi}} e^{-y^2/4t} - y\, \mathrm{erf}\, c\left(\frac{y}{2\sqrt{t}}\right)\right], \end{aligned} \tag{17}$$

$$\begin{aligned} u_s(y,t) &= -\frac{1}{4i} e^{-i\omega t} \\ &\times \left[e^{-y\sqrt{-i\omega a}}\, \mathrm{erf}\, c\left(\frac{y}{2}\sqrt{\frac{a}{t}} - \sqrt{-i\omega t}\right) \right. \\ &\left. + e^{y\sqrt{-i\omega a}}\, \mathrm{erf}\, c\left(\frac{y}{2}\sqrt{\frac{a}{t}} + \sqrt{-i\omega t}\right)\right] \\ &+ \frac{1}{4i} e^{i\omega t} \left[e^{-y\sqrt{i\omega a}}\, \mathrm{erf}\, c\left(\frac{y}{2}\sqrt{\frac{a}{t}} - \sqrt{i\omega t}\right) \right. \\ &\left. + e^{y\sqrt{i\omega a}}\, \mathrm{erf}\, c\left(\frac{y}{2}\sqrt{\frac{a}{t}} + \sqrt{+i\omega t}\right)\right] \\ &+ \frac{a\mathrm{Gr}\, y}{2}\left[2\sqrt{\frac{t}{\pi}} e^{-y^2/4t} - y\, \mathrm{erf}\, c\left(\frac{y}{2\sqrt{t}}\right)\right]. \end{aligned} \tag{18}$$

Note that, in (14) and (15), the first two terms in each equation account for the contribution from mechanical parts while the last two terms show the thermal effects. On the other hand in (17) and (18), the last term in each equation shows the contribution from the thermal part.

The nondimensional skin friction is calculated from the velocity field (14), using the relation

$$\tau = -\mu\left(1 + \frac{1}{\gamma}\right)\left.\frac{\partial u}{\partial y}\right|_{y=0},$$

$$\begin{aligned} \tau &= \frac{1}{2a\sqrt{\pi}} \\ &\times \left[e^{-it\omega} \left[2e^{it\omega} \left\{ H\sqrt{\frac{a}{t}} + \sqrt{ab}\sqrt{t} - ab\sqrt{\mathrm{Pr}}\sqrt{t} \right. \right. \right. \\ &\left. + b\sqrt{\frac{a}{t}}t + ab\sqrt{\frac{\mathrm{Pr}}{t}}t \right\} \\ &+ H\sqrt{\pi}\left\{\sqrt{-ia\omega}\, \mathrm{erf}\left(\sqrt{-it\omega}\right) \right. \\ &\left. \left. \left. + e^{2it\omega}\sqrt{ia\omega}\, \mathrm{erf}\left(\sqrt{it\omega}\right)\right\}\right]\right]. \end{aligned} \tag{19}$$

The expression of Nusselt number is given by

$$\mathrm{Nu} = -\frac{\nu}{U_0(T - T_\infty)}\left.\frac{\partial T^*}{\partial y^*}\right|_{y^*=0} = \sqrt{\frac{\mathrm{Pr}}{\pi t}}. \tag{20}$$

4. Limiting Cases

The following solutions from the literature appear as the limiting cases of our general solutions.

(i) By taking $\gamma \to \infty$ into (14) and (15), the corresponding solutions for viscous fluid can be obtained as a special case:

$$\begin{aligned} u_c(y,t) &= \frac{H(t)}{4} e^{-i\omega t} \\ &\times \left[e^{-y\sqrt{-i\omega}}\, \mathrm{erf}\, c\left(\frac{y}{2}\sqrt{\frac{1}{t}} - \sqrt{-i\omega t}\right) \right. \\ &\left. + e^{y\sqrt{-i\omega}}\, \mathrm{erf}\, c\left(\frac{y}{2}\sqrt{\frac{1}{t}} + \sqrt{-i\omega t}\right)\right] \\ &+ \frac{H(t)}{4} e^{i\omega t} \left[e^{-y\sqrt{i\omega}}\, \mathrm{erf}\, c\left(\frac{y}{2}\sqrt{\frac{1}{t}} - \sqrt{i\omega t}\right) \right. \\ &\left. + e^{y\sqrt{i\omega}}\, \mathrm{erf}\, c\left(\frac{y}{2}\sqrt{\frac{1}{t}} + \sqrt{+i\omega t}\right)\right] \\ &+ b\left[\left(t + \frac{y^2}{2}\right)\mathrm{erf}\, c\left(\frac{y}{2}\sqrt{\frac{1}{t}}\right) - y\sqrt{\frac{t}{\pi}} e^{-y^2/4t}\right] \\ &+ b\left[\left(t + \frac{\mathrm{Pr}\, y^2}{2}\right)\mathrm{erf}\, c\left(\frac{y}{2}\sqrt{\frac{\mathrm{Pr}}{t}}\right) \right. \\ &\left. - y\sqrt{\mathrm{Pr}}\sqrt{\frac{t}{\pi}} e^{-\mathrm{Pr}\, y^2/4t}\right], \end{aligned}$$

$$
\begin{aligned}
&u_s(y,t)\\
&= -\frac{1}{4i}e^{-i\omega t}\\
&\quad\times\left[e^{-y\sqrt{-i\omega}}\,\mathrm{erfc}\left(\frac{y}{2}\sqrt{\frac{1}{t}}-\sqrt{-i\omega t}\right)\right.\\
&\qquad\left.+e^{y\sqrt{-i\omega}}\,\mathrm{erfc}\left(\frac{y}{2}\sqrt{\frac{1}{t}}+\sqrt{-i\omega t}\right)\right]\\
&\quad+\frac{1}{4i}e^{i\omega t}\left[e^{-y\sqrt{i\omega}}\,\mathrm{erfc}\left(\frac{y}{2}\sqrt{\frac{1}{t}}-\sqrt{i\omega t}\right)\right.\\
&\qquad\left.+e^{y\sqrt{i\omega}}\,\mathrm{erfc}\left(\frac{y}{2}\sqrt{\frac{1}{t}}+\sqrt{+i\omega t}\right)\right]\\
&\quad+b\left[\left(t+\frac{y^2}{2}\right)\mathrm{erfc}\left(\frac{y}{2}\sqrt{\frac{1}{t}}\right)-y\sqrt{\frac{t}{\pi}}e^{-y^2/4t}\right]\\
&\quad+b\left[\left(t+\frac{\mathrm{Pr}\,y^2}{2}\right)\mathrm{erfc}\left(\frac{y}{2}\sqrt{\frac{\mathrm{Pr}}{t}}\right)\right.\\
&\qquad\left.-y\sqrt{\mathrm{Pr}}\sqrt{\frac{t}{\pi}}e^{-\mathrm{Pr}\,y^2/4t}\right].
\end{aligned}
\tag{21}
$$

(ii) By taking $\omega = 0$, which corresponds to impulsive motion of the plate, then (14) and (17) yield

$$
\begin{aligned}
&u_c(y,t)\\
&= H(t)\left[\mathrm{erfc}\left(\frac{y}{2}\sqrt{\frac{a}{t}}\right)\right]\\
&\quad+ab\left[\left(t+\frac{ay^2}{2}\right)\mathrm{erfc}\left(\frac{y}{2}\sqrt{\frac{a}{t}}\right)-y\sqrt{a}\sqrt{\frac{t}{\pi}}e^{-ay^2/4t}\right]\\
&\quad+ab\left[\left(t+\frac{\mathrm{Pr}\,y^2}{2}\right)\mathrm{erfc}\left(\frac{y}{2}\sqrt{\frac{\mathrm{Pr}}{t}}\right)\right.\\
&\qquad\left.-y\sqrt{\mathrm{Pr}}\sqrt{\frac{t}{\pi}}e^{-\mathrm{Pr}\,y^2/4t}\right];\quad \mathrm{Pr}\neq 1,
\end{aligned}
\tag{22}
$$

$$
\begin{aligned}
&u_c(y,t)\\
&= H(t)\left[\mathrm{erfc}\left(\frac{1}{2}\sqrt{\frac{a1}{t}}y\right)\right]\\
&\quad+\frac{a\mathrm{Gr}\,y}{2}\left[2\sqrt{\frac{t}{\pi}}e^{-y^2/4t}-y\,\mathrm{erfc}\left(\frac{y}{2\sqrt{t}}\right)\right];\quad \mathrm{Pr}=1,
\end{aligned}
\tag{23}
$$

respectively, and (22) and (23) describe the corresponding solution of Stokes' first problem for Casson fluid. It is important to note that exact solutions of Stokes' first problem for Casson fluid (22) and (23) are also not reported in the literature and hence are new.

(iii) In this last case, we assume that the flow is induced only due to bounding plate and the corresponding buoyancy forces are zero equivalently; it shows the absence of free convection ($\mathrm{Gr} = 0$) due to the differences in temperature gradient. This shows that the thermal parts of velocities in (14) and (15) are zero. Hence the flow is only governed by the corresponding mechanical parts given by

$$
\begin{aligned}
&u_c(y,t)\\
&= \frac{H(t)}{4}e^{-i\omega t}\left[e^{-y\sqrt{-i\omega a}}\,\mathrm{erfc}\left(\frac{y}{2}\sqrt{\frac{a}{t}}-\sqrt{-i\omega t}\right)\right.\\
&\qquad\left.+e^{y\sqrt{-i\omega a}}\,\mathrm{erfc}\left(\frac{y}{2}\sqrt{\frac{a}{t}}+\sqrt{-i\omega t}\right)\right]\\
&\quad+\frac{H(t)}{4}e^{i\omega t}\left[e^{-y\sqrt{i\omega a}}\,\mathrm{erfc}\left(\frac{y}{2}\sqrt{\frac{a}{t}}-\sqrt{i\omega t}\right)\right.\\
&\qquad\left.+e^{y\sqrt{i\omega a}}\,\mathrm{erfc}\left(\frac{y}{2}\sqrt{\frac{a}{t}}+\sqrt{+i\omega t}\right)\right],\\
&u_s(y,t)\\
&= -\frac{1}{4i}e^{-i\omega t}\left[e^{-y\sqrt{-i\omega a}}\,\mathrm{erfc}\left(\frac{y}{2}\sqrt{\frac{a}{t}}-\sqrt{-i\omega t}\right)\right.\\
&\qquad\left.+e^{y\sqrt{-i\omega a}}\,\mathrm{erfc}\left(\frac{y}{2}\sqrt{\frac{a}{t}}+\sqrt{-i\omega t}\right)\right]\\
&\quad+\frac{1}{4i}e^{i\omega t}\left[e^{-y\sqrt{i\omega a}}\,\mathrm{erfc}\left(\frac{y}{2}\sqrt{\frac{a}{t}}-\sqrt{i\omega t}\right)\right.\\
&\qquad\left.+e^{y\sqrt{i\omega a}}\,\mathrm{erfc}\left(\frac{y}{2}\sqrt{\frac{a}{t}}+\sqrt{+i\omega t}\right)\right].
\end{aligned}
\tag{24}
$$

Note that (24) are identical to those obtained by Fetecau et al. [9]; see (9) and (11). This fact is also shown in Figure 8.

5. Graphical Results and Discussion

In this section, the obtained exact solutions are studied numerically in order to determine the effects of several involved parameters such as Prandtl number Pr, Grashof number Gr, Casson parameter γ, phase angle ωt, and time t. Numerical values of skin friction and Nusselt number are computed and presented in tables for different parameters. For the sake of correctness and verification, we have compared our results with those of Fetecau et al. [9]. This comparison is shown in Figure 2. It is found that our limiting solutions (24) are identical to (9) and (11) obtained by Fetecau et al. [9]. This confirms the accuracy of our obtained results.

The velocity profiles for different values of Prandtl number Pr are shown in Figure 3, when the other parameters are fixed. It is observed that velocity of the fluid decreases with increasing Prandtl number. Figure 4 illustrates the profiles of velocity for different values of Gr. It is observed that velocity increases with increasing values of Gr.

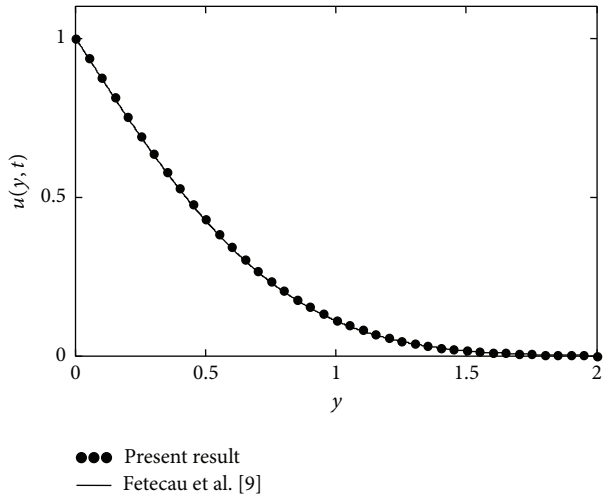

Figure 2: Comparison of the present results (see (24)) with those obtained by Fetecau et al. [9] (see (9) and (11)), when $t = 0.2$, $\omega = 0$, $a = 1$, $U = 1$, and $\nu = 1$.

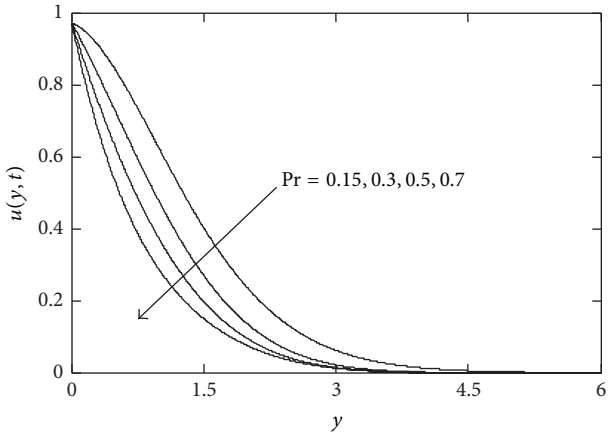

Figure 3: Profiles of velocity for different values of Pr, when $\omega = \pi/4$, $t = 0.2$, and Gr = 3.

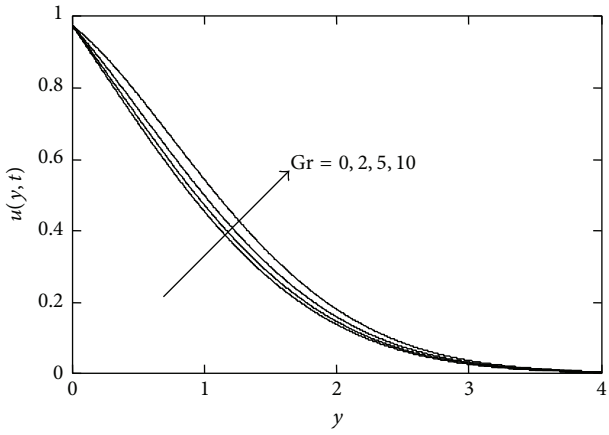

Figure 4: Profiles of velocity for different values of Gr, when Pr = 0.3, $\gamma = 0.6$, $t = 0.3$, and $\omega = \pi/4$.

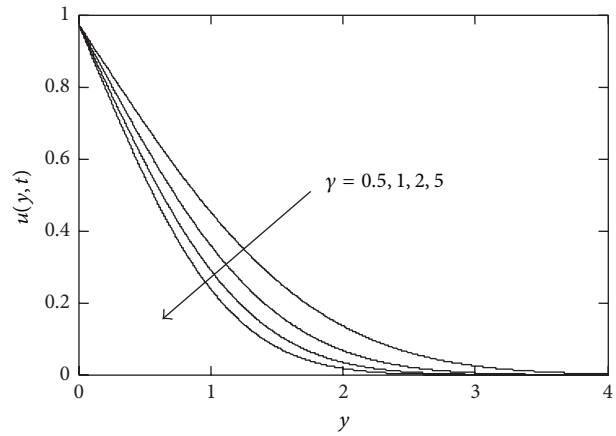

Figure 5: Profiles of velocity for different values of γ, when Pr = 0.3, Gr = 0, $t = 0.3$, and $\omega = \pi/4$.

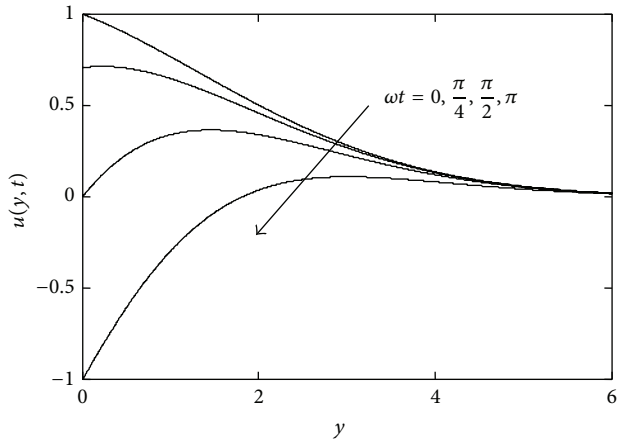

Figure 6: Profiles of velocity for different values of ωt, when Gr = 3, Pr = 0.3, $t = 1$, and $\gamma = 0.5$.

The influence of Casson fluid parameter on velocity profiles is shown in Figure 5. It is found that velocity decreases with increasing values of γ. It is important to note that an increase in Casson parameter makes the velocity boundary layer thickness shorter. It is further observed from this graph that when the Casson parameter γ is large enough, that is, $\gamma \to \infty$, the non-Newtonian behaviours disappear and the fluid purely behaves like a Newtonian fluid. Thus, the velocity boundary layer thickness for Casson fluid is larger than the Newtonian fluid. It occurs because of plasticity of Casson fluid. When Casson parameter decreases, the plasticity of the fluid increases, which causes the increment in velocity boundary layer thickness. The graphical results for the phase angle, ωt, are shown in Figure 6. It is observed that the fluid is oscillating between −1 and 1. These fluctuations near the plate are maximum and decrease for further values of independent variable y. This figure can easily help us to check the accuracy of our results. For illustration of such results we have concentrated more on the values of $\omega t = 0, \pi/2$ and π. We can see that, for these values of ωt, the velocity shows its values either 1, 0, or −1 which are identical with the

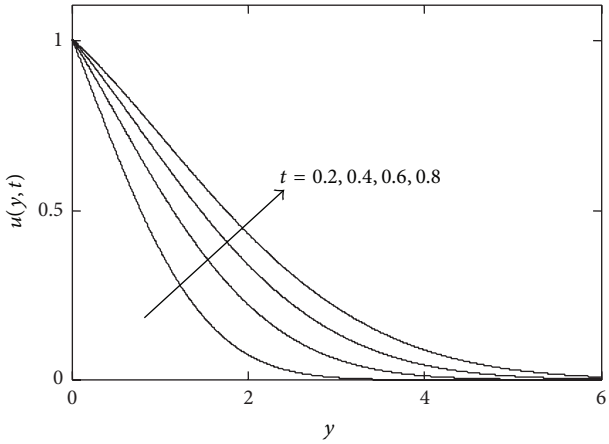

Figure 7: Profiles of velocity for different values of t, when Pr = 0.3, Gr = 3, $\gamma = 0.5$, and $\omega = 0$.

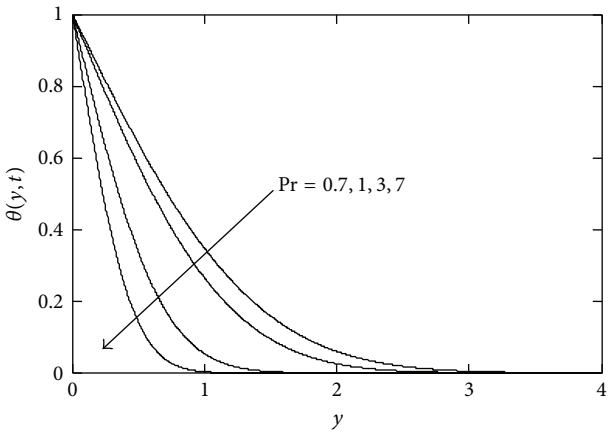

Figure 8: Profiles of temperature for different values of Pr, when $t = 0.4$.

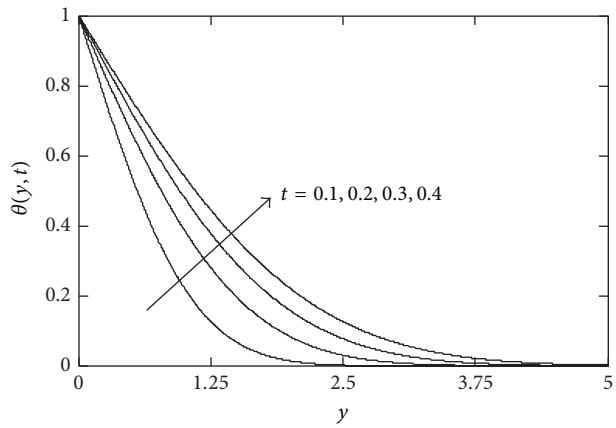

Figure 9: Profiles of temperature for different values of t, when Pr = 0.71.

Table 1: Skin friction variations.

Pr	Gr	γ	ωt	t	τ
0.3	3	0.5	$\pi/4$	0.3	3.384043
0.71	3	0.5	$\pi/4$	0.3	0.437932
0.3	**5**	0.5	$\pi/4$	0.3	0.200932
0.3	3	**1.0**	$\pi/4$	0.3	0.536355
0.3	3	0.5	$\boldsymbol{\pi/2}$	0.3	0.422417
0.3	3	0.5	$\pi/4$	**0.4**	0.307634

Table 2: Nusselt number variations.

Pr	t	Nu
0.3	0.3	0.564
0.71	0.3	0.867
0.3	**0.6**	0.398

imposed boundary conditions of velocity in (11). Hence, both the graphical and mathematical results are found in excellent agreement. In Figure 7 the influence of dimensionless time t on the velocity profiles is shown. It is found that the velocity is an increasing function of time t.

It is depicted from Figure 8 that the temperature profile decreases with increasing values of Prandtl number Pr. The specific values of Prandtl number such as Pr = 0.71, Pr = 1.0, and Pr = 7.0 are important in the sense that, physically, they correspond to air, electrolytic solution, and water, respectively. It is observed that the thermal boundary layer thickness is maximum near the plate and decreases with increasing distance from the leading edge and finally approaches to zero. It is also noticed from this figure that the magnitude of temperature is greater for air compared to electrolytic solution and water. It is justified due to the fact that thermal conductivity of the fluid decreases with increasing Prandtl number Pr and hence decreases the thermal boundary layer thickness and finally the temperature profiles.

Figure 9 is plotted to show the effects of the dimensionless time t on the temperature profiles. Four different values of time $t = 0.1$, $t = 0.2$, $t = 0.3$, and $t = 0.1$ are chosen. Obviously the temperature increases with increasing time t. This graphical behaviour of temperature is in good agreement with the corresponding boundary conditions of temperature profiles as shown in (9). Results for skin friction and Nusselt number are computed in Tables 1 and 2. The computations of skin friction give complex results. Therefore, for the sake of convenience we have considered in Table 1 only its real part. Table 1 shows that skin friction increases with increasing values of Pr, Gr, γ, and ωt, whereas it decreases with increasing values of t. On the other hand, it is found from Table 2 that Nusselt number increases with increasing Pr whereas it decreases with increasing t.

6. Conclusion

In this paper an exact analysis is performed to investigate the unsteady boundary layer flow of a Casson fluid past an oscillating vertical plate with constant wall temperature. The dimensionless governing equations are solved by using the Laplace transform technique. The results for velocity and temperature are obtained and plotted graphically. The numerical results for skin friction and Nusselt number are

computed in tables. The main conclusions of this study are as follows.

(1) Velocity increases with increasing Gr and t, whereas it decreases with increasing values of Pr, γ, and ωt.

(2) Temperature increases with increasing t, whereas it decreases when Pr is increased.

(3) Skin friction is increasing with increasing values of Pr, γ, and ωt, whereas it decreases with increasing values of Gr and t.

(4) Nusselt number increases with increasing Pr, whereas it decreases with increasing t.

(5) Solutions (24) are found in excellent agreement with those obtained by Fetecau et al. [9].

Conflict of Interests

The authors declare that there is no conflict of interests regarding the publication of this paper.

Acknowledgments

The authors would like to acknowledge the SBKWU (HEC), Pakistan, Ministry of Education (MOE), Malaysia, and the Research Management Centre, UTM, for the financial support through vote numbers 06H67 and 4F255 for this research.

References

[1] M. Sajid, I. Pop, and T. Hayat, "Fully developed mixed convection flow of a viscoelastic fluid between permeable parallel vertical plates," *Computers & Mathematics with Applications*, vol. 59, no. 1, pp. 493–498, 2010.

[2] I. Khan, K. Fakhar, and S. Sharidan, "Magnetohydrodynamic rotating flow of a generalized Burgers' fluid in a porous medium with Hall current," *Transport in Porous Media*, vol. 91, no. 1, pp. 49–58, 2012.

[3] M. I. Anwar, I. Khan, S. Shafie, and M. Z. Salleh, "Conjugate effects of heat and mass transfer of nano fluids over a non-linear stretching sheet," *International Journal of Physical Sciences*, vol. 7, no. 26, pp. 4081–4092, 2012.

[4] M. Khan, S. Nadeem, T. Hayat, and A. M. Siddiqui, "Unsteady motions of a generalized second-grade fluid," *Mathematical and Computer Modelling*, vol. 41, no. 6-7, pp. 629–637, 2005.

[5] N. Ali, T. Hayat, and S. Asghar, "Peristaltic flow of a Maxwell fluid in a channel with compliant walls," *Chaos, Solitons and Fractals*, vol. 39, no. 1, pp. 407–416, 2009.

[6] I. Khan, K. Fakhar, and M. Anwar, "Hydromagnetic rotating flows of an oldroyd-B fluid in a porous medium," *Special Topics and Reviews in Porous Media*, vol. 3, no. 1, pp. 89–95, 2012.

[7] T. Hayat, M. Awais, and A. Alsaedi, "Newtonian heating and magnetohydrodynamic effects in flow of a Jeffery fluid over a radially stretching surface," *International Journal of Physical Sciences*, vol. 7, pp. 2838–2844, 2012.

[8] F. Ali, I. Khan, S. Ul Haq, and S. Shafie, "Influence of thermal radiation on unsteady free convection MHD flow of Brinkman type fluid in a porous medium with Newtonian heating," *Mathematical Problems in Engineering*, vol. 2013, Article ID 632394, 13 pages, 2013.

[9] C. Fetecau, D. Vieru, and C. Fetecau, "A note on the second problem of Stokes for Newtonian fluids," *International Journal of Non-Linear Mechanics*, vol. 43, no. 5, pp. 451–457, 2008.

[10] M. E. Erdogan, "A note on an unsteady flow of a viscous fluid due to an oscillating plane wall," *International Journal of Non-Linear Mechanics*, vol. 35, no. 1, pp. 1–6, 2000.

[11] W. A. Khan and A. Aziz, "Natural convection flow of a nanofluid over a vertical plate with uniform surface heat flux," *International Journal of Thermal Sciences*, vol. 50, no. 7, pp. 1207–1214, 2011.

[12] C. Fetecau and M. Rana, "General solutions for the unsteady flow of second-grade fluids over an infinite plate that applies arbitrary shear to the fluid," *Zeitschrift für Naturforschung A: A Journal of Physical Science*, vol. 66, no. 12, pp. 753–759, 2011.

[13] N. Casson, "A flow equation for the pigment oil suspensions of the printing ink type," in *Rheology of Disperse Systems*, pp. 84–102, Pergamon, New York, NY, USA, 1959.

[14] T. Hayat, M. Awais, and M. Sajid, "Mass transfer effects on the unsteady flow of UCM fluid over a stretching sheet," *International Journal of Modern Physics B*, vol. 25, no. 21, pp. 2863–2878, 2011.

[15] R. K. Dash, K. N. Mehta, and G. Jayaraman, "Casson fluid flow in a pipe filled with a homogeneous porous medium," *International Journal of Engineering Science*, vol. 34, no. 10, pp. 1145–1156, 1996.

[16] Y. C. Fung, *Biodynamics Circulation*, Springer, New York, NY, USA, 1984.

[17] A. G. Fredrickson, *Principles and Applications of Rheology*, Prentice-Hall, Englewood Cliffs, NJ, USA, 1964.

[18] J. Boyd, J. M. Buick, and S. Green, "Analysis of the Casson and Carreau-Yasuda non-Newtonian blood models in steady and oscillatory flows using the lattice Boltzmann method," *Physics of Fluids*, vol. 19, no. 9, Article ID 093103, 2007.

[19] A. V. Mernone, J. N. Mazumdar, and S. K. Lucas, "A mathematical study of peristaltic transport of a Casson fluid," *Mathematical and Computer Modelling*, vol. 35, no. 7-8, pp. 895–912, 2002.

[20] M. Mustafa, T. Hayat, I. Pop, and A. Aziz, "Unsteady boundary layer flow of a Casson fluid due to an impulsively started moving flat plate," *Heat Transfer—Asian Research*, vol. 40, no. 6, pp. 563–576, 2011.

[21] T. Hayat, S. A. Shehzad, A. Alsaedi, and M. S. Alhothuali, "Mixed convection stagnation point flow of casson fluid with convective boundary conditions," *Chinese Physics Letters*, vol. 29, no. 11, Article ID 114704, 2012.

[22] S. Mukhopadhyay, "Effects of thermal radiation on Casson fluid flow and heat transfer over an unsteady stretching surface subjected to suction/blowing," *Chinese Physics B*, vol. 22, no. 11, Article ID 114702, 2013.

[23] S. Mukhopadhyay, P. R. De, K. Bhattacharyya, and G. C. Layek, "Casson fluid flow over an unsteady stretching surface," *Ain Shams Engineering Journal*, vol. 4, no. 4, pp. 933–938, 2013.

[24] K. Bhattacharyya, "Boundary layer stagnation-point flow of casson fluid and heat transfer towards a shrinking/stretching sheet," *Frontiers in Heat and Mass Transfer*, vol. 4, no. 2, Article ID 023003, 2013.

[25] S. Pramanik, "Casson fluid flow and heat transfer past an exponentially porous stretching surface in presence of thermal radiation," *Ain Shams Engineering Journal*, vol. 5, no. 1, pp. 205–212, 2014.

[26] S. Kim, *Study of non-Newtonian viscosity and yield stress of blood in a scanning capillary-tube rheometer (A) [Ph.D. thesis]*, Mechanical Engineering and Mechanics, 2002.

Hindawi Publishing Corporation
Abstract and Applied Analysis
Volume 2015, Article ID 539652, 12 pages
http://dx.doi.org/10.1155/2015/539652

Research Article

A Strongly A-Stable Time Integration Method for Solving the Nonlinear Reaction-Diffusion Equation

Wenyuan Liao

Department of Mathematics and Statistics, University of Calgary, 2500 University Drive NW, Calgary, AB, Canada T2N 1N4

Correspondence should be addressed to Wenyuan Liao; wliao@ucalgary.ca

Received 28 July 2014; Accepted 17 October 2014

Academic Editor: Santanu Saha Ray

Copyright © 2015 Wenyuan Liao. This is an open access article distributed under the Creative Commons Attribution License, which permits unrestricted use, distribution, and reproduction in any medium, provided the original work is properly cited.

The semidiscrete ordinary differential equation (ODE) system resulting from compact higher-order finite difference spatial discretization of a nonlinear parabolic partial differential equation, for instance, the reaction-diffusion equation, is highly stiff. Therefore numerical time integration methods with stiff stability such as implicit Runge-Kutta methods and implicit multistep methods are required to solve the large-scale stiff ODE system. However those methods are computationally expensive, especially for nonlinear cases. Rosenbrock method is efficient since it is iteration-free; however it suffers from order reduction when it is used for nonlinear parabolic partial differential equation. In this work we construct a new fourth-order Rosenbrock method to solve the nonlinear parabolic partial differential equation supplemented with Dirichlet or Neumann boundary condition. We successfully resolved the phenomena of order reduction, so the new method is fourth-order in time when it is used for nonlinear parabolic partial differential equations. Moreover, it has been shown that the Rosenbrock method is strongly A-stable hence suitable for the stiff ODE system obtained from compact finite difference discretization of the nonlinear parabolic partial differential equation. Several numerical experiments have been conducted to demonstrate the efficiency, stability, and accuracy of the new method.

1. Introduction

Let us consider the following parabolic partial differential equation:

$$u_t = Du_{xx} + f(u, x, t), \quad (x, t) \in (a, b) \times (0, T], \tag{1}$$

with the initial condition:

$$u(x, 0) = u_0(x), \quad x \in [a, b], \tag{2}$$

where D is a positive constant describing the diffusion property and $f(u, x, t)$ is a function representing the reaction term, which is nonlinear on u. The unknown function u represents, depending on the applications, variables such as mass concentration in chemical reaction process, temperature in heat conduction, neutron flux in nuclear reactors, and population density in population dynamics. On the boundary, either Dirichlet condition

$$u(a, t) = g_1(t), \quad u(b, t) = g_2(t), \quad 0 \le t \le T \tag{3}$$

or Neumann condition

$$u_x(a, t) = g_3(t), \quad u_x(b, t) = g_4(t), \quad 0 \le t \le T \tag{4}$$

is specified, where g_1, g_2, g_3, and g_4 are sufficiently smooth functions. Here in this paper we restrict our attention on Dirichlet and Neumann boundary conditions, while the developed techniques can be easily extended to Robin boundary condition.

Efficient and accurate numerical methods for solving (1) had attracted great attentions from scientists and engineers, as for many application problems in science and engineering, it is preferable to use high-order compact numerical algorithms to compute accurate solutions. In the past several decades a great deal of work has been done in the development of efficient, accurate, and robust numerical algorithm for solving such problem. For more details, the reader is referred to [1–4].

Since both temporal and spatial derivatives are involved in the equation, we discuss the numerical treatments in

time and space separately. Here we first apply the high-order compact finite difference approximation to the spatial derivative, so a semidiscrete ODE system is obtained, which is then solved by a fourth-order Rosenbrock method that will be discussed later.

Recently there have been attempts to develop high-order compact scheme for the spatial derivative. In [5], a three-point combined compact difference scheme was proposed to approximate the first and second derivatives for problem with periodic boundary condition. The resulting scheme has up to sixth-order accuracy at all grid points including the boundary nodes for periodic boundaries; however it is only fourth-order accurate for nonperiodic boundary condition.

Because the semidiscrete ODE system obtained from spatial discretization, such as method of lines, of the nonlinear parabolic partial differential equation is highly stiff, the choices of time integration methods are limited to implicit methods only. Explicit algorithm is efficient in a single time step but suffers from strict step size restriction, which makes it less efficient. Implicit method, on the other side, is less efficient in a single step but the unconditional stability allows the use of larger time step; hence the overall computational efficiency can be significantly improved. One issue, however, is that the iteration is usually slow when large step size Δt is used. Also, due to the stiffness of the ODE system, only Newton-type iterative methods are applicable to solve the nonlinear algebraic system. Furthermore, strong A-stability or L-stability of the time integration method is necessary for error damping. A great deal of work has been done in the development of efficient time stepping methods for the stiff ODE system. In [6] explicit exponential Rosenbrock methods of order five have been constructed to solve the large-scale stiff ODE system. Through the derivation of stiff order condition, new pairs of embedded methods of higher-order can be obtained. Similarly, fifth-order explicit exponential Runge-Kutta methods were constructed to efficiently integrate the semilinear stiff problems in [7]. The authors have also shown that there does not exist an explicit exponential Runge-Kutta method of order 5 with less than or equal to 6 stages; therefore the resultant methods are 8-stage methods. In [8] a fourth-order time stepping method, which is a modification of the exponential time-differencing fourth-order Runge-Kutta method, has been developed for stiff ODEs. These methods are efficient and accurate. However, A-stability of the time stepping method is not sufficient for highly stiff problem. To overcome these difficulties, it is desirable to construct new algorithms with strong A-stability or L-stability that are free of solving nonlinear equations. It turns out that the Rosenbrock method, which was firstly reported by Rosenbrock [9] and then improved by Haines [10], responded to these issues with considerably satisfying and promising results.

The objective herein is to develop a strongly A-stable Rosenbrock method to solve the semidiscrete stiff ODEs resulting from compact high-order finite difference approximation of a semilinear parabolic partial differential equation. The rest of the paper is organized as the following. In Section 2, we discretize the spatial derivatives of the semilinear parabolic partial differential equation using a fourth-order compact finite difference scheme, which is then combined with a newly proposed compact fourth-order boundary condition treatment to form the semidiscrete ODE system. In Section 3 we focus on the development of a fourth-order strongly A-stable Rosenbrock method and the stability analysis. Several numerical examples are used to demonstrate the accuracy and efficiency of the new algorithm in Section 4, which is followed by conclusions and possible future work.

2. Compact Fourth-Order Spatial Discretization

For the sake of simplicity, we assume that the 1D spatial domain $\Omega = [a, b]$ is divided into M subintervals with equal length $h = (b-a)/M$. Let $x_i = a + i \cdot h$, $i = 0, 1, \ldots, M$, be the grid points. A variety of compact high-order discretizations can be utilized to approximate the second derivative u_{xx} in (1).

Here we introduce a compact finite difference scheme to approximate u_{xx}, such that the resulting semidiscrete ODE system is an accurate and compact approximation to the original semilinear parabolic partial differential equation. This operator-approximation based method has been widely used to solve various multidimensional problems. We first define the central finite difference operator δ_x^2 as

$$\delta_x^2 u_i = u_{i+1} - 2u_i + u_{i-1}; \tag{5}$$

then δ_x^2/h^2 gives second-order accurate approximation to u_{xx}. Using Taylor series to expand all terms on the right-hand side of (5), under the assumption that $u(x)$ is sufficiently smooth, we have

$$\frac{\delta_x^2}{h^2} u_i = u_{xx}(x_i) + \frac{h^2}{12} u_{xxxx}(x_i) + O\left(h^4\right), \quad 1 \le i \le M-1. \tag{6}$$

To improve the above finite difference approximation to fourth-order accurate, one just needs to eliminate the second-order error term. Applying $\delta_x^2/12$ to both sides of (6), we have

$$\frac{\delta_x^2}{h^2} \frac{\delta_x^2}{12} u_i = u_{xxxx}(x_i) + O\left(h^4\right), \quad 1 \le i \le M-1. \tag{7}$$

Combining (6) with (7), neglecting $O(h^4)$, we obtain the following fourth-order accurate approximation to u_{xx} at node x_i:

$$u_{xx}(x_i) \approx \frac{1}{h^2} \delta_x^2 \left(1 - \frac{\delta_x^2}{12}\right) u_i, \quad 1 \le i \le M-1. \tag{8}$$

The drawback is that a five-point stencil is required; therefore the compactness is destroyed so the method becomes less efficient. Further investigation shows that the difference between $1 - \delta_x^2/12$ and $(1 + \delta_x^2/12)^{-1}$ is $O(h^4)$, so a natural way is to approximate $u_{xx}(x_i)$ as $\delta_x^2(1 + \delta_x^2/12)^{-1} u_i$, which is fourth-order accurate and compact.

Applying the fourth-order Padé approximation to u_{xx} in (1), we obtain the following ODE system

$$u_i'(t) = \frac{D}{h^2}\frac{\delta_x^2}{1+\delta_x^2/12}u_i(t) + f\left(u_i(t), x_i, t\right), \quad 1 \le i \le M-1, \tag{9}$$

which is a fourth-order accurate approximation (in space) to the original semilinear parabolic partial differential equation defined in (1).

However, the above algorithm is difficult to implement, so we multiply $1+\delta_x^2/12$ to both sides to obtain the following implicit ODE system:

$$\left(1+\frac{\delta_x^2}{12}\right)u_i'(t) = \frac{D}{h^2}\delta_x^2 u_i(t) + \left(1+\frac{\delta_x^2}{12}\right)f\left(u_i(t), x_i, t\right), \quad 1 \le i \le M-1, \quad 0 < t \le T, \tag{10}$$

which can be written in vector form as

$$AU'(t) = F(U, X, t), \quad 0 < t \le T, \tag{11}$$

where $U(t) = (u_1(t), u_2(t), \ldots, u_{M-1}(t))$ is the discrete solution of (1) at time t, with $u_i(t) = u(x_i, t)$, A is an $(M-1)\times(M-1)$ tridiagonal matrix, and F is a vector-valued function defined through (10). To complete the ODE system, we need the boundary conditions at $x = x_0$ and $x = x_M$, which can be derived from the original boundary conditions defined in (3) or (4).

First, if the Dirichlet boundary condition (3) is specified, one can add the following two ODEs to (9):

$$u_0'(t) = g_1'(t), \qquad u_M'(t) = g_2'(t). \tag{12}$$

Consequently the matrix is modified as

$$A = \begin{pmatrix} 1 & 0 & 0 & 0 & \cdots & 0 & 0 & 0 \\ \frac{1}{12} & \frac{5}{6} & \frac{1}{12} & 0 & \cdots & 0 & 0 & 0 \\ \cdots & \cdots & \cdots & \cdots & \cdots & \cdots & \cdots & \cdots \\ 0 & 0 & 0 & 0 & \cdots & \frac{1}{12} & \frac{5}{6} & \frac{1}{12} \\ 0 & 0 & 0 & 0 & \cdots & \cdots & \cdots & 1 \end{pmatrix}, \tag{13}$$

while the vector-valued function $F(U, X, t)$, after modifications, is defined as

$$F_0 = g_1'(t), \qquad F_i = \frac{D}{h^2}\delta_x^2 u_i(t) + \left(1+\frac{\delta_x^2}{12}\right)f\left(u_i(t), x_i, t\right), \quad 1 \le i \le M-1, \qquad F_M = g_2'(t). \tag{14}$$

Alternatively, we can incorporate the boundary condition by replacing $u_0(t)$ and $u_M(t)$ in (10) with $g_1(t)$ and $g_2(t)$, respectively, so the ODE system equation (11) has only $M-2$ equations.

As one can imagine, the situation is more complicated when the Neumann boundary condition (4) is specified. To complete the ODE system and maintain the higher-order overall accuracy, a compact fourth-order approximation of the Neumann boundary condition is needed. Let us use the boundary condition at $x = a$ as the example to demonstrate the idea of the new algorithm.

Unlike the Dirichlet boundary condition, which specifies the solution u on the boundary point explicitly, the Neumann boundary condition defines u_x at the boundary points; thus $u_0(t)$ and $u_M(t)$ need to be calculated along with solution at the interior grid points. Consequently, the range for i in (10) should be changed to $0 \le i \le M$, so A is an $(M+1)\times(M+1)$ matrix. To approximate the derivative at x_0, we introduce a ghost point $x_{-1} = a - h$ and assume that (1) holds and the solution u is sufficiently smooth on the extended domain $[a-h, b]$. Let $u_{-1}(t)$ denote the solution at $x_{-1} = a - h$ and then apply the second-order central finite difference approximation to $u_x(a, t)$,

$$\frac{u_1(t) - u_{-1}(t)}{2h} = u_x(a,t) + \frac{h^2}{6}u_{xxx}(a,t) + O\left(h^4\right). \tag{15}$$

Taking partial derivative with respect to x on both sides of (1), we have

$$u_{xxx} = \frac{1}{D}\left(u_{xt} - f_x - f_u \cdot u_x\right). \tag{16}$$

Letting $x \to a$ in (16) and then applying the Neumann boundary condition (4), we obtain

$$u_{xxx}(a) = \frac{1}{D}\left(g_3'(t) - f_x\left(u_0(t), a, t\right) - f_u\left(u_0(t), a, t\right)\cdot g_3(t)\right). \tag{17}$$

Combining (15) with (17), we obtain the following fourth-order compact approximation for $u_{-1}(t)$:

$$u_{-1}(t) = u_1(t) - 2hg_3(t) - \frac{h^3}{3D}\left(g_3'(t) - f_x\left(u_0(t), a, t\right) - f_u\left(u_0(t), a, t\right)\cdot g_3(t)\right), \tag{18}$$

which involves $u_0(t)$ and $u_1(t)$ only, so the compact structure is preserved.

Similarly, the fourth-order compact approximation for $u_{M+1}(t)$ can be derived as

$$\begin{aligned} u_{M+1}(t) &= u_{M-1}(t) + 2hg_4(t) \\ &\quad + \frac{h^3}{3D}\left(g_4'(t) - f_x(u_M(t), b, t)\right. \\ &\qquad \left. - f_u(u_M(t), b, t)\cdot g_4(t)\right). \end{aligned} \tag{19}$$

Now the matrix A involves t and U, and the first and last rows are modified as

$$\begin{aligned} A_{0,0\cdots M} &= \left(\frac{10}{12} + \frac{h^3}{36D}\left(f_{xu}(u_0, a, t)\right.\right. \\ &\qquad \left.\left. + f_{uu}(u_0, a, t)\cdot g_3(t)\right), \frac{1}{6}, \ldots, 0\right), \\ A_{M,0\cdots M} &= \left(0, \ldots, \frac{1}{6}, \frac{10}{12} - \frac{h^3}{36D}\left(f_{xu}(u_M, b, t)\right.\right. \\ &\qquad \left.\left. + f_{uu}(u_M, b, t)\cdot g_4(t)\right)\right). \end{aligned} \tag{20}$$

Consequently the first and last components of F are

$$\begin{aligned} F_0 &= \frac{D}{h^2}(2u_1 - 2u_0 - 2hg_3) \\ &\quad + \frac{1}{12}(10f(u_0, a, t) + f(u_1, a + h, t)) \\ &\quad - \frac{h}{3}\left(g_3' - f_x(u_0, a, t) - f_u(u_0, a, t)\cdot g_3\right) + \frac{h}{6}g_3' \\ &\quad + \frac{h^3}{36D}\left(g_3'' - f_{xt}(u_0, a, t) - f_u(u_0, a, t)\cdot g_3'\right. \\ &\qquad \left. - f_{ut}(u_0, a, t)\cdot g_3\right) \\ &\quad + \frac{1}{12}f\left(u_1 - 2hg_3 - \frac{h^3}{3D}\right. \\ &\qquad \left.\times\left(g_3' - f_x(u_0, a, t) - f_u(u_0, a, t)\cdot g_3\right),\right. \\ &\qquad \left. a - h, t\right), \\ F_M &= \frac{2D}{h^2}(u_{M-1} - u_M + hg_4) \\ &\quad + \frac{1}{12}(10f(u_M, b, t) + f(u_{M-1}, b - h, t)) \\ &\quad - \frac{h}{3}\left(g_4' - f_x(u_M, b, t) - f_u(u_M, b, t)\cdot g_4\right) - \frac{h}{6}g_4' \\ &\quad - \frac{h^3}{36D}\left(g_4'' - f_{xt}(u_M, b, t) - f_u(u_M, b, t)\cdot g_4'\right. \\ &\qquad \left. - f_{ut}(u_M, b, t)\cdot g_4\right) \\ &\quad + \frac{1}{12}f\left(u_{M-1} + 2hg_4 + \frac{h^3}{3D}\right. \\ &\qquad \left.\times\left(g_4' - f_x(u_M, b, t) - f_u(u_M, b, t)\cdot g_4\right),\right. \\ &\qquad \left. b + h, t\right). \end{aligned} \tag{21}$$

Finally, the ODE system is written in the form of $A(t, U)U' = F(U, t)$. Apparently, the matrix A preserves tridiagonal structure, but it depends on t and U; hence the development of Rosenbrock method becomes difficult. Fortunately, we notice that t and U are involved in two entries: $A_{0,0}$ and $A_{M,M}$ only. Further investigation shows that the extra terms in (20) are

$$\frac{h^3}{36D}\left(f_{xu}(u_0, a, t) + f_{uu}(u_0, a, t)\cdot g_1(t)\right), \tag{22}$$

$$-\frac{h^3}{36D}\left(f_{xu}(u_M, b, t) + f_{uu}(u_M, b, t)\cdot g_4(t)\right), \tag{23}$$

respectively. We can eliminate these two extra terms by incorporating them into vector F; therefore F_0 and F_M are modified as

$$\begin{aligned} \overline{F}_0 &= F_0 \\ &\quad - \frac{h^3}{36D}\left[\left(f_{xu}(u_0, a, t) + f_{uu}(u_0, a, t)\cdot g_3(t)\right)\right]\cdot u_0'(t), \end{aligned} \tag{24}$$

$$\begin{aligned} \overline{F}_M &= F_M \\ &\quad + \frac{h^3}{36D}\left[\left(f_{xu}(u_M, b, t) + f_{uu}(u_M, b, t)\cdot g_4(t)\right)\right] \\ &\quad \cdot u_M'(t). \end{aligned} \tag{25}$$

Using (1), we have

$$\begin{aligned} u_0'(t) &= \frac{2D}{h^2}(u_1(t) - u_0(t) - hg_3(t)) \\ &\quad + f(u_0(t), a, t) + O(h), \end{aligned} \tag{26}$$

$$\begin{aligned} u_M'(t) &= \frac{2D}{h^2}(u_{M-1}(t) - u_M(t) + hg_4(t)) \\ &\quad + f(u_M(t), b, t) + O(h). \end{aligned} \tag{27}$$

Inserting (26) into (24) and then ignoring the fourth-order error term $O(h^4)$, we obtain

$$\overline{F}_0 = F_0 - \frac{h^3}{36D}\left[\left(f_{xu}\left(u_0,a,t\right) + f_{uu}\left(u_0,a,t\right)\cdot g_3\left(t\right)\right)\right] \times\left(\frac{2D}{h^2}\left(u_1 - u_0 - hg_3\left(t\right)\right) + f\left(u_0,a,t\right)\right). \tag{28}$$

Similarly, inserting (27) into (25) and then ignoring the fourth-order error term, we obtain

$$\overline{F}_M = F_M - \frac{h^3}{36D}\left[\left(f_{xu}\left(u_M,b,t\right) + f_{uu}\left(u_M,b,t\right)\cdot g_4\left(t\right)\right)\right] \times\left(\frac{2D}{h^2}\left(u_{M-1}\left(t\right) - u_M\left(t\right) + hg_4\left(t\right)\right) + f\left(u_M\left(t\right),b,t\right)\right). \tag{29}$$

We then obtain the closed ODE system $AU'(t) = F(U,t)$, where the vector-valued function is given as $F = (\overline{F}_0, F_1, \ldots, F_{M-1}, \overline{F}_M)$, and A is a nonsingular $(M+1)\times(M+1)$ constant matrix given as

$$A = \begin{pmatrix} \frac{5}{6} & \frac{1}{12} & 0 & 0 & \cdots & 0 & 0 & 0 \\ \frac{1}{12} & \frac{5}{6} & \frac{1}{12} & 0 & \cdots & 0 & 0 & 0 \\ \cdots & \cdots & \cdots & \cdots & \cdots & \cdots & \cdots & \cdots \\ 0 & 0 & 0 & 0 & \cdots & \frac{1}{12} & \frac{5}{6} & \frac{1}{12} \\ 0 & 0 & 0 & 0 & \cdots & \cdots & \frac{1}{12} & \frac{5}{6} \end{pmatrix}. \tag{30}$$

If the Robin boundary condition is specified, a similar numerical technique can be used to derive the semidiscrete ODE system.

Here we mention, without theoretical proof, that the resulting semidiscrete ODE system (9) is a fourth-order accurate approximation to the original semilinear parabolic partial differential equation given in (1), supplemented with either Dirichlet or Neumann boundary conditions. Interested readers can find a similar theorem and proof in [11].

3. Fourth-Order Strongly A-Stable Rosenbrock Method

Various numerical methods can be used to solve the ODE system in (11). However, due to the stiffness of the problem, only stiffly stable methods are applicable; thus the choices are limited to the subclass of implicit methods such as implicit linear multistep methods and implicit Runge-Kutta methods. It is known that A-stability is necessary for stiff problem, and in general strong A-stable or even L-stable methods are preferred. The A-stability was firstly introduced and defined by Dahlquist [12] as the following.

Definition 1. A numerical method is called A-stable if there is no restriction on the step size, when it is applied to solve the test equation $y' = \lambda y$, where $\mathrm{Re}(\lambda) < 0$.

For a single-step method such as Runge-Kutta method that can be written as $y_{n+1} = R(y_n)$, the A-stability is equivalent to the condition $|R(z)| \le 1$ for any $z \in \mathbb{C}^{-1}$, where $R(z)$ is called the stability function of the method. Although successfully used in various applications, an A-stable linear multistep method has the highest order of 2. In fact, the second-order A-stable linear multistep method with optimal error constant is the Trapezium rule [12]. Further, Gourlay [13] pointed out that an A-stable method is necessary but not sufficient for very stiff system as it has the incorrect damping rate. For example, the widely used Trapezium rule has stability function $R(z) = (1+z)/(1-z)$ satisfying $|R(z)| < 1$ for any $z \in \mathbb{C}^{-1}$, but its damping rate converges to -1 when $z \to -\infty$. To overcome this difficulty, strong A-stability was introduced.

Definition 2. A numerical method is called strongly A-stable if it is A-stable and $|R(-\infty)| < 1$.

It has been shown that a numerical method with strong A-stability is effective in damping numerical oscillations for highly stiff system. For more details about the description and comparison of A-stability and strong A-stability, the readers are referred to [14].

Implicit Runge-Kutta method is usually unconditionally stable but suffers from the issue of high computational complexity, especially for nonlinear ODE system. For example, during each time step, an algebraic system with $s \times M$ unknown variables needs to be solved, if an s-stage implicit Runge-Kutta method is used to solve an ODE system with M equations. Therefore, fully implicit Runge-Kutta methods are too computationally expensive to be useful for large-scale problems. In the past several decades, efforts have been made to reduce the computational cost, which results in various modified implicit Runge-Kutta methods, such as diagonally implicit Runge-Kutta method, singly diagonally implicit Runge-Kutta method, explicit-implicit Runge-Kutta method, to name a few. For more details of these methods, the reader is referred to [15–19].

To completely avoid solving a nonlinear algebraic system, Rosenbrock method, which is a special class of Runge-Kutta method, had been proposed. Since the spatial discretization is fourth-order, our aim herein is to develop a strongly A-stable fourth-order Rosenbrock method for solving the ODE system (11), so the new algorithm is fourth-order accurate in both temporal and spatial dimensions.

3.1. Rosenbrock Method for Scalar Equation. We first derive the Rosenbrock method based on an autonomous scalar equation $y' = f(y)$, for which the initial condition is given as $y(t_0) = y_0$. Nonautonomous equations can be converted to autonomous form by adding an extra equation to the system. Some previous research [20] suggested that it is unlikely to find a 3-stage fourth-order Rosenbrock method with strong A-stability or L-stability, so herein we focus on

the development of a 4-stage Rosenbrock method. Suppose the numerical solution at time t_n is known as y_n, the 4-stage Rosenbrock method calculates the numerical solution at t_{n+1} as

$$y_{n+1} = y_n + b_1k_1 + b_2k_2 + b_3k_3 + b_4k_4, \tag{31}$$

$$k_i = \Delta t f\left(y_n + \sum_{j=1}^{i-1}\alpha_{ij}k_j\right) + \Delta t J(y_n)\sum_{j=1}^{i}\gamma_{ij}k_j, \quad i = 1,2,3,4, \tag{32}$$

where b_i, α_{ij}, and γ_{ij} are coefficients to be determined and $J(y_n) = f_y(y_n)$.

To extend the above algorithm to the nonautonomous problems $y' = f(y,t)$, we first convert it to autonomous form by adding a new equation $t' = 1$ and then apply the algorithm (31) to the augmented system. Note that the components corresponding to the last variable can be computed explicitly; thus we can derive the modified algorithm as the following:

$$\begin{aligned} y_{n+1} &= y_n + b_1k_1 + b_2k_2 + b_3k_3 + b_4k_4, \\ k_i &= \Delta t f\left(y_n + \sum_{j=1}^{i-1}\alpha_{ij}k_j, t_n + \alpha_i\Delta t\right) \\ &\quad + \gamma_i\Delta t^2 f_t(y_n,t_n) + \Delta t f_y(y_n,t_n)\sum_{j=1}^{i}\gamma_{ij}k_j, \\ &\qquad i = 1,2,3,4, \end{aligned} \tag{33}$$

where

$$\alpha_i = \sum_{j=1}^{i-1}\alpha_{ij}, \qquad \gamma_i = \sum_{j=1}^{i}\gamma_{ij}. \tag{34}$$

A Rosenbrock method of order p is obtained through choosing coefficients in (31)-(32) so that the local error satisfies $y(t_n + \Delta t) - y_{n+1} = O(\Delta t^{p+1})$. This can be done either by solving the so-called *Butcher Series* [14] or by straightforward differentiation. Here we derive the order conditions for the fourth-order Rosenbrock method in a different way using Taylor series. First, both $y(t_n + \Delta t)$ and k_i are expanded as Taylor series so that the difference $y(t_n+\Delta t) - y_{n+1}$ can be expressed as a Taylor series and its coefficients of the terms up to $O(\Delta t^4)$ are set to 0, which results in a set of equations involving these coefficients.

Given $y(t_n) = y_n$, the Taylor series of $y(t_n + \Delta t)$ at t_n is expanded as

$$\begin{aligned} y(t_n + \Delta t) &= y_n + \Delta t f_n + \frac{\Delta t^2}{2}J_nf_n + \frac{\Delta t^3}{6}\left(J_n^2f_n + J_n'f_n^2\right) \\ &\quad + \frac{\Delta t^4}{24}\left(J_n''f_n^3 + 2J_n'J_nf_n^2 + 2J_nJ_n'f_n^2 + J_n^3f_n\right) \\ &\quad + O\left(\Delta t^5\right), \end{aligned} \tag{35}$$

where $f_n = f(y_n)$, $J_n = (\partial f/\partial y)(y_n)$, $J_n' = (\partial^2 f/\partial y^2)(y_n)$, and $J_n'' = (\partial^3 f/\partial y^3)(y_n)$. For the sake of simplicity, let $\beta_{ij} = \alpha_{ij}+\gamma_{ij}$ and $\alpha_{ii} = 0$.

Letting $i = 1$ in (32) we have

$$\begin{aligned} k_1 &= \Delta t\left(1 - \Delta t\gamma_{11}J_n\right)^{-1}f_n \\ &= \Delta t f_n + \Delta t^2\gamma_{11}J_nf_n + \Delta t^3\gamma_{11}^2J_n^2f_n \\ &\quad + \Delta t^4\gamma_{11}^3J_n^3f_n + O\left(\Delta t^5\right). \end{aligned} \tag{36}$$

Similarly, letting $i = 2$ in (32) we have

$$k_2 = \Delta t\left(1 - \Delta t\gamma_{22}J_n\right)^{-1}\left(f\left(y_n + \alpha_{21}k_1\right) + \gamma_{21}J_nk_1\right). \tag{37}$$

Combining it with the Taylor series of k_1 in (36), we obtain

$$\begin{aligned} k_2 &= \Delta t f_n + \Delta t^2\left(\alpha_{21} + \gamma_{21} + \gamma_{22}\right)J_nf_n \\ &\quad + \Delta t^3\left[\left(\gamma_{11} + \gamma_{22}\right)\left(\alpha_{21} + \gamma_{21}\right) + \gamma_{22}^2\right]J_n^2f_n + \frac{\Delta t^3}{2}\alpha_{21}^2J_n'f_n^2 \\ &\quad + \Delta t^4\left[\left(\gamma_{11}\gamma_{22} + \gamma_{11}^2 + \gamma_{22}^2\right)\left(\alpha_{21} + \gamma_{21}\right) + \gamma_{22}^3\right]J_n^3f_n \\ &\quad + \Delta t^4\gamma_{11}\alpha_{21}^2J_n'J_nf_n^2 + \frac{\Delta t^4}{2}\gamma_{22}\alpha_{21}^2J_nJ_n'f_n^2 \\ &\quad + \frac{\Delta t^4}{6}\alpha_{21}^3J_n''f_n^3 + O\left(\Delta t^5\right). \end{aligned} \tag{38}$$

Following the same way, we have

$$\begin{aligned} k_3 &= \Delta t f_n + \Delta t^2\left(\beta_{31} + \beta_{32} + \gamma_{33}\right)J_nf_n \\ &\quad + \Delta t^3\left[\sum_{j=1}^{3}\left(\left(\alpha_{3j} + \gamma_{3j}\right)\cdot\sum_{l=1}^{j}\left(\alpha_{jl} + \gamma_{jl}\right)\right)\right]J_n^2f_n \\ &\quad + \frac{\Delta t^3}{2}\alpha_3^2J_n'f_n^2 \\ &\quad + \Delta t^4\left[\sum_{i=1}^{3}\left(\left(\alpha_{3i} + \gamma_{3i}\right)\cdot\sum_{j=1}^{i}\left(\left(\alpha_{ij} + \gamma_{ij}\right)\cdot\sum_{l=1}^{j}\left(\alpha_{jl} + \gamma_{jl}\right)\right)\right)\right]J_n^3f_n \\ &\quad + \frac{\Delta t^4}{2}\left[\alpha_2^2\beta_{32} + \gamma_{33}\alpha_3^2\right]J_nJ_n'f_n^2 \\ &\quad + \Delta t^4\left[\alpha_3\left(\left(\beta_{21} + \gamma_{22}\right)\alpha_{32} + \gamma_{11}\alpha_{31}\right)\right]J_n'J_nf_n^2 \\ &\quad + \frac{\Delta t^4}{6}\left(\alpha_{31} + \alpha_{32}\right)^3J_n''f_n^3 + O\left(\Delta t^5\right), \end{aligned}$$

$$
\begin{aligned}
k_4 = {} & \Delta t f_n + \Delta t^2 \left(\beta_{41} + \beta_{42} + \beta_{42} + \gamma_{44}\right) J_n f_n \\
& + \Delta t^3 \left[\sum_{j=1}^{4} \left(\left(\alpha_{4j} + \gamma_{4j}\right) \cdot \sum_{l=1}^{j} \left(\alpha_{jl} + \gamma_{jl}\right) \right) \right] J_n^2 f_n \\
& + \frac{\Delta t^3}{2} \alpha_4^2 J_n' f_n^2 \\
& + \Delta t^4 \left[\sum_{i=1}^{4} \left(\left(\alpha_{4i} + \gamma_{4i}\right) \cdot \sum_{j=1}^{i} \left(\left(\alpha_{ij} + \gamma_{ij}\right) \right.\right.\right. \\
& \qquad \left.\left.\left. \cdot \sum_{l=1}^{j} \left(\alpha_{jl} + \gamma_{jl}\right) \right) \right) \right] J_n^3 f_n \\
& + \Delta t^4 \left[\alpha_4 \left(\left(\gamma_{33} + \beta_{32} + \beta_{31}\right) \alpha_{43} \right.\right. \\
& \qquad \left.\left. + \left(\gamma_{22} + \beta_{21}\right) \alpha_{42} + \gamma_{11} \alpha_{41} \right) \right] J_n' J_n f_n^2 \\
& + \frac{\Delta t^4}{2} \left[\gamma_{44} \alpha_4^2 + \beta_{43} \alpha_3^2 + \beta_{42} \alpha_2^2 \right] J_n J_n' f_n^2 \\
& + \frac{\Delta t^4}{6} \left(\alpha_{41} + \alpha_{42} + \alpha_{43}\right)^3 J_n'' f_n^3 + O\left(\Delta t^5\right).
\end{aligned} \tag{39}
$$

Inserting the four Taylor series into (35) and matching the coefficients of Δt^p for $p = 0, 1, 2, 3, 4$ on both sides of (31), we obtain the following order conditions:

$$1 = \sum_{i=1}^{4} b_i, \tag{40}$$

$$\frac{1}{2} = \sum_{i=1}^{4} b_i \cdot \left(\gamma_{ii} + \sum_{j=1}^{i-1} \beta_{ij} \right), \tag{41}$$

$$\frac{1}{6} = \sum_{i=1}^{4} b_i \cdot \left(\sum_{j=1}^{i} \beta_{ij} \cdot \sum_{l=1}^{j} \beta_{jl} \right), \tag{42}$$

$$\frac{1}{3} = \sum_{i=1}^{4} b_i \cdot \left(\sum_{j=1}^{i-1} \alpha_{ij} \right)^2, \tag{43}$$

$$\frac{1}{4} = \sum_{i=1}^{4} b_i \cdot \left(\sum_{j=1}^{i-1} \alpha_{ij} \right)^3, \tag{44}$$

$$\frac{1}{24} = \sum_{i=1}^{4} b_i \cdot \left(\alpha_i \sum_{j=1}^{i-1} \alpha_{ij} \cdot \left(\gamma_{jj} + \sum_{l=1}^{j-1} \beta_{jl} \right) \right), \tag{45}$$

$$\frac{1}{12} = \sum_{i=1}^{4} b_i \cdot \left(\sum_{j=1}^{i} \beta_{ij} \cdot \left(\sum_{l=1}^{j-1} \alpha_{jl} \right)^2 \right), \tag{46}$$

$$\frac{1}{24} = \sum_{i=1}^{4} b_i \cdot \left(\sum_{j=1}^{i} \left(\beta_{ij} \cdot \sum_{l=1}^{j} \left(\beta_{jl} \cdot \sum_{k=1}^{l} \beta_{lk} \right) \right) \right). \tag{47}$$

Note that the set of order conditions obtained by using Butcher series [14, page 108] is a special case here when $\gamma_{ii} = \gamma$.

Also it is worthy to point out that if $f(y)$ is a scalar function of a single variable, $J_n J_n' = J_n' J_n$, thus conditions (45) and (46) can be combined to one single condition. However here since the method is developed for ODE system, both conditions should be satisfied individually.

Apparently there are 12 degrees of freedom to determine the method defined in (32) since there are 20 parameters while only 8 constraints are given by (40)–(47). To simplify the procedure of determining these parameters and reduce the number of matrix inversion, we assume that $\beta_{ii} = \gamma$, for $i = 1, 2, 3, 4$, so that only one matrix inversion is required to solve all k_i during each time step. After this simplification, there are 17 parameters left, and the order conditions are simplified as well.

It is known that the Rosenbrock method suffers from order reduction when applied to nonlinear parabolic partial differential equations; see [20, 21]. In order to avoid such reduction of accuracy, the following two extra order conditions, simplified after taking into account the previous order conditions, should be satisfied [22]:

$$b_4 \beta_{43} \beta_{32} \alpha_2^2 = -2\gamma^4 + 4\gamma^3 - \frac{5}{3}\gamma^2 + \frac{\gamma}{6}, \tag{48}$$

$$b_4 \beta_{43} \beta_{32} \alpha_2^2 = -\frac{8\gamma^4}{3} + 5\gamma^3 - 2\gamma^2 + \frac{7\gamma}{36}, \tag{49}$$

which imply

$$\gamma^3 - \frac{3}{2}\gamma^2 + \frac{\gamma}{2} - \frac{1}{24} = 0. \tag{50}$$

Solving (50) results in three distinct real roots, while stability analysis shows that only one ($\gamma = 1.06857902130162885$) can ensure A-stability for the Rosenbrock method. More details regarding stability will be provided later.

To perform step size control and error estimation, we need a third-order embedded formula [23] defined as $y_{n+1} = y_n + \sum_{j=1}^{s} \widetilde{b}_j k_j$ which uses the same values of k_j's as the Rosenbrock method in (31) but coefficients of k_j's are different. To ensure the existence of such embedded formula, we need $\mathrm{Det}(\widehat{A}) = 0$, where $\widehat{A}$ is a 4×4 square matrix defined as

$$\widehat{A} = \begin{pmatrix} 1 & 1 & 1 & 1 \\ \beta_1 & \beta_2 & \beta_3 & \beta_4 \\ \beta_1^2 & \sum_{i=1}^{2} \beta_{2i} \cdot \beta_i & \sum_{i=1}^{3} \beta_{3i} \cdot \beta_i & \sum_{i=1}^{4} \beta_{4i} \cdot \beta_i \\ 0 & \alpha_2^2 & \alpha_3^2 & \alpha_4^2 \end{pmatrix} \tag{51}$$

and $\beta_i = \sum_{j=1}^{i} \beta_{ij}$.

Taking into account the order conditions, we obtain the simplified condition as $\overline{\beta}_3^2 \alpha_2^2 \beta_{43} = 0$, which unfortunately contradicts the order condition given in (47). Thus one can either sacrifices efficiency by relaxing the condition $\gamma_{ii} = \gamma$ for the existence of a third-order embedded formula or simply skip the condition and then ignore step size control and error estimation. In this work, we are interested in the

Table 1: Coefficients of the 4th-order Rosenbrock method.

$b_1 = 0.4074074074074$	$b_2 = -0.2568608534470$	$b_3 = 0.2$
$b_4 = 0.6494534460396$	$\alpha_{21} = 0.75$	$\alpha_{31} = 0.75$
$\alpha_{32} = 0$	$\alpha_{41} = 2.9193596398302$	$\alpha_{42} = 0.4$
$\alpha_{43} = -2.5693596398302$	$\gamma_{21} = -0.75$	$\gamma_{31} = -1.3152686912402$
$\gamma_{32} = 0.75$	$\gamma_{41} = -2.8738466294648$	$\gamma_{42} = -3.3778743470341$
$\gamma_{43} = 4.5693596398302$	$\gamma = 1.068579021301629$	

efficiency and order reduction of the Rosenbrock method, so the condition for step size control is bypassed.

Upon the determination of γ, there are 17 free parameters remaining while the order conditions are simplified as the following:

$$b_1 + b_2 + b_3 + b_4 = 1, \tag{52}$$

$$b_2\overline{\beta}_2 + b_3\overline{\beta}_3 + b_4\overline{\beta}_4 = \frac{1}{2} - \gamma, \tag{53}$$

$$b_3\beta_{32}\overline{\beta}_2 + b_4\left(\beta_{42}\overline{\beta}_2 + \beta_{43}\overline{\beta}_3\right) = \frac{1}{6} - \gamma + \gamma^2, \tag{54}$$

$$b_2\alpha_{21}^2 + b_3\alpha_3^2 + b_4\alpha_4^2 = \frac{1}{3}, \tag{55}$$

$$b_2\alpha_{21}^3 + b_3\alpha_3^3 + b_4\alpha_4^3 = \frac{1}{4}, \tag{56}$$

$$b_3\alpha_3\alpha_{32}\overline{\beta}_2 + b_4\alpha_4\left(\alpha_{42}\overline{\beta}_2 + \alpha_{43}\overline{\beta}_3\right) = \frac{1}{8} - \frac{\gamma}{3}, \tag{57}$$

$$b_3\beta_{32}\alpha_2^2 + b_4\left(\beta_{42}\alpha_2^2 + \beta_{43}\alpha_3^2\right) = \frac{1}{12} - \frac{\gamma}{3}, \tag{58}$$

$$b_4\beta_{43}\beta_{32}\overline{\beta}_2 = \frac{1}{24} - \frac{\gamma}{2} + \frac{3}{2}\gamma^2 - \gamma^3, \tag{59}$$

which are equivalent to those given in [14, page 108], where $\overline{\beta}_i = \sum_{j=1}^{i-1}\beta_{ij}$.

Since γ is a root of (50), $b_4\beta_{43}\beta_{32}\overline{\beta}_2 = 0$, but $b_4\beta_{43}\beta_{32}\alpha_2^2 \neq 0$, thus $\beta_{21} = 0$. Then the order conditions in (52)–(58) can be further simplified.

We now choose the coefficients α_{ij} with the purpose of reducing the number of functional evaluations. Particularly, letting $\alpha_2 = \alpha_3 = \alpha_4$, (55)-(56) imply that $\alpha_{21} = \alpha_2 = 3/4$, which further implies $b_2 + b_3 + b_4 = 16/27$, so $b_1 = 11/27$. Letting $\alpha_{31} = \alpha_{21}$ and $\alpha_{32} = 0$, we can reduce the number of functional evaluation by 1.

We choose β_{43} as a free parameter, so

$$\begin{aligned} b_4\overline{\beta}_3 &= \frac{1 - 6\gamma + 6\gamma^2}{6\beta_{43}}, \\ \alpha_{43} &= \frac{\left(1 - 8\gamma/3\right)\beta_{43}}{1 - 6\gamma + 6\gamma^2}. \end{aligned} \tag{60}$$

By choosing α_{42} as a free parameter, we have

$$\alpha_{41} = \frac{3}{4} - \alpha_{42} - \frac{\left(1 - 8\gamma/3\right)\beta_{43}}{1 - 6\gamma + 6\gamma^2}. \tag{61}$$

Letting β_{32} be a free parameter, we obtain

$$\begin{aligned} b_4 &= \frac{16\left(-2\gamma^4 + 4\gamma^3 - 5\gamma^2/3 + \gamma/6\right)}{9\beta_{43}\beta_{32}}, \\ \beta_{31} &= \frac{1 - 6\gamma + 6\gamma^2}{6\beta_{43}b_4} - \beta_{32}. \end{aligned} \tag{62}$$

Finally, choose b_3 as free parameter, so we have $b_2 = 16/27 - b_3 - b_4$ and

$$\begin{aligned} \beta_{42} &= \frac{\left(4 - 16\gamma - 27b_3\beta_{32}\right)}{\left(27b_4\right)} - \beta_{43}, \\ \beta_{41} &= \frac{\left(1/2 - \gamma - b_3\left(\beta_{31} + \beta_{32}\right)\right)}{b_4} - \beta_{42} - \beta_{43}. \end{aligned} \tag{63}$$

In summary, the coefficients of the Rosenbrock method are listed in Table 1.

Note that one can also use these free parameters to eliminate some fifth-order truncation error terms, so the truncation error constant can be further optimized.

3.2. Extend the Rosenbrock Method to ODE System. We now extend the Rosenbrock algorithm to the ODE system $AU'(t) = F(U,t)$. Suppose that $U^n = (u_0^n, u_1^n, \ldots, u_M^n)$ is the numerical solution of (10) at time t_n; then U^{n+1} is calculated as

$$U^{n+1} = U^n + b_1K_1 + b_2K_2 + b_3K_3 + b_4K_4, \tag{64}$$

$$\begin{aligned} \left(A - \gamma\Delta t J_n\right)K_i = {} & F\left(U_n + \sum_{j=1}^{i-1}\alpha_{ij}K_j, t_n + \sigma_i\Delta t\right) \\ & + \mu_i\Delta t^2\frac{\partial F}{\partial t}\left(U_n, t_n\right) + \Delta t\mathcal{J}_n\left(\sum_{j=1}^{i-1}\gamma_{ij}K_j\right), \\ & i = 1, 2, 3, 4, \end{aligned} \tag{65}$$

where $J_n = (\partial F/\partial U)(U_n, t_n)$ is the Jacobi matrix σ_i and μ_i are defined through (34).

Obviously, each stage of this method consists of solving a linear system of $M + 1$ equations. Since $\gamma_{11} = \cdots = \gamma_{44} = \gamma$, only one LU-decomposition is required during each time step.

3.3. Stability of the Rosenbrock Method. We now study the stability of the Rosenbrock method defined by (31)-(32) with coefficients given in Table 1. Applying the Rosenbrock method to the linear test equation $y' = \lambda y$, $\lambda < 0$, and taking into account the order condition equation (49), we obtain the stability function of the Rosenbrock method as

$$R(z) = \left(1 + (1-4\gamma)z + \left(\frac{1}{2} - 4\gamma + 6\gamma^2\right)z^2 - \left(\frac{5\gamma^2}{4} - \frac{5\gamma}{8} + \frac{1}{16}\right)z^4\right) \times \left((1-\gamma z)^4\right)^{-1}, \tag{66}$$

where $z = \lambda \Delta t$.

In order for the Rosenbrock method to be strongly A-stable, we need

$$|R(z)| \le 1, \quad \forall z \in \mathbb{C}^-, \tag{67}$$

$$\lim_{z \to -\infty} |R(z)| < 1. \tag{68}$$

Apparently,

$$\lim_{z \to -\infty} |R(z)| = \left|\frac{5\gamma^2/4 - 5\gamma/8 + 1/16}{\gamma^4}\right| = 0.6304149382 < 1, \tag{69}$$

so (68) is satisfied.

To prove (67), we can substitute z with $x + iy$ and then show that $|R(x + iy)| \le 1$ for any $x < 0$. However such proof is technically tedious although possible. Here we use the Boundary-Locus method to draw the region of absolute stability of the method, which is shown in Figure 1. Obviously, the region of absolute stability contains the whole half-plane $\mathbb{C}^-$, so the Rosenbrock method is A-stable. Combined with (69), we can prove that the Rosenbrock method is strongly A-stable.

4. Numerical Examples and Discussions

We solve three numerical examples to demonstrate the accuracy and efficiency of the new algorithm. The first and second examples are reaction-diffusion equations supplemented with Dirichlet and Neumann boundary conditions, respectively. The two examples are solved by the new method to demonstrate the fourth-order accuracy in time and space. The third example is used to demonstrate that the new algorithm is free of order reduction and more efficient than several other existing fourth-order Rosenbrock methods. For comparison, the rate of convergence is compared with several other fourth-order methods which suffer from order reduction. In what follows, we use *HOC-ROSB4* to represent

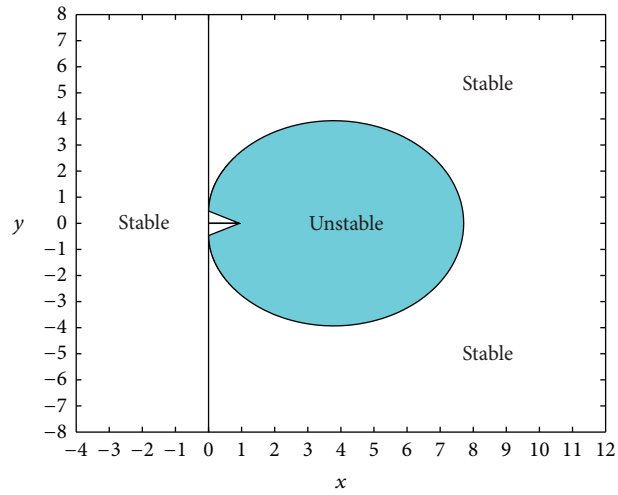

Figure 1: Absolute stable region of the Rosenbrock method.

the new algorithm developed in this paper and *HOC-GRK4A* to represent the fourth-order method that combines high-order compact finite difference scheme and fourth-order *GRK4A* [23]. *HOC-SHAMP* represents the algorithm that combines high-order compact finite difference scheme with the fourth-order Rosenbrock method *Shampine* [24]. *HOC-LSTAB* represents the algorithm that combines the high-order compact finite difference scheme in space and the L-stable fourth-order Rosenbrock method [14] in time. Finally, we use *HOC-VELD* to represent the algorithm that combines the high-order compact finite difference scheme in space with fourth-order Rosenbrock method proposed in [25].

4.1. Example 1. Consider the following reaction-diffusion equation:

$$u_t = u_{xx} + \cos(u) - \cos\left(e^{-t}\cos(x)\right), \quad (x,t) \in (0,2) \times (0,1], \quad u(x,0) = \cos(x), \quad x \in [0,2], \quad u(0,t) = e^{-t}, \quad u(2,t) = \cos(2)e^{-t}, \quad t \in [0,1], \tag{70}$$

for which the analytical solution is $u(x,t) = e^{-t}\cos(x)$.

We first show that the compact finite difference scheme for spatial discretization and the compact boundary condition treatment are fourth-order accurate. In order to do so, we fixed $\Delta t = 0.0001$ so the truncation error from time discretization is negligible. The results included in Table 2 clearly demonstrate the fourth-order convergence in space, as the maximal error reduced by a factor of 16 (roughly) when the grid size h is halved.

We then show the fourth-order accuracy in time by fixing $h = 0.001$. The data in Table 3 confirmed that the Rosenbrock method is fourth-order accurate in time, so the new algorithm is free of order reduction.

Since the method is fourth-order accurate in both temporal and spatial dimensions, we can write the leading term of

Table 2: Numerical results of *example 1* by *HOC-ROSB4* with $\Delta t = 0.0001$.

h	1/10	1/20	1/40	1/80	1/160
$E(h)$	$7.38e-08$	$4.62e-09$	$2.89e-10$	$1.80e-11$	$1.06e-12$
$E(h)/E(h/2)$	—	15.9562	16.0049	16.0607	17.0153
Convergence rate	—	3.9960	4.0004	4.0055	4.0888

Table 3: Numerical results of *example 1* by *HOC-ROSB4* with $h = 0.001$.

Δt	1/10	1/20	1/40	1/80	1/160
$E(\Delta t)$	$9.03e-06$	$6.16e-07$	$3.96e-08$	$2.45e-09$	$1.49e-10$
$E(\Delta t)/E(\Delta t/2)$	—	14.6679	15.5402	16.1607	16.4631
Convergence rate	—	3.8746	3.9579	4.0144	4.0412

Table 4: Numerical results of *example 1* by *HOC-ROSB4* with $h/\Delta t = 3.2$.

h	1/10	1/20	1/40	1/80	1/160
Δt	1/32	1/64	1/128	1/256	1/512
$E(\Delta t, h)$	$5.94e-08$	$4.09e-09$	$2.73e-10$	$1.78e-11$	$1.15e-12$
$E(\Delta t, h)/E(\Delta t/2, h/2)$	—	14.4970	14.9793	15.3189	15.4959
Convergence rate	—	3.8577	3.9049	3.9372	3.9538

the truncation error as $E(h, \Delta t) = C_1 h^4 + C_2 \Delta t^4$, where C_1 and C_2 are two constants. To obtain optimal performance, we can adjust the ratio $\Delta t/h$ to balance the two error terms. To do so, we adjust Δt and h so that the two error terms are balanced, which is utilized by letting $|C_2 \Delta t^4 / C_1 h^4| \approx 1$, from which we can estimate the optimal ratio as $(C_1/C_2)^{1/4}$. To estimate C_1, we solve the example using small Δt and then $C_1 \approx E(h)/h^4$. Similarly, we can estimate C_2 using the same method.

Simple calculation based on numerical results from Tables 2 and 3 suggests that the optimal ratio for this example is $h/\Delta t \approx 3.2$. We then solve the reaction-diffusion equation using the optimal ratio to show that the new algorithm is fourth-order accurate in both temporal and spatial dimensions. The numerical results in Table 4 indicate that the new algorithm is fourth-order accurate in both temporal and spatial dimensions, as the maximal error is reduced by a factor of 16 (roughly) when Δt and h are halved simultaneously. We also notice that the algorithm is very efficient as the maximal error drops to the level of 10^{-12} when h and Δt are still reasonably large.

4.2. Example 2. We solve the following semilinear parabolic partial differential equation with the Neumann boundary conditions:

$$u_t = 2u_{xx} + u + u^2 - e^{-2t}\cos^2(x), \quad (x,t) \in (0,2) \times (0,1],$$
$$u(x,0) = \cos(x), \quad x \in [0,2],$$
$$u_x(0,t) = 0, \quad u_x(2,t) = -\sin(2)\, e^{-t}, \quad t \in [0,1], \tag{71}$$

for which the analytical solution is $u(x,t) = e^{-t}\cos(x)$.

Notice that the boundary conditions are approximated by the compact fourth-order boundary scheme given in (18)-(19), so the compactness of the resulting linear system is preserved; consequently, in each time step, only a tridiagonal system is solved for each k_i, so the solution procedure is very efficient. However we point out that some tedious work is needed to form the semidiscrete ODE system, for instance, the first and last rows of the matrix A in (20) and the first and last components of F in (28)-(29).

To obtain the optimal performance, we choose the optimal ratio as Δt as $h/\Delta t = 2.5$ to balance the two error terms. The data in Table 5 shows that the method is fourth-order accurate in both time and space, as the maximum error is reduced by a factor of 16 (roughly), when h and Δt are halved.

It is worthy to mention that one can also use any other one-sided formula to approximate the Neumann boundary condition, which apparently reduces the effort to derive the semidiscrete ODE system, but will destroy the tridiagonal structure of the matrix A and consequently affect the efficiency of the algorithm. Another side-effect of using one-sided approximation on the boundary is the stability issue that may arise because the modifications to matrix A may result in positive eigenvalues of A.

4.3. Example 3. In this example we compare the new algorithm with several other fourth-order Rosenbrock methods in terms of the rate of convergence in time and efficiency. The nonlinear parabolic partial differential equation to be solved is defined as

$$u_t = u_{xx} + u^3 - e^{-3t}\cos^3(x), \quad (x,t) \in (0,1) \times (0,1]$$
$$u(x,0) = \cos(x), \quad x \in [0,1], \tag{72}$$
$$u(0,t) = e^{-t}, \quad u(1,t) = \cos(1)\, e^{-t}, \quad t \in [0,1],$$

for which the exact solution is $u(x,t) = e^{-t}\cos(x)$.

The data in Table 6 shows that *HOC-ROSB4* is fourth-order accurate and thus is free of order reduction, while the

Table 5: Numerical results of *example 2* by *HOC-ROSB4* with $h/\Delta t = 2.5$.

h	1/10	1/20	1/40	1/80	1/160
Δt	1/25	1/50	1/100	1/200	1/400
$E(h, \Delta t)$	$6.27e-06$	$4.40e-07$	$2.95e-08$	$1.96e-09$	$1.31e-10$
$E(h, \Delta t)/E(h/2, \Delta t/2)$	—	14.2495	14.9178	15.0510	15.0135
Convergence rate	—	3.8328	3.8990	3.9118	3.9082

Table 6: Comparison of the rate of convergence among the five fourth-order Rosenbrock methods for *example 3* with $h = 0.001$. $E(\Delta t)$ represents the maximum error of the numerical solution obtained by using Δt.

	Δt	1/10	1/20	1/40	1/80
HOC-ROSB4	$E(\Delta t)$	$9.59e-06$	$6.94e-0$	$4.58e-08$	$2.88e-09$
	Rate of Conv.	—	3.78757	3.9221	3.9896
HOC-GRK4A	$E(\Delta t)$	$5.88e-06$	$6.16e-07$	$6.83e-08$	$7.56e-09$
	Rate of Conv.	—	3.2552	3.1728	3.1757
HOC-LSTAB	$E(\Delta t)$	$3.96e-06$	$4.56e-07$	$5.23e-08$	$6.19e-09$
	Rate of Conv.	—	3.1205	3.1223	3.0795
HOC-VELD	$E(\Delta t)$	$8.41e-06$	$8.77e-07$	$9.77e-08$	$1.14e-08$
	Rate of Conv.	—	3.2613	3.1653	3.0996
HOC-SHAMP	$E(\Delta t)$	$6.35e-06$	$6.34e-07$	$6.92e-08$	$8.01e-09$
	Rate of Conv.	—	3.3230	3.1965	3.1099

Table 7: Comparison of the efficiency among the five fourth-order Rosenbrock methods for *example 3*.

Method	$(\Delta t, h)$	Max. error	CPU time (seconds)
HOC-ROSB4	(1/180, 1/40)	$7.72e-011$	0.107
HOC-GRK4A	(1/256, 1/40)	$7.28e-011$	0.134
HOC-LSTAB	(1/360, 1/40)	$7.83e-011$	0.174
HOC-VELD	(1/400, 1/40)	$7.77e-011$	0.188
HOC-SHAMP	(1/360, 1/40)	$7.60e-011$	0.170

other four fourth-order Rosenbrock methods, which obviously suffer from order reduction, show rates of convergence ranging from 3.0 to 3.25. Note that $h = 0.001$ is fixed and the same spatial discretization method is used for all five methods, so the demonstrated rate of convergence is in time. One can see that the *HOC-LSTAB* method has the most optimal error constant, while the *HOC-ROSB4* method has the largest error constant. However, due to the freedom in determining those coefficients in Rosenbrock method, better error constant can be accomplished by eliminating several fifth-order truncation error terms.

Finally, we show that *HOC-ROSB4* is the most efficient method. For consistency, we adjust Δt and h for each method to reach the same error level and record the average CPU time of 5 simulation runs. Since all of the five methods use the same spatial discretization, the same h is used for all methods; hence we adjust Δt only. The comparison result included in Table 7 clearly indicates that the new method is the most efficient one. The higher efficiency apparently is obtained from the fact that the new method is free of order reduction; hence large time step can be used to reach the same error level.

5. Conclusion

An efficient fourth-order numerical algorithm that combines the Padé approximation in space and fourth-order accurate Rosenbrock method in time is proposed in this paper. Our investigation shows that many widely used fourth-order Rosenbrock methods (A-stable or L-stable) suffer from order reduction when they are used to solve nonlinear parabolic partial differential equation. To avoid order reduction, extra order conditions are required, which are implemented in this paper to develop the new algorithm. Also, it has been shown [26] that the extra condition to resolve order reduction contradicts the L-stability of the Rosenbrock method, so there is no L-stable Rosenbrock method that is also free of order reduction. The new method can be used to solve nonlinear parabolic partial differential equation with all types of boundary conditions; however, for Neumann or Robin boundary condition, extra efforts are needed to form the semidiscrete ODE system. Two numerical examples are solved to demonstrate that the new method is fourth-order accurate in both time and space, while the third example shows that the new method is free of order reduction and

is very efficient. In the future, we plan to extend the new method to multidimensional problems supplemented with various types of boundary conditions.

Conflict of Interests

The author declares that there is no conflict of interests regarding the publication of this paper.

Acknowledgment

This work of was supported by the Natural Sciences & Engineering Research Council of Canada (NSERC) through the individual Discovery Grant program. The author gratefully acknowledges the financial support from NSERC.

References

[1] Y. Adam, "Highly accurate compact implicit methods and boundary conditions," *Journal of Computational Physics*, vol. 24, no. 1, pp. 10–22, 1977.

[2] A. R. Mitchell and D. F. Griffths, *The Finite Difference Method in Partial Differential Equations*, John Wiley & Sons, New York, NY, USA, 1980.

[3] J. I. Ramos, "Linearization methods for reaction-diffusion equations: multidimensional problems," *Applied Mathematics and Computation*, vol. 88, no. 2-3, pp. 225–254, 1997.

[4] J. I. Ramos, "Implicit, compact, linearized θ-methods with factorization for multidimensional reaction-diffusion equations," *Applied Mathematics and Computation*, vol. 94, no. 1, pp. 17–43, 1998.

[5] P. C. Chu and C. Fan, "A three-point combined compact difference scheme," *Journal of Computational Physics*, vol. 140, no. 2, pp. 370–399, 1998.

[6] V. Luan and A. Ostermann, "Exponential Rosenbrock methods of order five—construction, analysis and numerical comparisons," *Journal of Computational and Applied Mathematics*, vol. 255, no. 1, pp. 417–431, 2014.

[7] V. T. Luan and A. Ostermann, "Explicit exponential Runge-Kutta methods of high order for parabolic problems," *Journal of Computational and Applied Mathematics*, vol. 256, pp. 168–179, 2014.

[8] A.-K. Kassam and L. N. Trefethen, "Fourth-order time-stepping for stiff PDEs," *SIAM Journal on Scientific Computing*, vol. 26, no. 4, pp. 1214–1233, 2005.

[9] H. Rosenbrock, "Some general implicit processes for the numerical solution of differential equations," *The Computer Journal*, vol. 5, pp. 329–330, 1963.

[10] C. F. Haines, "Implicit integration processes with error estimate for the numerical solution of differential equations," *The Computer Journal*, vol. 12, no. 2, pp. 183–188, 1969.

[11] W. Liao and Y. Yan, "Singly diagonally implicit Runge-Kutta method for time-dependent reaction-diffusion equation," *Numerical Methods for Partial Differential Equations*, vol. 27, no. 6, pp. 1423–1441, 2011.

[12] G. G. Dahlquist, "A special stability problem for linear multistep methods," *BIT Numerical Mathematics*, vol. 3, pp. 27–43, 1963.

[13] A. R. Gourlay, "A note on trapezoidal methods for the solution of initial value problems," *Mathematics of Computation*, vol. 24, pp. 629–633, 1970.

[14] E. Hairer and G. Wanner, *Solving Ordinary Differential Equations, II, Stiff and Algebraic Problems*, Springer, Berlin , Germany, 2nd edition, 1996.

[15] R. Alexander, "Diagonally implicit Runge-Kutta methods for stiff O.D.E.'s," *SIAM Journal on Numerical Analysis*, vol. 14, no. 6, pp. 1006–1021, 1977.

[16] K. Burrage, J. C. Butcher, and F. H. Chipman, "An implementation of singly-implicit Runge-Kutta methods," *BIT Numerical Mathematics*, vol. 20, no. 3, pp. 326–340, 1980.

[17] H. Claus, "Singly-implicit Runge-Kutta methods for retarded and ordinary differential equations," *Computing*, vol. 43, no. 3, pp. 209–222, 1990.

[18] W. Liniger and R. A. Willoughby, "Efficient integration methods for stiff systems of ordinary differential equations," *SIAM Journal on Numerical Analysis*, vol. 7, pp. 47–66, 1970.

[19] J. G. Verwer, E. J. Spee, J. G. Blom, and W. Hundsdorfer, "A second-order Rosenbrock method applied to photochemical dispersion problems," *SIAM Journal on Scientific Computing*, vol. 20, no. 4, pp. 1456–1480, 1999.

[20] J. Lang and J. Verwer, "ROS3P—an accurate third-order Rosenbrock solver designed for parabolic problems," *BIT Numerical Mathematics*, vol. 41, no. 4, pp. 731–738, 2001.

[21] W. H. Hundsdorfer, "Stability and B-convergence of linearly implicit Runge-Kutta methods," *Numerische Mathematik*, vol. 50, no. 1, pp. 83–95, 1986.

[22] C. Lubich and A. Ostermann, "Linearly implicit time discretization of non-linear parabolic equations," *IMA Journal of Numerical Analysis*, vol. 15, no. 4, pp. 555–583, 1995.

[23] P. Kaps and P. Rentrop, "Generalized Runge-Kutta methods of order four with stepsize control for stiff ordinary differential equations," *Numerische Mathematik*, vol. 33, no. 1, pp. 55–68, 1979.

[24] L. F. Shampine, "Implementation of Rosenbrock methods," *ACM Transactions on Mathematical Software*, vol. 8, no. 2, pp. 93–113, 1982.

[25] M. van Veldhuizen, "D-stability and Kaps-Rentrop-methods," *Computing. Archives for Scientific Computing*, vol. 32, no. 3, pp. 229–237, 1984.

[26] T. D. Bui, "On an L-stable method for stiff differential equations," *Information Processing Letters*, vol. 6, no. 5, pp. 158–161, 1977.

Hindawi Publishing Corporation
Abstract and Applied Analysis
Volume 2014, Article ID 926838, 7 pages
http://dx.doi.org/10.1155/2014/926838

Research Article

Traveling Wave Solutions of the Benjamin-Bona-Mahony Water Wave Equations

A. R. Seadawy[1,2] and A. Sayed[2]

[1] *Mathematics Department, Faculty of Science, Taibah University, Al-Ula 41921-259, Saudi Arabia*
[2] *Mathematics Department, Faculty of Science, Beni-Suef University, Egypt*

Correspondence should be addressed to A. R. Seadawy; aly742001@yahoo.com

Received 5 August 2014; Revised 1 September 2014; Accepted 4 September 2014; Published 15 October 2014

Academic Editor: Santanu Saha Ray

Copyright © 2014 A. R. Seadawy and A. Sayed. This is an open access article distributed under the Creative Commons Attribution License, which permits unrestricted use, distribution, and reproduction in any medium, provided the original work is properly cited.

The modeling of unidirectional propagation of long water waves in dispersive media is presented. The Korteweg-de Vries (KdV) and Benjamin-Bona-Mahony (BBM) equations are derived from water waves models. New traveling solutions of the KdV and BBM equations are obtained by implementing the extended direct algebraic and extended sech-tanh methods. The stability of the obtained traveling solutions is analyzed and discussed.

1. Introduction

Many nonlinear evolution equations are playing important role in the analysis of some phenomena and including ion acoustic waves in plasmas, dust acoustic solitary structures in magnetized dusty plasmas, and electromagnetic waves in size-quantized films [1–4]. To obtain the traveling wave solutions to these nonlinear evolution equations, many methods were attempted, such as the inverse scattering method [5], Hirotas bilinear transformation [6], the tanh-sech method, extended tanh method, sine-cosine method [7], homogeneous balance method, Bäcklund transformation [8], the theory of Weierstrass elliptic function method [9], the factorization technique [10, 11], the Wadati trace method, pseudospectral method, Exp-function method, and the Riccati equation expansion method were used to investigate these types of equations [12, 13]. The above methods derived many types of solutions from most nonlinear evolution equations [14].

The Benjamin-Bona-Mahony (BBM) equation is well known in physical applications [15]; it describes the model for propagation of long waves which incorporates nonlinear and dissipative effects; it is used in the analysis of the surface waves of long wavelength in liquids, hydromagnetic waves in cold plasma, acoustic-gravity waves in compressible fluids, and acoustic waves in harmonic crystals [15]. Many mathematicians paid their attention to the dynamics of the BBM equation [16].

The BBM equation has been investigated as a regularized version of the KdV equation for shallow water waves [17]. In certain theoretical investigations the equation is superior as a model for long waves; from the standpoint of existence and stability, the equation offers considerable technical advantages over the KdV equation [18]. In addition to shallow water waves, the equation is applicable to the study of drift waves in plasma or the Rossby waves in rotating fluids. Under certain conditions, it also provides a model of one-dimensional transmitted waves.

The main mathematical difference between KdV and BBM models can be most readily appreciated by comparing the dispersion relation for the respective linearized equations. It can be easily seen that these relations are comparable only for small wave numbers and they generate drastically different responses to short waves. This is one of the reasons why, whereas existence and regularity theory for the KdV equation is difficult, the theory of the BBM equation is comparatively simple [19], where the BBM equation does not take into account dissipation and is nonintegrable [20–22]. The KdV equation describes long nonlinear waves of small amplitude on the surface of inviscid ideal fluid [22].

The KdV equation is integrable by the inverse scattering transform. Solitons exist due to the balance between the weak nonlinearity and dispersion of the KdV equation. Soliton is a localized wave that has an infinite support or a localized wave with exponential wings. The solutions of the BBM equation and the KdV equation have been of considerable concern. Zabusky and Kruskal investigated the interaction of solitary waves and the recurrence of initial states [23]. The term soliton is coined to reflect the particle like behavior of the solitary waves under interaction. The interaction of two solitons emphasized the reality of the preservation of shapes and speeds and of the steady pulse like character of solitons [24–27].

This paper is organized as follows: an introduction is in Section 1. In Section 2, the problem formulations to derive the nonlinear BBM and KdV equations are formulated. The extended direct algebraic and sech-tanh methods are analyzed in Section 3. In Section 4, the traveling solutions of the BBM and KdV equations are obtained.

2. Problem Formulation

In water wave equations, a two-dimensional inviscid, incompressible fluid with constant gravitational field is considered. The physical parameters are scaled into the definition of space, (x, y), time t and the gravitational acceleration g is in the negative y direction. Let h_0 be the undisturbed depth of the fluid and let $y = \eta(x,t)$ represent the free surface of the fluid. We also assume that the motion is irrotational and let $\phi(x, y, t)$ denote the velocity potential ($u = \nabla\phi$). The divergence-free condition on the velocity field implies that the velocity potential ϕ satisfies the Laplaces equation [28, 29]:

$$\frac{\partial^2\phi}{\partial x^2} + \frac{\partial^2\phi}{\partial y^2} = 0, \quad \text{at } -h_0 < y < \eta(x,t). \tag{1}$$

On a solid fixed boundary, the normal velocity of the fluid must vanish. For a horizontal flat bottom, we have

$$\frac{\partial\phi}{\partial y} = 0 \quad \text{at } y = -h_0. \tag{2}$$

The boundary conditions at the free surface $y = \eta(x,t)$ are given by

$$\frac{\partial\phi}{\partial y} - \frac{\partial\eta}{\partial t} - \frac{\partial\phi}{\partial x}\frac{\partial\eta}{\partial x} = 0, \tag{3}$$

$$\frac{\partial\phi}{\partial t} + \frac{1}{2}\left(\left(\frac{\partial\phi}{\partial x}\right)^2 + \left(\frac{\partial\phi}{\partial y}\right)^2\right) + g\eta = 0. \tag{4}$$

Equation (3) is a kinematic boundary condition, while (4) represents the continuity of pressure at the free surface, as derived from Bernoullis equation. The Laplace equation (1) and the boundary conditions (2) on the bottom are already linear and are independent of η. Moreover, η can be eliminated from the linear versions of (3) and (4). The first order equations for ϕ in the form

$$\frac{\partial^2\phi}{\partial x^2} + \frac{\partial^2\phi}{\partial y^2} = 0, \quad \text{at } -h_0 < y < 0, \tag{5}$$

$$\frac{\partial\phi}{\partial y} = 0, \quad \text{at } y = -h_0, \tag{6}$$

$$\frac{\partial^2\phi}{\partial t^2} + g\frac{\partial\phi}{\partial y} = 0, \quad \text{at } y = 0. \tag{7}$$

The progressive wave solution of the first order system is

$$\phi(x, y, t) = \varphi(y)\, e^{i(kx - wt)}. \tag{8}$$

Then, (5) has the solution

$$\varphi(y) = A\cosh k(y + h_0) + B\sinh k(y + h_0), \tag{9}$$

where A and B are arbitrary constants. The boundary condition (6) implies $B = 0$, while the remaining condition (7) gives the dispersion relation

$$w^2 = gk\tanh kh_0. \tag{10}$$

The dispersive effects can be combined with nonlinear effects to give

$$u_t + \frac{3}{2}\frac{c_0}{h_0}uu_x + \int_{-\infty}^{\infty} K(x - \xi)\, u_\xi(\xi, t)\, d\xi = 0, \tag{11}$$

where $u(x,t)$ is the water wave velocity and h_0 is the depth of the fluid and $c_0 = \sqrt{gh_0}$, with a kernel, $K(x)$, that is given by

$$K(x) = \frac{1}{2\pi}\int_{-\infty}^{\infty} c(k)\, e^{ikx} dx. \tag{12}$$

From Taylor expansion, the partial deferential equation (11) reduces to the KdV equation:

$$u_t + c_0u_x + \frac{3}{2}\frac{c_0}{h_0}uu_x + \frac{1}{6}c_0h_0^2u_{xxx} = 0. \tag{13}$$

The BBM model was introduced in [18] as an alternative to the KdV equation. The main argument is that the phase velocity ω/k and the group velocity $d\omega/dk$ in the KdV model are not bounded from below. In contrast, the BBM equation has a phase velocity and a group velocity both of which are bounded for all k. They also approach zero as $k \to \infty$.

The derivation of the KdV equation in [18] uses a scaling of the variables u, x, and t, and a perturbation expansion argument in such a way that the dispersive and the nonlinear effects become small. The main argument that was used in [18] to derive the BBM equation is that, to the first order in ϵ, the scaled KdV equation is equivalent to

$$u_t + u_x + uu_x - a^2u_{xxx} - b^2u_{xxt} = 0. \tag{14}$$

While the derivation presented in [18] is formally valid, it is important to note that the particular choice of the mixed derivative $-u_{xxt}$ as a replacement of u_{xxx} may seem arbitrary from the point of view of asymptotic expansions. Indeed, any admissible combination of these two terms could be valid based on the zero-order correspondence between the derivatives in space and time ($u_t = -u_x$).

3. An Analysis of the Methods

The following is given nonlinear partial differential equations (BBM and KdV equations) with two variables x and t as

$$F\left(u, u_t, u_x, u_{xx}, u_{xxx}\right) = 0 \tag{15}$$

can be converted to ordinary deferential equations:

$$F\left(u, u', u'', u'''\right) = 0, \tag{16}$$

by using a wave variable $\xi = x - ct$. The equation is integrated as all terms contain derivatives where integration constants are considered zeros.

3.1. Extended Direct Algebraic Methods. We introduce an independent variable, where $u = \phi(\xi)$ is a solution of the following third-order ODE:

$$\phi'^2 = \pm\alpha\phi^2(\xi) \pm \beta\phi^4(\xi), \tag{17}$$

where α, β are constants. We expand the solution of (16) as the following series:

$$u(\xi) = \sum_{k=0}^{m} a_k \phi^k + \sum_{k=1}^{m} b_k \phi^{-k}, \tag{18}$$

where m is a positive integer, in most cases, that will be determined. The parameter m is usually obtained by balancing the linear terms of highest order in the resulting equation with the highest order nonlinear terms. Substituting from (18) into the ODE (16) results in an algebraic system of equations in powers of ϕ that will lead to the determination of the parameters $a_k, (k = 0, 1, \ldots, m)$ and c by using Mathematica.

3.2. The Sech-Tanh Method. We suppose that $u(x,t) = u(\xi)$, where $\xi = x - ct$ and $u(\xi)$ has the following formal travelling wave solution:

$$u(\xi) = \sum_{i=1}^{n} \operatorname{sech}^{i-1}\xi \left(A_i \operatorname{sech}\xi + B_i \tanh\xi\right), \tag{19}$$

where $A_0, A_1, \ldots, A_n$ and $B_1, \ldots, B_n$ are constants to be determined.

Step 1. Equating the highest-order nonlinear term and highest-order linear partial derivative in (16) yields the value of n.

Step 2. Setting the coefficients of $(\operatorname{sech}^j \tanh^i)$ for $i = 0, 1$ and $j = 1, 2, \ldots$ to zero, we have the following set of overdetermined equations in the unknowns A_0, A_i, B_i, and c for $i = 1, 2, \ldots, n$.

Step 3. Using Mathematica and Wu ŝ elimination methods, the algebraic equations in Step 2 can be solved.

4. Application of the Methods

4.1. Exact Solutions for KdV Equation. We will employ the proposed methods to solve the KdV equation:

$$u_t + c_0 u_x + \frac{3}{2}\frac{c_0}{h_0} u u_x + \frac{1}{6} c_0 h_0^2 u_{xxx} = 0. \tag{20}$$

By assuming travelling wave solutions of the form $u(x,t) = u(\xi)$, $\xi = x - ct$, (20) is equivalent to

$$\left(c_0 - c\right) u' + \frac{3}{2}\frac{c_0}{h_0} u u' + \frac{1}{6} c_0 h_0^2 u''' = 0. \tag{21}$$

Balancing u''' with uu' in (21) gives $m = 2$; then

$$u(\xi) = a_0 + a_1\phi + a_2\phi^2 + \frac{b_1}{\phi} + \frac{b_2}{\phi^2}. \tag{22}$$

Substituting into (21) and collecting the coefficient of ϕ, we obtain a system of algebraic equations for a_0, a_1, a_2, b_1, b_2, and c. Solving this system gives the following real exact solutions.

Case I. Suppose that

$$\phi'^2 = -\alpha\phi^2(\xi) + \beta\phi^4(\xi), \tag{23}$$

by comparing them with the coefficients of ϕ^i $(i = -5, -4, -3, -2, -1, 0, 1, 2, 3)$ where $\alpha > 0$:

$$\phi(\xi) = \sqrt{\frac{\alpha}{\beta}} \sec\left(\sqrt{\alpha}\xi + \xi_0\right), \tag{24}$$

where ξ_0 is constant of integration; then we have

$$\begin{aligned} a_0 &= \frac{2}{9c_0}\left(3ch_0 - 3c_0h_0 + 2\alpha c_0 h_0^3\right), \\ a_2 &= -\frac{4}{3}\beta h_0^3, \qquad a_1 = b_1 = b_2 = 0. \end{aligned} \tag{25}$$

In this case, the generalized soliton solution can be written as

$$u_1(x,t) = \frac{2}{9}h_0 \times \left(-3 + 3\frac{c}{c_0} + 2\alpha h_0^2\left(1 - 3\sec^2\left(\sqrt{\alpha}\left(x - ct\right) + \xi_0\right)\right)\right). \tag{26}$$

Figure 1 shows the travelling wave solutions with $(\alpha = 0.16, \beta = 0.25, k = 0.5, h_0 = 0.25, c_0 = 2)$ in the interval $[-10, 10]$ and time in the interval $[0, 0.1]$.

Case II. Suppose that

$$\phi'^2 = \alpha\phi^2(\xi) - \beta\phi^4(\xi), \tag{27}$$

by comparing them with the coefficients of ϕ^i and $\alpha > 0$ under condition $\phi(0) = \sqrt{\alpha/\beta}$, so

$$\phi(\xi) = \sqrt{\frac{\alpha}{\beta}} \operatorname{sech}\left(\sqrt{\alpha}\xi\right); \tag{28}$$

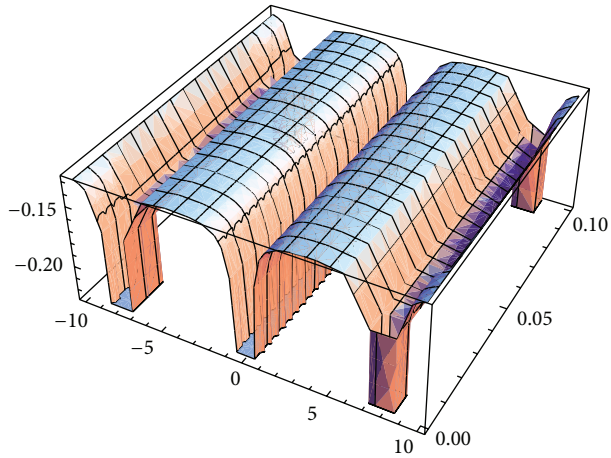

Figure 1: Travelling waves solutions (26) are plotted: periodic solitary waves.

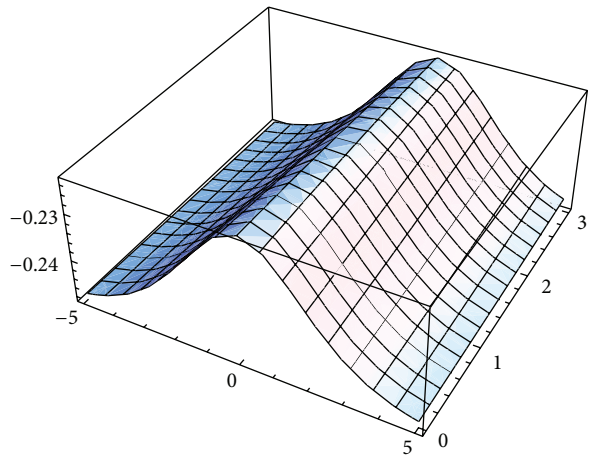

Figure 2: Travelling waves solutions (30) are plotted: bright solitary waves.

then we have

$$a_0 = \frac{2}{9c_0}\left(-3c_0h_0 + 3ch_0 - 2\alpha c_0 h_0^3\right),$$
$$a_2 = -\frac{4}{3}\beta h_0^3, \qquad a_1 = b_1 = b_2 = 0. \tag{29}$$

In this case, the generalized soliton solution can be written as

$$u_2(x,t) = \frac{2}{9}h_0\left(-3+3\frac{c}{c_0} - 2\alpha h_0^2\left(1+3\operatorname{sech}^2\left(\sqrt{\alpha}\,(x-ct)\right)\right)\right). \tag{30}$$

Figure 2 shows the travelling wave solutions with ($\alpha = 0.16, k = 0.25, h_0 = 0.5, c_0 = 0.9$) in the interval $[-5, 5]$ and time in the interval $[0, 3]$.

The stability of soliton solution is stable at $t = 0, \alpha = 0.16$ if

$$k > c_0\left[1 - 0.048h_0^2\right]. \tag{31}$$

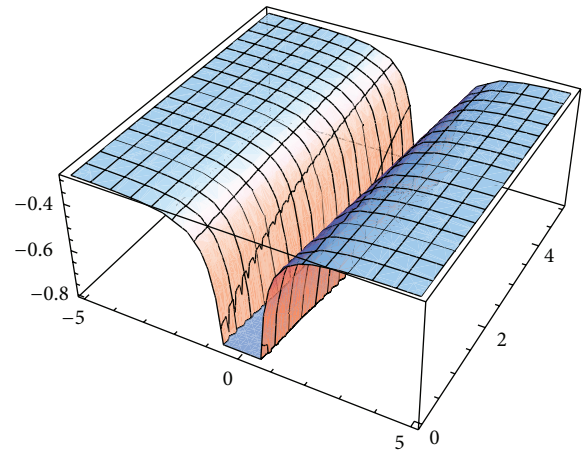

Figure 3: Travelling waves solutions (35) are plotted: dark solitary waves.

Case III. Suppose that

$$\phi'^2 = \alpha\phi^2(\xi) + \beta\phi^4(\xi), \tag{32}$$

by comparing them with the coefficients of ϕ^i and $\alpha > 0$ under condition $\beta = 1/4$ so

$$\phi(\xi) = 2\sqrt{\alpha}\operatorname{csch}\left(\sqrt{\alpha}\xi\right) \tag{33}$$

and we have

$$a_0 = \frac{2}{9c_0}\left(-3c_0h_0 + 3ch_0 - 2\alpha c_0 h_0^3\right),$$
$$a_2 = -\frac{h_0^3}{3}, \qquad a_1 = b_1 = b_2 = 0. \tag{34}$$

In this case, the generalized soliton solution can be written as

$$u_3(x,t) = \frac{2}{9}h_0\left(-3+3\frac{c}{c_0} - 2\alpha h_0^2\left(1+3\operatorname{csch}^2\left[\sqrt{\alpha}\,(x-ct)\right]\right)\right). \tag{35}$$

Figure 3 shows the travelling wave solutions with ($\alpha = 0.25, k = 0.16, h_0 = 0.5, c_0 = 0.9$) in the interval $[-5, 5]$ and time in the interval $[0, 5]$.

Using Sech-Tanh Method. Consider

$$u(\xi) = A_0 + A_1\operatorname{sech}\xi + B_1\tanh\xi + A_2\operatorname{sech}\xi^2 + B_2\tanh\xi\operatorname{sech}\xi. \tag{36}$$

Substituting from (36) into (21), setting the coefficients of $(\operatorname{sech}^j \tanh^i)$ for $i = 0, 1$ and $j = 1, 2, 3, 4$ to zero, we have the following set of overdetermined equations in the unknowns A_0, A_1, A_2, B_1, B_2, and c. Solve the set of equations

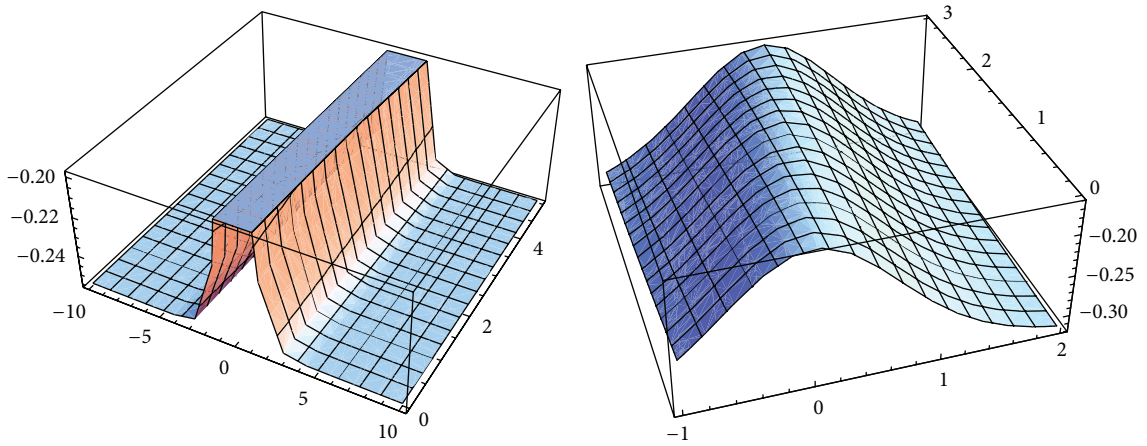

(a) (b)

Figure 4: Travelling waves solutions (40) are plotted: bright solitary waves.

of coefficients of $(\operatorname{sech}^j \tanh^i)$, by using Mathematica and Wu ŝ elimination method; we obtain the following solutions:

$$\text{(i)}\ A_0 = -\frac{h_0\left(-6k + 6c_0 + c_0h_0^2\right)}{9c_0}$$
$$A_2 = \frac{2h_0^3}{3}, \qquad B_2 = \mp\frac{2}{3}ih_0^3, \qquad A_1 = B_1 = 0, \tag{37}$$

and then the solution of KdV equation as

$$u_4(x,t) = \frac{h_0}{9c_0}\Big(6k + c_0 \times \Big(-6 + h_0^2\,(-1 + 6\operatorname{sech}[x - kt] \times (\operatorname{sech}[x - kt] \pm i\tanh[x - kt]))\Big)\Big). \tag{38}$$

This soliton solution is stable if

$$k > c_0\left(1 + \frac{\left(4 + e^{20}\right)h_0^2}{15\left(1 + e^{20}\right)}\right)$$

$$\text{(ii)}\ A_0 = \frac{2}{9}\left(-3h_0 + \frac{3kh_0}{c_0} - 2h_0^3\right), \tag{39}$$
$$A_2 = \frac{4h_0^3}{3}, \qquad A_1 = B_1 = B_2 = 0,$$

and the solution of KdV equation is

$$u_5(x,t) = \frac{2}{9}h_0\left(-3 + \frac{3k}{c_0} + \left(-2 + 6\operatorname{sech}^2[x - kt]\right)h_0^2\right). \tag{40}$$

Figure 4(a) shows the travelling wave solutions with $(k = 0.1, h_0 = 0.5, c_0 = 0.25)$ in the interval $[-10, 10]$ and time in the interval $[0, 5]$.

Figure 4(b) shows the travelling wave solutions with $(k = 0.16, h_0 = 0.5, c_0 = 0.9)$ in the interval $[-1, 2]$ and time in the interval $[0, 3]$.

This soliton solution is stable if

$$k > c_0\left(1 + \frac{\left(13 + 7e^{20}\right)h_0^2}{15\left(1 + e^{20}\right)}\right). \tag{41}$$

4.2. Solutions for Benjamin-Bona-Mahony Equation. The Benjamin-Bona-Mahony equation (14) can be transformed to ODE as

$$(k - c)u' + kuu' + \left(b^2k^2c - a^2k^3\right)u''' = 0. \tag{42}$$

Balancing u''' with uu' in (21) gives $m = 2$.

First Case. Let finite expansion

$$u(\xi) = A_0 + A_1\operatorname{sech}\xi + A_2\operatorname{sech}^2\xi + B_1\cosh\xi + B_2\cosh^2\xi. \tag{43}$$

Substituting from (43) into (42) and setting the coefficients of $(\operatorname{sech}^j \cosh^i)$ for $i, j = 1, 2, 3, 4$ to zero, we have the following set of overdetermined equations in the unknowns A_0, A_1, B_1, and B_2. By solving the set of equations of coefficients of $(\operatorname{sech}^j \cosh^i)$ by using Mathematica method, we obtain the following solution:

$$A_1 = B_1 = B_2 = 0, \qquad A_0 = \frac{c - k - 4b^2k^2c + 4a^2k^3}{k},$$
$$A_2 = 12\left(b^2ck - a^2k^2\right). \tag{44}$$

The exact soliton solution of Benjamin-Bona-Mahony equation is

$$u(x,t) = \left(\frac{c - k - 4b^2k^2c + 4a^2k^3}{k}\right) + 12\left(b^2ck - a^2k^2\right)\operatorname{sech}^2(kx - ct). \tag{45}$$

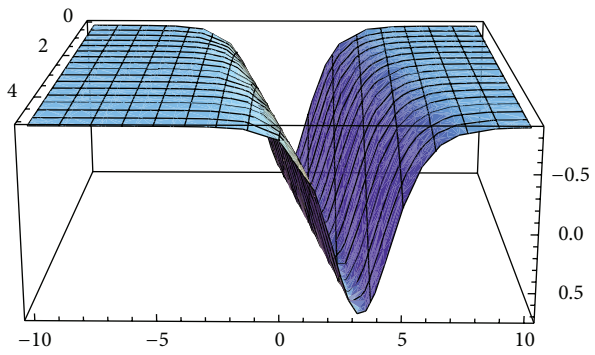

Figure 5: Travelling waves solutions (45) are plotted: dark solitary waves.

Figure 5 shows the travelling wave solutions with ($k = 0.6, c = 0.4, a^2 = 9/10, b^2 = 19/10$) in the interval $[-10, 10]$ and time in the interval $[0, 5]$.

Second Case. Let finite expansion

$$u(\xi) = A_0 + A_1 \coth\xi + A_2 \coth^2\xi + B_1 \tanh\xi + B_2 \tanh^2\xi. \tag{46}$$

Then, we obtain the following solutions:

$$A_1 = B_1 = 0, \qquad A_0 = \frac{c - k + 8b^2k^2c - 8a^2k^3}{k}, \qquad A_2 = B_2 = -12\left(b^2ck - a^2k^2\right) \tag{47}$$

so that the exact soliton solution be

$$u(x,t) = \left(\frac{c - k + 8b^2k^2c - 8a^2k^3}{k}\right) - 12\left(b^2ck - a^2k^2\right) \times \left(\tanh^2(kx - ct) + \coth^2(kx - ct)\right). \tag{48}$$

Figure 6 shows the travelling wave solutions with ($k = 0.6, c = 0.4, a^2 = 9/10, b^2 = 19/10$) in the interval $[-10, 10]$ and time in the interval $[0, 5]$.

5. Conclusion

By implementing the extended direct algebraic and modified sech-tanh methods, we presented new traveling wave solutions of the KdV and BBM equations. We obtained the water wave velocity potential of KdV equation in periodic form and bright and dark solitary wave solutions by using the extended direct algebraic method. Using the modified sech-tanh method, the water wave velocity of KdV equation in form of bright and dark solitary wave solutions. The water wave velocity potentials of BBM equation are deduced in form of dark solitary wave solutions. The structures of the obtained solutions are distinct and stable.

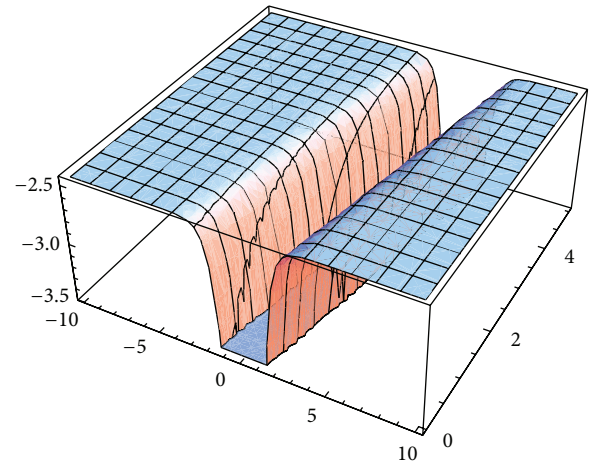

Figure 6: Travelling waves solutions (48) are plotted: dark solitary waves.

Conflict of Interests

The authors declare that there is no conflict of interests regarding the publication of this paper.

References

[1] A. R. Seadawy, "New exact solutions for the KdV equation with higher order nonlinearity by using the variational method," *Computers & Mathematics with Applications*, vol. 62, no. 10, pp. 3741–3755, 2011.

[2] M. A. Helal and A. R. Seadawy, "Benjamin-Feir instability in nonlinear dispersive waves," *Computers & Mathematics with Applications*, vol. 64, no. 11, pp. 3557–3568, 2012.

[3] A. R. Seadawy and K. El-Rashidy, "Traveling wave solutions for some coupled nonlinear evolution equations," *Mathematical and Computer Modelling*, vol. 57, no. 5-6, pp. 1371–1379, 2013.

[4] F. Yan, H. Liu, and Z. Liu, "The bifurcation and exact travelling wave solutions for the modified Benjamin-BONa-Mahoney (mBBM) equation," *Communications in Nonlinear Science and Numerical Simulation*, vol. 17, no. 7, pp. 2824–2832, 2012.

[5] M. J. Ablowitz and P. A. Clarkson, *Soliton, Nonlinear Evolution Equations and Inverse Scattering*, Cambridge University Press, New York, NY, USA, 1991.

[6] R. Hirota, "Exact solution of the korteweg-de vries equation for multiple Collisions of solitons," *Physical Review Letters*, vol. 27, no. 18, pp. 1192–1194, 1971.

[7] A.-M. Wazwaz, "New travelling wave solutions of different physical structures to generalized BBM equation," *Physics Letters A: General, Atomic and Solid State Physics*, vol. 355, no. 4-5, pp. 358–362, 2006.

[8] M. R. Miurs, *Backlund Transformation*, Springer, Berlin, Germany, 1978.

[9] X. Liu, L. Tian, and Y. Wu, "Exact solutions of the generalized Benjamin-BONa-Mahony equation," *Mathematical Problems in Engineering*, vol. 2010, Article ID 796398, 5 pages, 2010.

[10] Ş. Kuru, "Traveling wave solutions of the BBM-like equations," *Journal of Physics A: Mathematical and Theoretical*, vol. 42, no. 37, Article ID 375203, 12 pages, 2009.

[11] P. G. Estévez, Ş. Kuru, J. Negro, and L. M. Nieto, "Travelling wave solutions of the generalized Benjamin-Bona-Mahony

equation," *Chaos, Solitons & Fractals*, vol. 40, no. 4, pp. 2031–2040, 2009.

[12] A. Wazwaz, "Exact solutions with compact and noncompact structures for the one-dimensional generalized Benjamin-Bona-Mahony equation," *Communications in Nonlinear Science and Numerical Simulation*, vol. 10, no. 8, pp. 855–867, 2005.

[13] Q.-H. Feng, F.-W. Meng, and Y.-M. Zhang, "Traveling wave solutions for two nonlinear evolution equations with nonlinear terms of any order," *Chinese Physics B*, vol. 20, no. 12, Article ID 120202, 2011.

[14] X. Liu, L. Tian, and Y. Wu, "Exact solutions of four generalized Benjamin-Bona-Mahony equations with any order," *Applied Mathematics and Computation*, vol. 218, no. 17, pp. 8602–8613, 2012.

[15] S. Abbasbandy and A. Shirzadi, "The first integral method for modified Benjamin-Bona-Mahony equation," *Communications in Nonlinear Science and Numerical Simulation*, vol. 15, no. 7, pp. 1759–1764, 2010.

[16] B. Hong and D. Lu, "New exact solutions for the generalized BBM and Burgers-BBM equations," *World Journal of Modelling and Simulation*, vol. 4, pp. 243–249, 2008.

[17] W. Hereman, "Shallow water waves and solitary waves," in *Mathematics of Complexity and Dynamical Systems*, pp. 1520–1532, 2011.

[18] J. Nickel, "Elliptic solutions to a generalized BBM equation," *Physics Letters. A*, vol. 364, no. 3-4, pp. 221–226, 2007.

[19] K. Singh, R. K. Gupta, and S. Kumar, "Benjamin-Bona-Mahony (BBM) equation with variable coefficients: similarity reductions and Painlevé analysis," *Applied Mathematics and Computation*, vol. 217, no. 16, pp. 7021–7027, 2011.

[20] T. B. Benjamin, J. L. Bona, and J. J. Mahony, "Model equations for long waves in nonlinear dispersive systems," *Philosophical Transactions of the Royal Society of A: Mathematical and Physical Sciences*, vol. 272, no. 1220, pp. 47–78, 1972.

[21] J. Saut and N. Tzvetkov, "Global well-posedness for the KP-BBM equations," *Applied Mathematics Research eXpress*, no. 1, pp. 1–16, 2004.

[22] V. Varlamov and Y. Liu, "Cauchy problem for the Ostrovsky equation," *Discrete and Continuous Dynamical Systems A*, vol. 10, no. 3, pp. 731–753, 2004.

[23] N. J. Zabusky and M. D. Kruskal, "Interaction of "solitons" in a collisionless plasma and the recurrence of initial states," *Physical Review Letters*, vol. 15, no. 6, pp. 240–243, 1965.

[24] A. Wazwaz and M. A. Helal, "Nonlinear variants of the BBM equation with compact and noncompact physical structures," *Chaos, Solitons and Fractals*, vol. 26, no. 3, pp. 767–776, 2005.

[25] M. A. Helal and A. R. Seadawy, "Variational method for the derivative nonlinear Schrödinger equation with computational applications," *Physica Scripta*, vol. 80, no. 3, Article ID 035004, 2009.

[26] A. R. Seadawy, "Exact solutions of a two-dimensional nonlinear Schrödinger equation," *Applied Mathematics Letters*, vol. 25, no. 4, pp. 687–691, 2012.

[27] A. R. Seadawy, "Stability analysis for Zakharov-Kuznetsov equation of weakly nonlinear ion-acoustic waves in a plasma," *Computers & Mathematics with Applications*, vol. 67, no. 1, pp. 172–180, 2014.

[28] A. Jeffrey and T. Kakutani, "Weak nonlinear dispersive waves: a discussion centered around the Korteweg-de Vries equation," *SIAM Review*, vol. 14, pp. 582–643, 1972.

[29] R. Fetecau and D. Levy, "Approximate model equations for water waves," *Communications in Mathematical Sciences*, vol. 3, no. 2, pp. 159–170, 2005.

Hindawi Publishing Corporation
Abstract and Applied Analysis
Volume 2014, Article ID 408230, 11 pages
http://dx.doi.org/10.1155/2014/408230

Research Article

Nonlinear Nanofluid Flow over Heated Vertical Surface with Sinusoidal Wall Temperature Variations

S. S. Motsa,[1] F. G. Awad,[2] and M. Khumalo[2]

[1] *School of Mathematical Sciences, University of KwaZulu-Natal, Private Bag X01, Scottsville, Pietermaritzburg 3209, South Africa*
[2] *Department of Pure and Applied Mathematics, University of Johannesburg, P.O. Box 524, Auckland Park, Johannesburg 2006, South Africa*

Correspondence should be addressed to S. S. Motsa; sandilemotsa@gmail.com

Received 15 July 2014; Revised 15 August 2014; Accepted 15 August 2014; Published 14 October 2014

Academic Editor: Santanu Saha Ray

Copyright © 2014 S. S. Motsa et al. This is an open access article distributed under the Creative Commons Attribution License, which permits unrestricted use, distribution, and reproduction in any medium, provided the original work is properly cited.

The nonlinear density temperature variations in two-dimensional nanofluid flow over heated vertical surface with a sinusoidal wall temperature are investigated. The model includes the effects of Brownian motion and thermophoresis. Using the boundary layer approximation, the two-dimensional momentum, heat, and mass transfer equations are transferred to nonlinear partial differential equations form and solved numerically using a new method called spectral local linearisation method. The effects of the governing parameters on the fluid properties and on the heat and nanomass transfer coefficients are determined and shown graphically.

1. Introduction

In recent years, nanofluids have attracted a considerable amount of interest due to their novel properties that make them potentially useful in a number of industrial applications including transportation, power generation, micromanufacturing, thermal therapy for cancer treatment, chemical and metallurgical sectors, heating, cooling, ventilation, and air-conditioning. The term nanofluid is used to refer to a solid-liquid mixture with a continuous phase in which nanoscale particles are dispersed in conventional base fluids. The nanofluid reference was first used by Choi [1]. The nanofluid can be readily configured either in a low state, where it conducts heat poorly, or in a high state, where the dissipation is more efficient [2]. The nanoparticles are made of various materials such as oxide ceramics, nitride ceramics, carbide ceramics, metals, semiconductors, and composite materials such as alloyed nanoparticles while the base fluids are usually water, ethylene glycol, toluene, and oil [3, 4]. They are also important for the production of nanostructured materials for the engineering of complete fluids and for cleaning oil from surfaces due to their excellent wetting and spreading behaviour [4, 5]. Nanofluids can also be used as smart materials working as a heat valve to control the flow of heat. A good review of the literature on nanofluids can be found in Buongiorno [6]. Kuznetsov and Nield [7] investigated the problem of natural convective boundary-layer flow of a nanofluid past a vertical plate. Their model considered the nanoparticle Brownian motion and thermophoresis with simple boundary conditions; namely, both the temperature and the nanoparticle fraction were constant along the wall. Using the Darcy model, Nield and Kuznetsov [8] studied the Cheng-Minkowycz problem of natural convection past a vertical plate in a porous medium saturated with a nanofluid. Khan and Pop [9] considered the effects of Brownian motion and thermophoresis in the laminar fluid flow from a stretching flat surface in a nanofluid. An experimental study of the problem was made for flow in vertical square enclosures of different sizes by Ho et al. [10]. Similar investigations have been conducted by, among others, Khan and Aziz [11], Rashad et al. [12], Aziz et al. [13], Rana et al. [14], Hajipour and Molaei Dehkordi [15], and Chanda and Rana [16].

The nonlinear temperature-density relationship in which the flow is driven by buoyancy may exert a strong influence on the flow and heat transfer characteristics. It is of practical importance in geothermal and engineering applications; for example, the residual warm water discharged from a geothermal power plant is usually disposed off

from wells through subsurface reinjection. Using a parabolic temperature-density relationship, Korovkin and Andrievskii [17] investigated a fully developed free-convective flow above a horizontal linear heat source and on a flat impermeable vertical semi-infinite plate for three types of thermal boundary conditions, namely, an adiabatic surface, a constant temperature, and a constant heat flux on the surface. Vajravelu et al. [18] studied the problem of free convection flow at a vertical flat plate embedded in a saturated porous medium in the presence of heat sources (or sinks) with nonlinear density temperature variation. Fluid flow problems involving the nonlinear density temperature variation have been investigated by [19–22] among others. The recent study by Motsa et al. [23] investigated the problem of unsteady double diffusive convection flow over a stretching flat plate with nonlinear density temperature variation using a new version of the spectral homotopy analysis method.

The objective of this study is to consider the effects of the nonlinear density temperature variations as well as the Brownian motion and thermophoresis on nanofluid flow over heated vertical surface with a sinusoidal wall temperature. It is well known that power law surface temperature distributions give rise to self-similar boundary-layer flows (see [24, 25]). To define the periodic array of heaters behind or within the wall, Rees [26] proposed another form of surface temperature variation with sinusoidal variations about the mean temperature which is held above the ambient temperature of the fluid. These types of boundary heating have been investigated by, among others, Pop and Ingham [27], Roy and Hossain [28], Saha et al. [29], Molla et al. [30], and Rana and Bhargava [31]. The momentum, heat, and mass transfer equations are reduced into nonlinear partial differential equations form. The high nonlinear systems governing the model are solved using a new method of solving systems of differential equations called the local linearisation method (LLM). The LLM is an innovative method that seeks to decouple systems of nonlinear differential equation and applies the Chebyshev spectral collocation in solving the resulting sequence of decoupled equations. The LLM was introduced by Motsa [32] for the solution of general nonlinear boundary-layer flow equations defined as systems of ordinary differential equations. The method has also been successfully used with domain transformation techniques in [33] to solve natural convection boundary-layer flow problem. In all the cited works, where the LLM has previously been applied, the governing equations were systems of ordinary differential equations. In this work we extend the application of the LLM to systems of nonlinear partial differential equations.

2. Mathematical Formulation

We consider nonlinear convection from a vertical flat surface embedded in a nanofluid of ambient temperature $\overline{T}_\infty$. We assume that the surface is kept at a steady temperature

$$\overline{T} = \overline{T}_\infty + \left(\overline{T}_w - \overline{T}_\infty\right)\left(1 + A\sin\left(\frac{\pi\overline{x}}{L}\right)\right), \tag{1}$$

where A is the relative amplitude of the surface temperature variations and $2L$ is the wavelength of the variations, $\overline{T}_w > \overline{T}_\infty$ for a heated surface and $\overline{T}_w < \overline{T}_\infty$ corresponding to a cooled surface. The temperature between the surface and the medium is assumed to be sufficiently large; hence the convection region is thick. In the buoyancy driven flow it is assumed that the density of the fluid ρ depends nonlinearly on the temperature $\overline{T}$ of the fluid. In presence of Boussinesq's approximation the governing equations for the problem can be written in the form

$$\begin{aligned}
&\frac{\partial\overline{u}}{\partial\overline{x}} + \frac{\partial\overline{v}}{\partial\overline{y}} = 0,\\
&\rho_{f_\infty}\left[\overline{u}\frac{\partial\overline{u}}{\partial\overline{x}} + \overline{v}\frac{\partial\overline{u}}{\partial\overline{y}}\right] = \mu\frac{\partial^2\overline{u}}{\partial\overline{y}^2} + \left(1-\overline{\phi}_\infty\right)g\rho_{f_\infty}\\
&\qquad\times\left[\beta_0\left(\overline{T}-\overline{T}_\infty\right) + \beta_1\left(\overline{T}-\overline{T}_\infty\right)^2\right]\\
&\qquad-\left(\rho_p - \rho_{f_\infty}\right)g\left(\overline{\phi}-\overline{\phi}_\infty\right),\\
&\overline{u}\frac{\partial\overline{T}}{\partial\overline{x}} + \overline{v}\frac{\partial\overline{T}}{\partial\overline{y}} = \alpha_m\frac{\partial\overline{T}}{\partial\overline{y}^2} + \tau\left[D_B\frac{\partial\overline{\phi}}{\partial\overline{y}}\frac{\partial\overline{T}}{\partial\overline{y}} + \frac{D_T}{\overline{T}_\infty}\left(\frac{\partial\overline{T}}{\partial\overline{y}}\right)^2\right],\\
&\overline{u}\frac{\partial\overline{\phi}}{\partial\overline{x}} + \overline{v}\frac{\partial\overline{\phi}}{\partial\overline{y}} = D_B\frac{\partial^2\overline{\phi}}{\partial\overline{y}^2} + \frac{D_T}{\overline{T}_\infty}\frac{\partial^2\overline{T}}{\partial\overline{y}^2},
\end{aligned} \tag{2}$$

where $\overline{u}$ and $\overline{v}$ are the velocity components along the x- and y-directions, respectively, $\overline{T}$ and $\overline{\phi}$ are the local fluid temperature and nanoparticle volume fraction, ρ_∞ is the constant fluid density, $\overline{\phi}_\infty$ is the nanoparticle volume fraction, β_0, β_1 are thermal expansion coefficients, μ is the fluid viscosity, α_m is the effective thermal diffusivity, D_B is the Brownian diffusion coefficient, D_T is thermophoresis diffusion coefficient, ρ_{f_∞} is the fluid density, ρ_P is particle mass density, g is the acceleration due to the gravity, ρc_P is the effective heat capacity of the nanoparticle material, and τ is a parameter defined by $\rho c_f/\rho c_P$.

We introduce the following nondimensional variables:

$$\begin{aligned}
&(x,y) = \frac{\left(\overline{x},\overline{y}\mathrm{Gr}^{1/4}\right)}{L}, \qquad (u,v) = \frac{\left(\overline{u},\overline{v}\mathrm{Gr}^{1/4}\right)}{U_c},\\
&\frac{\overline{T}-\overline{T}_\infty}{\overline{T}_w-\overline{T}_\infty} = \theta, \qquad \frac{\overline{\phi}-\overline{\phi}_\infty}{\overline{\phi}_w-\overline{\phi}_\infty} = \phi.
\end{aligned} \tag{3}$$

The governing equations (2) can be presented as

$$\frac{\partial u}{\partial x} + \frac{\partial v}{\partial y} = 0, \tag{4}$$

$$u\frac{\partial u}{\partial x} + v\frac{\partial u}{\partial y} = \frac{\partial^2 u}{\partial y^2} + \theta + \sigma\theta^2 - \mathrm{Nr}\phi, \tag{5}$$

$$u\frac{\partial\theta}{\partial x}+v\frac{\partial\theta}{\partial y}=\frac{1}{\mathrm{Pr}}\frac{\partial^2\theta}{\partial y^2}+\mathrm{Nb}\frac{\partial\phi}{\partial y}\frac{\partial\theta}{\partial y}+\mathrm{Nt}\left(\frac{\partial\theta}{\partial y}\right)^2, \quad (6)$$

$$\mathrm{Le}\left(u\frac{\partial\phi}{\partial x}+v\frac{\partial\phi}{\partial y}\right)=\frac{\partial^2\phi}{\partial y^2}+\frac{\mathrm{Nt}}{\mathrm{Nb}}\frac{\partial^2\theta}{\partial y^2}, \quad (7)$$

subject to the boundary conditions

$$u=0,\quad v=0,\quad \theta=1+A\sin\pi x,\quad \phi=1 \text{ at } y=0, \quad (8)$$
$$u\longrightarrow 0,\quad \theta\longrightarrow 0,\quad \phi\longrightarrow 0 \text{ as } y\longrightarrow\infty.$$

The various nondimensional parameters appearing in (4)–(7) are the nanofluid Grashof number Gr, the nonlinear temperature parameter σ, the buoyancy ratio Nr, the Prandtl number Pr, the Lewis number Le, the Brownian motion parameter Nb, and the thermophoresis parameter Nt. These parameters are defined as

$$\mathrm{Gr}=\frac{\left(1-\phi_\infty\right)\beta_0 g\left(\overline{T}_w-\overline{T}_\infty\right)L^3}{\nu^2},\qquad \sigma=\frac{\beta_1}{\beta_0}\left(\overline{T}_w-\overline{T}_\infty\right),$$
$$\mathrm{Nr}=\frac{\left(\rho_p-\rho_{f_\infty}\right)}{\left(1-\overline{\phi}_\infty\right)\beta_0\rho_{f_\infty}}\frac{\left(\overline{\phi}_w-\overline{\phi}_\infty\right)}{\left(\overline{T}_w-\overline{T}_\infty\right)},\qquad \mathrm{Pr}=\frac{\nu}{\alpha_m},$$
$$\mathrm{Le}=\frac{\nu}{D_B},\qquad \mathrm{Nb}=\frac{\tau D_B\left(\overline{\phi}_w-\overline{\phi}_\infty\right)}{\nu},$$
$$U_c=\frac{\nu}{L}\mathrm{Gr}^{1/2}. \quad (9)$$

Introducing the stream function $\psi(x,y)$, where $u=\partial\psi/\partial y$ and $v=-\partial\psi/\partial x$, the two-dimensional equations (5)–(7) will take the form

$$\frac{\partial\psi}{\partial y}\frac{\partial^2\psi}{\partial x\partial y}-\frac{\partial\psi}{\partial x}\frac{\partial^2\psi}{\partial y^2}=\frac{\partial^3\psi}{\partial y^3}+\theta+\sigma\theta^2-\mathrm{Nr}\phi,$$
$$\left(\frac{\partial\psi}{\partial y}\frac{\partial\theta}{\partial x}-\frac{\partial\psi}{\partial x}\frac{\partial\theta}{\partial y}\right)=\frac{1}{\mathrm{Pr}}\frac{\partial^2\theta}{\partial y^2}+\left[\mathrm{Nb}\frac{\partial\phi}{\partial y}\frac{\partial\theta}{\partial y}+\mathrm{Nt}\left(\frac{\partial\theta}{\partial y}\right)^2\right],$$
$$\mathrm{Le}\left(\frac{\partial\psi}{\partial y}\frac{\partial\phi}{\partial x}-\frac{\partial\psi}{\partial x}\frac{\partial\phi}{\partial y}\right)=\frac{\partial^2\phi}{\partial y^2}+\frac{\mathrm{Nt}}{\mathrm{Nb}}\frac{\partial^2\theta}{\partial y^2}. \quad (10)$$

The boundary conditions in (8) can be written in terms of the stream function as

$$\frac{\partial\psi}{\partial x}=0,\quad \frac{\partial\psi}{\partial y}=0,\quad \theta=1A\sin\pi x,\quad \phi=1 \text{ at } y=0,$$
$$\frac{\partial\psi}{\partial y}\longrightarrow 0,\quad \theta\longrightarrow 0,\quad \phi\longrightarrow 0 \text{ as } y\longrightarrow\infty. \quad (11)$$

Equations (10) can further be simplified by introducing the following variables:

$$\psi=x^{3/4}f(x,\eta),\qquad \theta=\theta(x,\eta),\qquad \phi=\phi(x,\eta),$$
$$\eta=yx^{-1/4}. \quad (12)$$

Using the similarity variables defined in (12), equations (10) along with the boundary conditions (11) reduce to the following two-dimensional boundary value problem:

$$\frac{\partial^3 f}{\partial\eta^3}+\frac{3}{4}f\frac{\partial^2 f}{\partial\eta^2}-\frac{1}{2}\left(\frac{\partial f}{\partial\eta}\right)^2+\theta+\sigma\theta^2-\mathrm{Nr}\phi=x\left(\frac{\partial f}{\partial\eta}\frac{\partial^2 f}{\partial x\partial\eta}-\frac{\partial^2 f}{\partial\eta^2}\frac{\partial f}{\partial x}\right), \quad (13)$$

$$\frac{1}{\mathrm{Pr}}\frac{\partial^2\theta}{\partial\eta^2}+\frac{3}{4}f\frac{\partial\theta}{\partial\eta}+\left[\mathrm{Nb}\frac{\partial\phi}{\partial\eta}\frac{\partial\theta}{\partial\eta}+\mathrm{Nt}\left(\frac{\partial\theta}{\partial\eta}\right)^2\right]=x\left(\frac{\partial f}{\partial\eta}\frac{\partial\theta}{\partial x}-\frac{\partial f}{\partial x}\frac{\partial\theta}{\partial\eta}\right), \quad (14)$$

$$\frac{1}{\mathrm{Le}}\frac{\partial^2\phi}{\partial\eta^2}+\frac{3}{4}f\frac{\partial\phi}{\partial\eta}+\frac{1}{\mathrm{Le}}\frac{\mathrm{Nt}}{\mathrm{Nb}}\frac{\partial^2\theta}{\partial\eta^2}=x\left(\frac{\partial f}{\partial\eta}\frac{\partial\phi}{\partial x}-\frac{\partial f}{\partial x}\frac{\partial\phi}{\partial\eta}\right), \quad (15)$$

with the boundary conditions

$$f(x,0)=0,\qquad \frac{\partial f}{\partial\eta}(x,0)=0,$$
$$\theta(x,0)=1+A\sin\pi x,\qquad \phi(x,0)=1, \quad (16)$$
$$\frac{\partial f}{\partial\eta}(x,\infty)=0,\qquad \theta(x,\infty)=0,\qquad \phi(x,\infty)=0.$$

3. Numerical Solution

In this section we present the numerical method used to solve the governing nonlinear system of PDEs (13)–(16). The local linearisation method (LLM) approach is used to decouple the equations leading to a linear system which is subsequently solved using the Chebyshev spectral collocation method. The basic idea behind the LLM stems from the combination of the Gauss-Seidel method for decoupling equations and the Newton-Raphson based quasilinearisation. In this regard, linearisation in the momentum equation (13) is applied only in terms involving $f(\eta)$ and its derivatives. All other terms are assumed to be known from previous iterations. In the energy equation (14), linearisation is applied only to terms involving $\theta(\eta)$ and its derivatives. The terms involving $\phi(\eta)$ are assumed to be known from previous iteration while the updated solution for f(η) at the current iteration is used. Similarly, in the mass transfer equation (15), only terms in $\phi(\eta)$ are linearised while terms in $f(\eta)$ and $\theta(\eta)$ are assumed to be now known at the current iteration (denoted by $r+1$). In each case, the quasilinearisation is applied by assuming that the difference between the functions at the current and previous iterations is small. For example, in the case of $f(\eta)$,

this difference is denoted by $f_{r+1} - f_r$. Thus applying the LLM on (13)–(16) gives

$$f'''_{r+1} + a_{1,r} f''_{r+1} + a_{2,r} f'_{r+1} + a_{3,r} f_{r+1} + a_{4,r} = a_{5,r} \frac{\partial f'_{r+1}}{\partial x} + a_{6,r} \frac{\partial f_{r+1}}{\partial x}, \tag{17}$$

$$\frac{1}{\mathrm{Pr}} \theta''_{r+1} + b_{1,r} \theta'_{r+1} + b_{2,r} = b_{3,r} \frac{\partial \theta_{r+1}}{\partial x}, \tag{18}$$

$$\frac{1}{\mathrm{Le}} \phi''_{r+1} + c_{1,r} \phi'_{r+1} + c_{2,r} = b_{3,r} \frac{\partial \phi_{r+1}}{\partial x}, \tag{19}$$

where the primes denote partial derivatives with respect to η. The boundary conditions are given by

$$f_{r+1}(x,0) = 0, \qquad f'_{r+1}(x,0) = 0,$$
$$\theta_{r+1}(x,0) = 1 + A \sin \pi x, \qquad \phi_{r+1}(x,0) = 1,$$
$$f'_{r+1}(x,\infty) = 0, \qquad \theta_{r+1}(x,\infty) = 0, \qquad \phi_{r+1}(x,\infty) = 0. \tag{20}$$

The coefficients in (17)–(19) are defined as

$$a_{1,r} = \frac{3}{4} f_r + x \frac{\partial f_r}{\partial x}, \qquad a_{2,r} = -f'_r - x \frac{\partial f'_r}{\partial x}, \qquad a_{3,r} = \frac{3}{4} f''_r,$$
$$a_{4,r} = \theta_r + \sigma \theta_r^2 - N_r \phi_r + \frac{1}{2}\left(f'_r\right)^2 - \frac{3}{4} f_r f''_r + x\left(f'_r \frac{\partial f'_r}{\partial x} - f''_r \frac{\partial f_r}{\partial x}\right),$$
$$a_{5,r} = x f'_r, \qquad a_{6,r} = -x f''_r,$$
$$b_{1,r} = \frac{3}{4} f_r + N_b \phi'_r + 2 N_t \theta'_r + x \frac{\partial f_r}{\partial x},$$
$$b_{2,r} = -N_t\left(\theta'_r\right)^2, \qquad b_{3,r} = x f'_r, \qquad c_{1,r} = \frac{3}{4} f_r + x \frac{\partial f_r}{\partial x},$$
$$c_{2,r} = \frac{1}{\mathrm{Le}} \frac{N_t}{N_b} \theta'_r, \qquad c_{3,r} = x f'_r. \tag{21}$$

To solve the linearised system of (17)-(18) we employ the Chebyshev spectral collocation method to discretize in the η-direction and use an implicit finite difference method in the x-direction. To this end, we define the grid points on (η, x) as

$$\eta_j = \cos \frac{\pi j}{N_x}, \qquad x^n = n \Delta x,$$
$$j = 0, 1, \ldots, N_x; \; n = 0, 1, \ldots, N_t, \tag{22}$$

where N_x, N_t are the total number of grid points in the η- and x-directions, respectively, and Δx is the spacing in the x-direction. The finite difference scheme is applied with centering about a midpoint halfway between x^{n+1} and x^n. This midpoint is defined as $x^{n+1/2} = (x^{n+1} + x^n)/2$. The derivatives with respect with η are discretized in terms of the Chebyshev differentiation matrices. Applying the centering about $x^{n+1/2}$ to any function, say $f(\eta, x)$ and its associated derivative, we obtain

$$f\left(\eta_j, x^{n+1/2}\right) = f_j^{n+1/2} = \frac{f_j^{n+1} + f_j^n}{2},$$
$$\left(\frac{\partial f}{\partial x}\right)^{n+1/2} = \frac{f_j^{n+1} - f_j^n}{\Delta x}. \tag{23}$$

In applying the Chebyshev spectral collocation method, the continuous derivatives in the unknown functions are approximated by matrix-vector products of the so-called differentiation matrices at the collocation points. Before the spectral method is applied, the domain $\eta \in [0, \eta_\infty]$ is transformed to the domain $Y \in [-1, 1]$ on which the spectral method can be implemented. Thus, the derivatives, say f', f'', at the collocation points $Y_j (j = 0, 1, \ldots, N_x)$, are given in matrix form in [34, 35] as a differentiation matrix D that maps a vector of the function values $\mathbf{F} = [f(Y_0), \ldots, f(Y_{N_x})]^T$ at the collocation points to a vector $\mathbf{F}'$ defined as

$$\mathbf{F}' = \sum_{k=0}^{N_x} D_{jk} f\left(Y_k\right) = \mathbf{D}\mathbf{F}, \quad j = 0, 1, \ldots, N_x. \tag{24}$$

In general, a derivative of order s for the function $f(\eta)$ can be transformed as

$$f^{(s)}(\eta) \longrightarrow \mathbf{D}^s \mathbf{F}. \tag{25}$$

Thus, applying the spectral method in η and finite difference method in x gives

$$A_1 \mathbf{F}_{r+1}^{n+1} = B_1 \mathbf{F}_{r+1}^n + K_1,$$
$$A_2 \mathbf{\Theta}_{r+1}^{n+1} = B_2 \mathbf{\Theta}_{r+1}^n + K_2, \tag{26}$$
$$A_3 \mathbf{\Phi}_{r+1}^{n+1} = B_3 \mathbf{\Phi}_{r+1}^n + K_3,$$

where

$$A_1 = \frac{1}{2}\left(\mathbf{D}^3 + \mathbf{a}_{1,r}^{n+1/2} \mathbf{D}^2 + \mathbf{a}_{2,r}^{n+1/2} \mathbf{D} + \mathbf{a}_{3,r}^{n+1/2}\right) - \frac{\mathbf{a}_{5,r}^{n+1/2} \mathbf{D}}{\Delta \xi} - \frac{\mathbf{a}_{6,r}^{n+1/2}}{\Delta \xi},$$

$$B_1 = -\frac{1}{2}\left(\mathbf{D}^3 + \mathbf{a}_{1,r}^{n+1/2} \mathbf{D}^2 + \mathbf{a}_{2,r}^{n+1/2} \mathbf{D} + \mathbf{a}_{3,r}^{n+1/2}\right) - \frac{\mathbf{a}_{5,r}^{n+(1/2)} \mathbf{D}}{\Delta \xi} - \frac{\mathbf{a}_{6,r}^{n+1/2}}{\Delta \xi},$$

$$A_2 = \frac{1}{2}\left(\frac{1}{\mathrm{Pr}} \mathbf{D}^2 + \mathbf{b}_{1,r}^{n+1/2} \mathbf{D}\right) - \frac{\mathbf{b}_{3,r}^{n+1/2}}{\Delta \xi},$$

$$B_2 = -\frac{1}{2}\left(\frac{1}{\mathrm{Pr}} \mathbf{D}^2 + \mathbf{b}_{1,r}^{n+1/2} \mathbf{D}\right) - \frac{\mathbf{b}_{3,r}^{n+1/2}}{\Delta \xi},$$

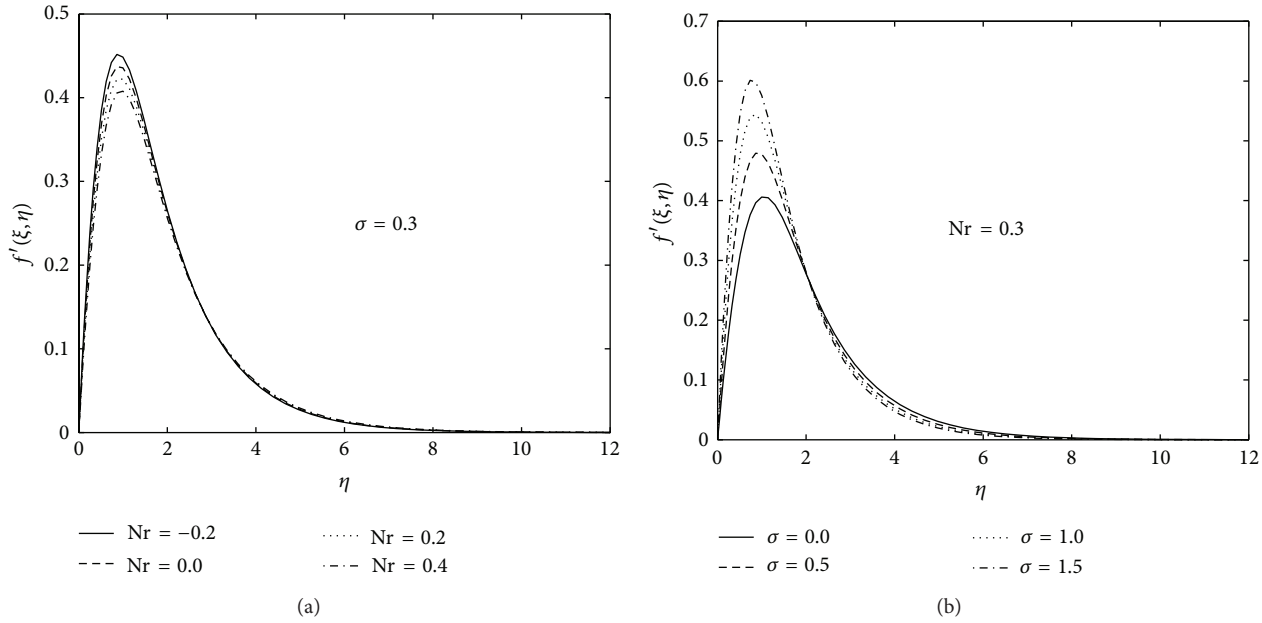

Figure 1: Effect of the buoyancy ratio Nr on $f(\eta)$ and $f'(\eta)$ for $\xi = 0.5$, Le = 10, Pr = 7, Nt = 0.1, Nb = 0.5, and $A = 0.1$.

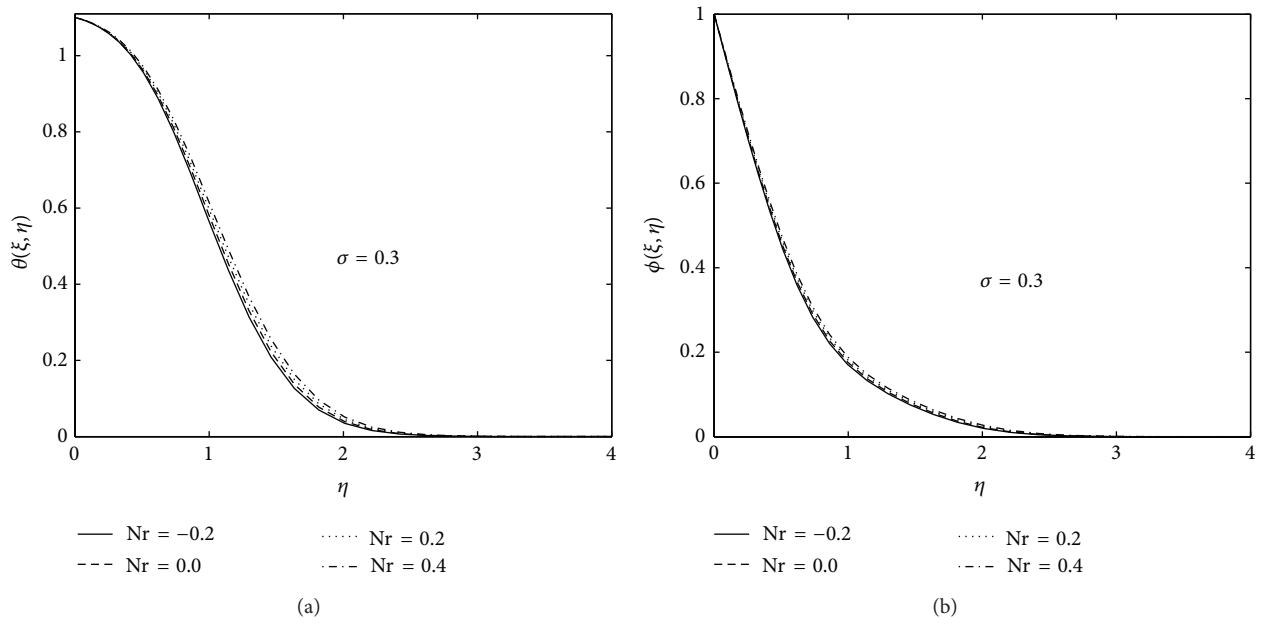

Figure 2: Effect of the buoyancy ratio Nr on $\theta(\eta)$ and $\phi(\eta)$ for $\xi = 0.5$, Le = 10, Pr = 7, Nt = 0.1, Nb = 0.5, and $A = 0.1$.

$$A_3 = \frac{1}{2}\left(\frac{1}{\mathrm{Le}}\mathbf{D}^2 + \mathbf{c}_{1,r}^{n+1/2}\mathbf{D}\right) - \frac{\mathbf{c}_{3,r}^{n+1/2}}{\Delta\xi},$$

$$B_3 = -\frac{1}{2}\left(\frac{1}{\mathrm{Le}}\mathbf{D}^2 + \mathbf{c}_{1,r}^{n+1/2}\mathbf{D}\right) - \frac{\mathbf{c}_{3,r}^{n+1/2}}{\Delta\xi},$$

$$K_1 = -\mathbf{a}_{4,r}^{n+1/2}, \quad K_2 = -\mathbf{b}_{2,r}^{n+1/2}, \quad K_3 = -\mathbf{c}_{2,r}^{n+1/2}. \tag{27}$$

In the above equations $\mathbf{\Phi}$, $\mathbf{\Theta}$, and $\mathbf{F}$ correspond to the approximate values of $\phi(\eta, x)$, $\theta(\eta, x)$, and $f(\eta, x)$ at the collocation points. The approximate solutions for f, θ, and ϕ are obtained by solving (26). The convergence and stability of the iteration schemes are assessed by considering the norm of the difference in the values of the approximate functions between two successive iterations. Thus, for each iteration scheme, we define the following maximum error E at the $(r+1)$th iteration:

$$E = \max\left(\left\|\mathbf{F}_{r+1} - \mathbf{F}_r\right\|_\infty, \left\|\mathbf{\Theta}_{r+1} - \mathbf{\Theta}_r\right\|_\infty, \left\|\mathbf{\Phi}_{r+1} - \mathbf{\Phi}_r\right\|_\infty\right). \tag{28}$$

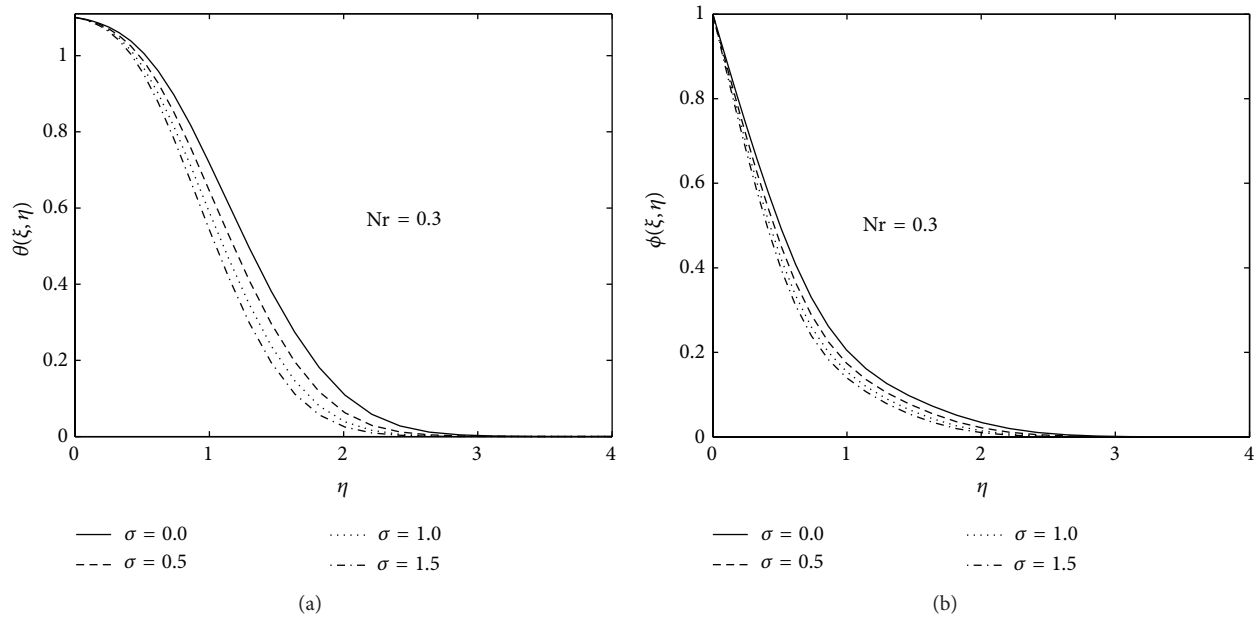

Figure 3: Effect of the σ on $\theta(\eta)$ and $\phi(\eta)$ for $x = 0.5$, Le = 10, Pr = 7, $A = 0.1$, Nr = 0.1, Nt = 0.1, and Nb = 0.5.

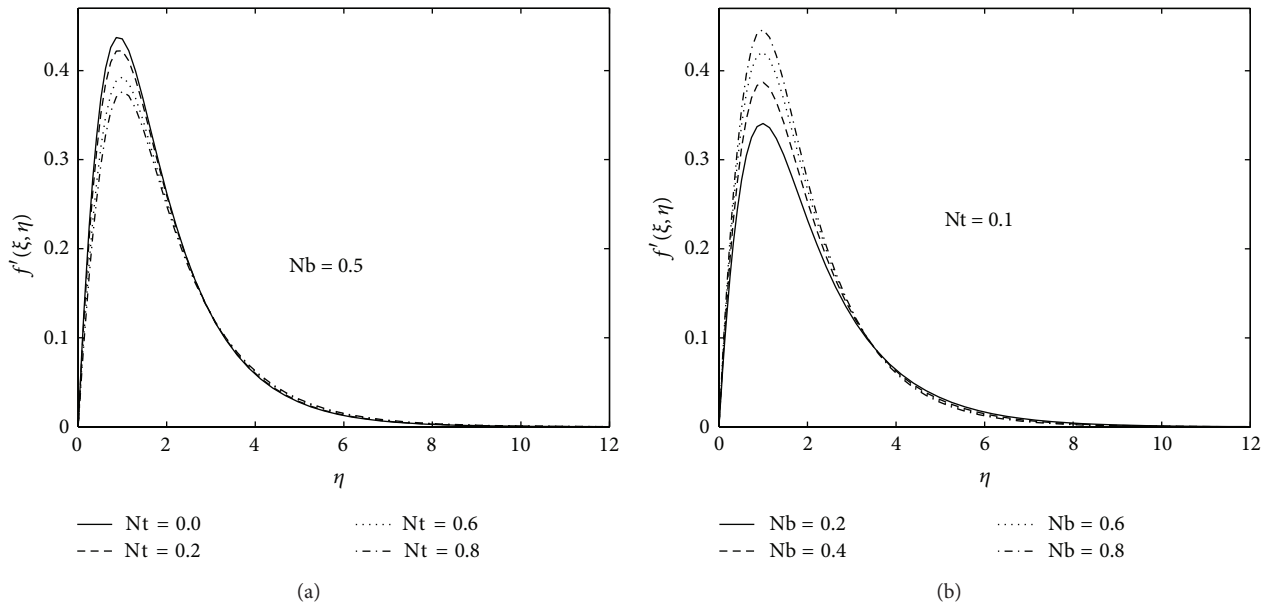

Figure 4: Effect of the Nt on $f'(\eta)$ for $\xi = 0.5$, Le = 10, Pr = 7, $\sigma = 0.3$, Nr = 0.1, and $A = 0.1$.

The unknowns f, θ, and ϕ were iteratively calculated, for a given number of collocation points N_x, until the following criteria for convergence was satisfied at iteration r:

$$E \leq \epsilon, \tag{29}$$

where ϵ is the convergence tolerance level which was chosen to be 10^{-7} in this work. The results are given in the next section.

4. Results and Discussions

In this section we present solutions of (13)–(15) along with the boundary conditions (16) which were generated using the local linearisation method described in the previous section. In order to obtain clear insights into the physics of the problem of nanofluid flow over heated vertical surface with sinusoidal wall temperature variations in presence of the nonlinear temperature-density relationship, analysis has been carried out for different values of our governing parameters,

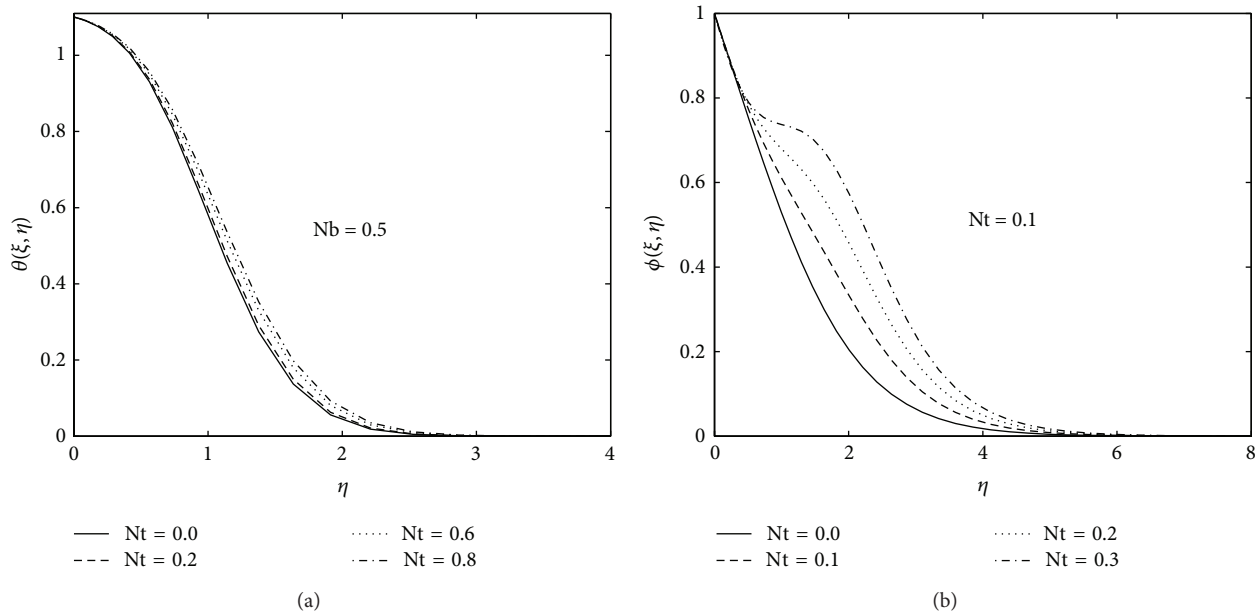

Figure 5: Effect of the Nt on $\theta(\eta)$ and $\phi(\eta)$ for $\xi = 0.5$, Le = 10, Pr = 7, $\sigma = 0.3$, Nr = 0.1, Nb = 0.5, and $A = 0.1$.

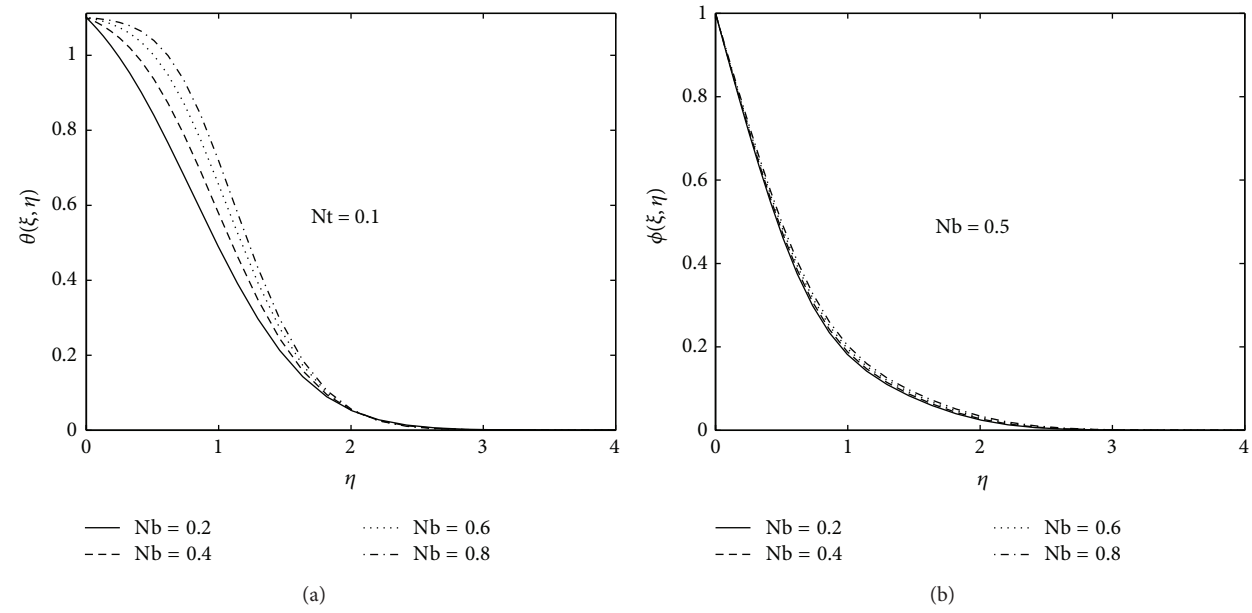

Figure 6: Effect of the Nb on $\theta(\eta)$ and $\phi(\eta)$ for $\xi = 0.5$, Le = 10, Pr = 7, $\sigma = 0.3$, Nr = 0.1, Nt = 0.1, and $A = 0.1$.

namely, the nonlinear temperature parameter σ, the Buoyancy ratio Nr, the Prandtl number Pr, the Lewis number Le, the Brownian motion parameter Nb, and the thermophoresis parameter Nt at some streamwise positions x. Table 1 gives a comparison between the present results and Rees [26] for the skin-friction and the heat transfer coefficient, respectively. Firstly we note a remarkable agreement between the two sets of results, and secondly as the Prandtl Pr increases, the skin-friction coefficient decreases and the rate of heat transfer increases with increasing Prandtl number.

Figure 1 shows the effect of increasing the buoyancy ratio and the nonlinear temperature parameter σ on the velocity component $f'(\eta)$. Increasing the buoyancy ratio parameter leads to increased thickness of the momentum boundary layer. We also observe that the velocity decelerates at the surface with an increase in the buoyancy ratio parameter. In addition, as σ increases, the velocity tends to increase very closely to the surface near the edge of boundary layer in a narrow region. The nonlinear temperature parameter is expected to alter the momentum boundary layer; hence

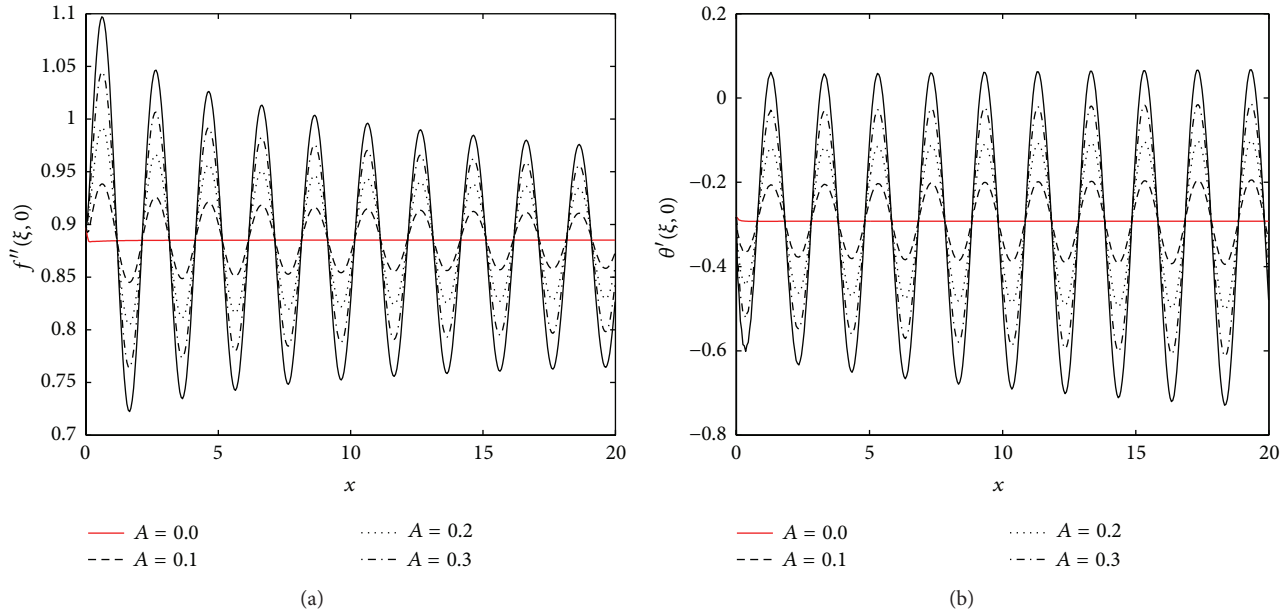

FIGURE 7: Effect of the A on $f''(x, 0)$ and $\theta'(x, 0)$ for Le = 10, Pr = 1, σ = 0.02, Nr = 0.1, Nt = 0.3, and Nb = 0.5.

TABLE 1: Comparisons of wall skin-friction coefficient $f''(0)$ and local Nusselt number $-\theta'(0)$ with those of Rees [26] for various values of Prandtl number Pr with Nt = 0, Nb = 0, Nr = 0, and σ = 0.

Pr	Rees [26]		Present results	
	$f''(0)$	$-\theta'(0)$	$f''(0)$	$-\theta'(0)$
0.50	1.0086	0.3120	1.00855006	0.31195217
0.70	0.9601	0.3532	0.96012412	0.35320776
1.00	0.9082	0.4010	0.90819121	0.40103314
1.50	0.8492	0.4607	0.84923678	0.46070468
2.00	0.8079	0.5066	0.80788807	0.50661849
3.00	0.7508	0.5767	0.75076470	0.57667739
4.00	0.7113	0.6304	0.71128220	0.63042597
5.00	0.6814	0.6746	0.68135380	0.67458252
6.00	0.6574	0.7123	0.65739280	0.71234690
7.00	0.6375	0.7455	0.63749977	0.74551232
8.00	0.6206	0.7752	0.62054992	0.77519223
10.00	0.5928	0.8268	0.59283303	0.82684396
20.00	0.5119	1.0052	0.51189002	1.00519108
40.00	0.4392	1.2146	0.43918933	1.21460776
70.00	0.3866	1.4104	0.38663181	1.41042858
100.00	0.3559	1.5495	0.35594693	1.54953322

the velocity decreases with the increase of σ. The influence of buoyancy parameter Nr on the local temperature and nanoparticle profiles is displayed in Figure 2. It can be noticed that both the thermal and the nanoparticle boundary layers thicknesses increase with an increase in Nr, so the local temperature and nanoparticle volume fraction profiles are seen to increase when Nr increases. Figure 3 depicts the influence of the nonlinear density temperature variation on the temperature and the nanoparticle volume fraction profiles in the boundary layer. From the graphical representation it is apparent that the fluid is brought closer to the surface and reduces the thermal and nanoparticle volume boundary-layer thickness with increasing σ. Hence, when σ increases there will be a decrease in the temperature profile and in the nanoparticle volume fraction.

Figure 4 illustrates the effects of the thermophoresis and Brownian motion parameters on the fluid velocity $f'(\eta)$. We observe that the velocity of the nanofluid decreases as the

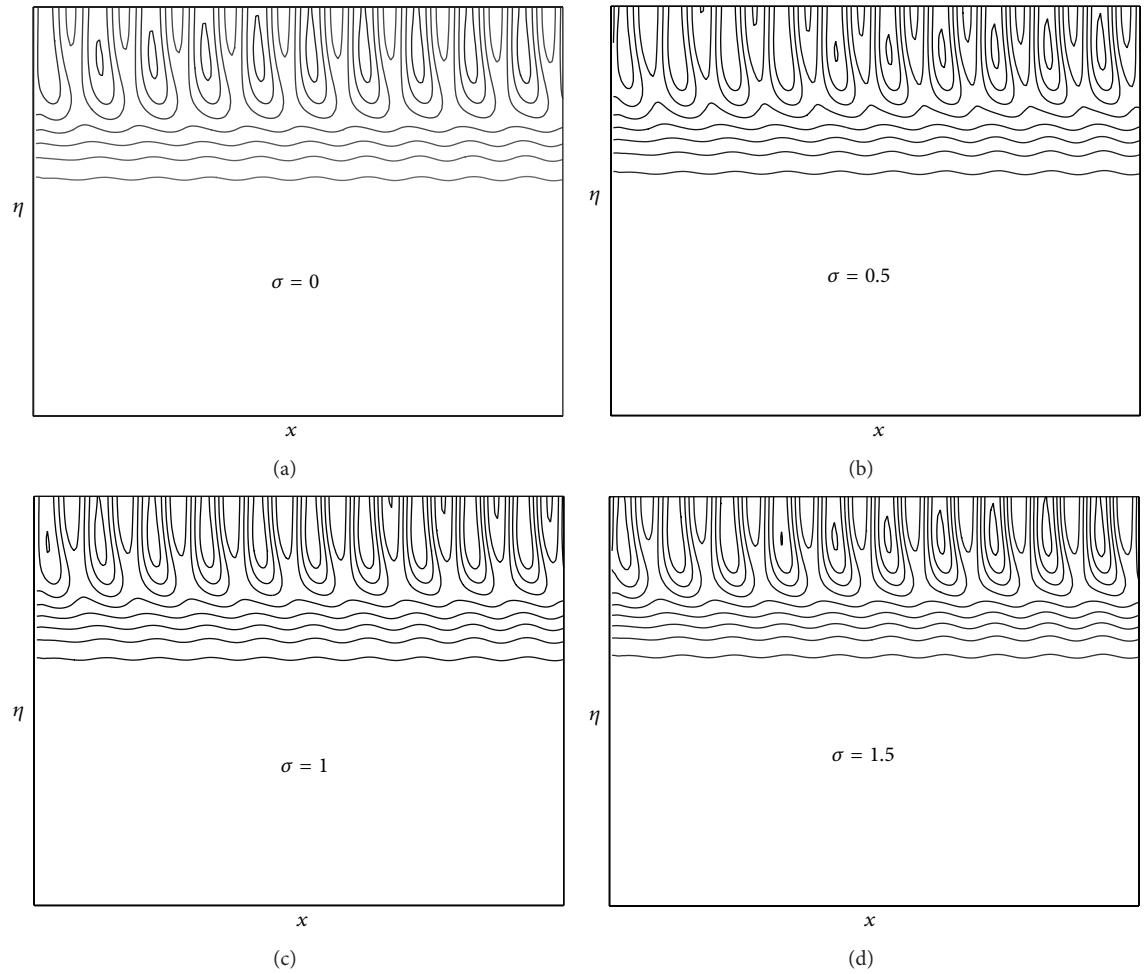

Figure 8: Le = 1, Pr = 1, A = 0.1, Nr = 0.1, Nt = 0.1, and Nb = 0.5.

thermophoresis parameter Nt increases; however, the Brownian motion parameter Nb makes the velocity component $f'(\eta)$ increase. As expected, the boundary-layer thickness of the momentum decreases with increasing Nt, whereas the opposite behaviour of the velocity component $f'(\eta)$ is observed with increasing Nb. The effect of thermophoresis parameter on the temperature and mass volume fraction profiles is shown in Figure 5. The thermophoresis force generated by the temperature gradient creates a fast flow away from the surface; hence more fluid is heated away from the surface, and, consequently, as Nt increases, the temperature within the boundary layer increases. The flow from the surface carries with it nanoparticles leading to increase in the mass volume fraction boundary-layer thickness. The effect of Brownian motion on the temperature and nanoparticle volume fraction has been plotted in Figure 6. The Brownian motion represents the random movement caused by the nanoparticles that are suspended within the fluid. The local temperature increases as the Brownian motion parameter Nb increases; hence the Brownian motion is an important mechanism for the enhancement of thermal conductivity of nanofluids. However, Brownian motion leads to repositioning of the nanoparticles away from the fluid regime which causes a clustering near the surface. This leads to a decrease in the mass volume fraction.

Figure 7 shows effects of the temperature wave amplitude A on both the scaled surface shear stress and the rate of surface heat transfer, respectively. As the temperature wave amplitude increases, the thickness of the momentum boundary layer increases; thus we can expect a decrease in the scaled surface shear stress. However, the fast flow from the surface increase leads to thinness in the boundary layer and hence increases the heat transfer rate. Thus the local temperature increases with increasing A; the same result has been reported by Rees [26] for regular fluids.

It is clear from Figure 8 that, as the streamwise distance x increases, there is an increase in the size of the inner isotherms cells while there is no variation in the outer cells. However increases in the nonlinear temperature parameter σ create more cells. This is because the thickness of the boundary layer varies with increasing both x and σ. Figure 9 shows the isotherms for several values of the temperature wave

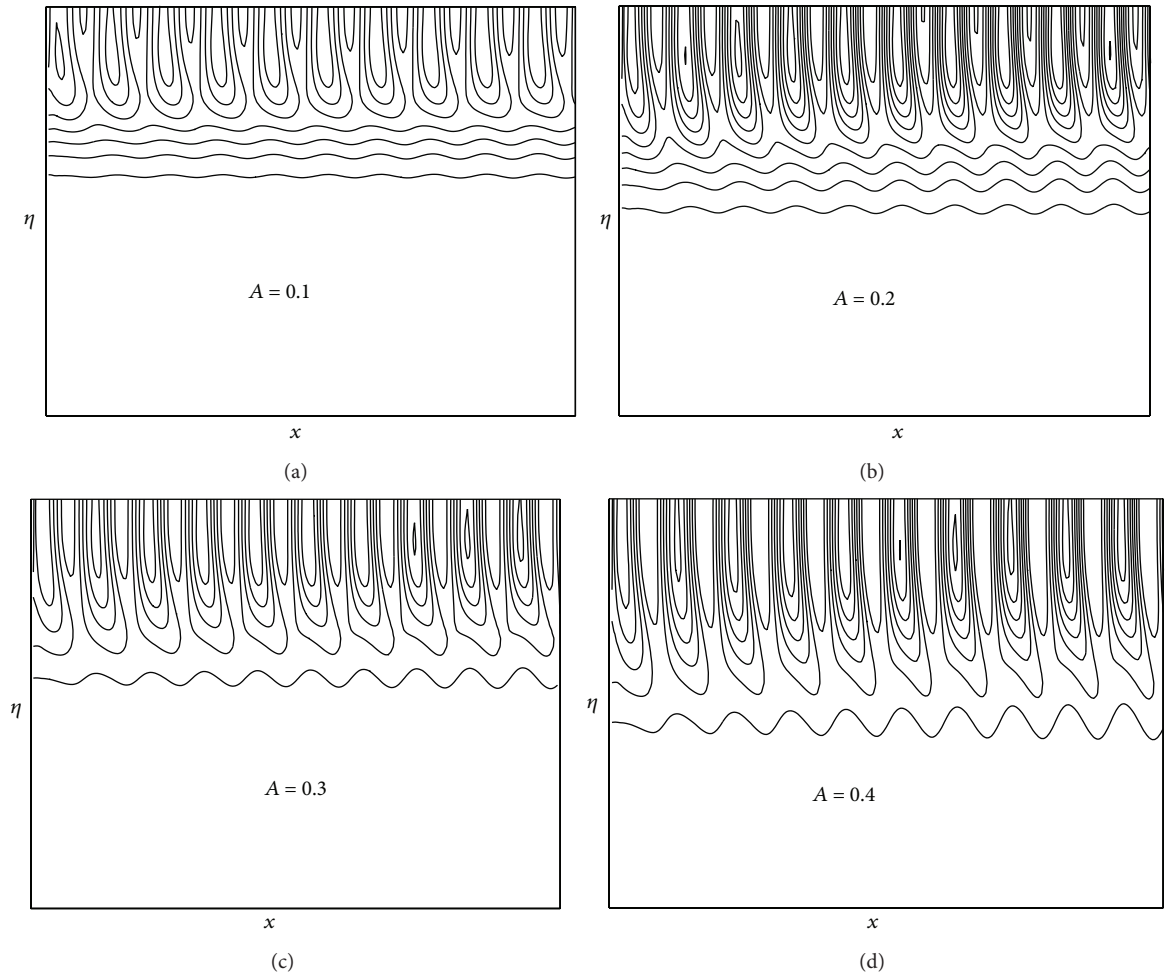

Figure 9: Le = 1, Pr = 1, A = 0.1, Nr = 0.1, Nt = 0.1, and Nb = 0.5.

amplitude A. The variation of temperature wave amplitude leads to an increase in boundary-layer thickness, so that the inner isotherms cell size increases and more inner isotherms cells are created.

5. Conclusions

In this investigation, the problem of nonlinear nanofluid flow over heated vertical surface with sinusoidal wall temperature variations has been considered. The model includes the effects of Brownian motion and thermophoresis effects. Numerical approximations for the coupled high nonlinear partial differential equations governing were obtained using the local linearisation method. The effects of various parameters on the fluid properties and on the scaled surface shear stress and rate of surface heat transfer were determined. It was found that as the nonlinear temperature parameter increases the velocity tends to increase very closely to the surface and then decreases. Moreover, it was observed that the boundary-layer thickness of the momentum decreases with an increase in the thermophoresis parameter. The random movement caused by the nanoparticles enhanced the temperature within the boundary layer when increased.

Conflict of Interests

The authors declare that there is no conflict of interests regarding the publication of this paper.

References

[1] S. U. S. Choi, "Enhancing thermal conductivity of fluids with nanoparticles," in *Proceedings of the International Mechanical Engineering Congress and Exhibition*, FED 231/MD, pp. 99–105, ASME, San Franciscos, Calif, USA, 1995.

[2] K. V. Wong and O. De Leon, "Applications of nanofluids: current and future," *Advances in Mechanical Engineering*, vol. 2010, Article ID 519659, 11 pages, 2010.

[3] J. A. Gbadeyan, M. A. Olanrewaju, and P. O. Olanrewaju, "Boundary layer flow of a nanofluid past a stretching sheet with a convective boundary condition in the presence of magnetic field and thermal radiation," *Australian Journal of Basic and Applied Sciences*, vol. 5, no. 9, pp. 1323–1334, 2011.

[4] R. Sharma, A. Ishak, and I. Pop, "Partial slip flow and heat transfer over a stretching sheet in a nanofluid," *Mathematical Problems in Engineering*, vol. 2013, Article ID 724547, 7 pages, 2013.

[5] Y. Ding, H. Chen, L. Wang et al., "Heat transfer intensification using nanofluids," *Kona*, vol. 25, pp. 23–38, 2007.

[6] J. Buongiorno, "Convective transport in nanofluids," *Journal of Heat Transfer*, vol. 128, no. 3, pp. 240–250, 2006.

[7] A. V. Kuznetsov and D. A. Nield, "Natural convective boundary-layer flow of a nanofluid past a vertical plate," *International Journal of Thermal Sciences*, vol. 49, no. 2, pp. 243–247, 2010.

[8] D. A. Nield and A. V. Kuznetsov, "The Cheng-Minkowycz problem for natural convective boundary-layer flow in a porous medium saturated by a nanofluid," *International Journal of Heat and Mass Transfer*, vol. 52, no. 25-26, pp. 5792–5795, 2009.

[9] W. A. Khan and I. Pop, "Boundary-layer flow of a nanofluid past a stretching sheet," *International Journal of Heat and Mass Transfer*, vol. 53, no. 11-12, pp. 2477–2483, 2010.

[10] C. J. Ho, W. K. Liu, Y. S. Chang, and C. C. Lin, "Natural convection heat transfer of alumina-water nanofluid in vertical square enclosures: an experimental study," *International Journal of Thermal Sciences*, vol. 49, no. 8, pp. 1345–1353, 2010.

[11] W. A. Khan and A. Aziz, "Double-diffusive natural convective boundary layer flow in a porous medium saturated with a nanofluid over a vertical plate: Prescribed surface heat, solute and nanoparticle fluxes," *International Journal of Thermal Sciences*, vol. 50, no. 11, pp. 2154–2160, 2011.

[12] A. M. Rashad, M. A. El-Hakiem, and M. M. M. Abdou, "Natural convection boundary layer of a non-Newtonian fluid about a permeable vertical cone embedded in a porous medium saturated with a nanofluid," *Computers & Mathematics with Applications*, vol. 62, no. 8, pp. 3140–3151, 2011.

[13] A. Aziz, W. A. Khan, and I. Pop, "Free convection boundary layer flow past a horizontal flat plate embedded in porous medium filled by nanofluid containing gyrotactic microorganisms," *International Journal of Thermal Sciences*, vol. 56, pp. 48–57, 2012.

[14] P. Rana, R. Bè, and O. A. Bég, "Numerical solution for mixed convection boundary layer flow of a nanofluid along an inclined plate embedded in a porous medium," *Computers and Mathematics with Applications*, vol. 64, no. 9, pp. 2816–2832, 2012.

[15] M. Hajipour and A. Molaei Dehkordi, "Analysis of nanofluid heat transfer in parallel-plate vertical channels partially filled with porous medium," *International Journal of Thermal Sciences*, vol. 55, pp. 103–113, 2012.

[16] R. Chand and G. C. Rana, "On the onset of thermal convection in rotating nanofluid layer saturating a Darcy-Brinkman porous medium," *International Journal of Heat and Mass Transfer*, vol. 55, no. 21-22, pp. 5417–5424, 2012.

[17] V. N. Korovkin and A. P. Andrievskii, "Free convection with a nonlinear dependence of density on temperature: plane problems," *Journal of Engineering Physics and Thermophysics*, vol. 73, no. 2, pp. 381–386, 2000.

[18] K. Vajravelu, J. R. Cannon, J. Leto et al., "Nonlinear convection at a porous flat plane with application to heat transfer from a dike," *Journal of Mathematical Analysis and Applications*, vol. 277, no. 2, pp. 609–623, 2003.

[19] H. Barrow and T. L. S. Rao, "The effect of variable beta on free convection," *British Chemical Engineering*, vol. 16, pp. 704–709, 1971.

[20] V. L. Streeter, *Handbook of Fluid Dynamics*, vol. 6, McGraw-Hill, New York, NY, USA, 1961.

[21] K. Vajravelu and K. S. Sastri, "Fully developed laminar free convection flow between two parallel vertical walls-I," *International Journal of Heat and Mass Transfer*, vol. 20, no. 6, pp. 655–660, 1977.

[22] K. V. Prasad, K. Vajravelu, and R. A. Van Gorder, "Non-Darcian flow and heat transfer along a permeable vertical surface with nonlinear density temperature variation," *Acta Mechanica*, vol. 220, no. 1–4, pp. 139–154, 2011.

[23] S. S. Motsa, F. G. Awad, Z. G. Makukula, and P. Sibanda, "The spectral homotopy analysis method extended to systems of partial differential equations," *Abstract and Applied Analysis*, vol. 2014, Article ID 241594, 11 pages, 2014.

[24] S. Ostrach, "An analysis of laminar free-convection flow and heat transfer about a flat plate parallel to the direction of the generating body force," *NACA*, vol. 2635, 1952.

[25] E. M. Sparrow and J. L. Gregg, "Similar solution for free convection from a non-isothermal vertical plate," *Journal of Heat Transfer*, vol. 80, pp. 379–384, 1958.

[26] D. A. S. Rees, "The effect of steady streamwise surface temperature variations on vertical free convection," *International Journal of Heat and Mass Transfer*, vol. 42, no. 13, pp. 2455–2464, 1999.

[27] I. Pop and D. B. Ingham, *Convective Heat Transfer: Mathematical and Computational Modelling of Viscous Fluids and Porous Media*, Pergamon, Oxford, UK, 2001.

[28] N. C. Roy and M. A. Hossain, "Numerical solution of a steady natural convection flow from a vertical plate with the combined effects of streamwise temperature and species concentration variations," *Heat and Mass Transfer*, vol. 46, no. 5, pp. 509–522, 2010.

[29] S. C. Saha, J. C. Patterson, and C. Lei, "Natural convection and heat transfer in attics subject to periodic thermal forcing," *International Journal of Thermal Sciences*, vol. 49, no. 10, pp. 1899–1910, 2010.

[30] M. M. Molla, S. C. Saha, and M. A. Hossain, "Radiation effect on free convection laminar flow along a vertical flat plate with streamwise sinusoidal surface temperature," *Mathematical and Computer Modelling*, vol. 53, no. 5-6, pp. 1310–1319, 2011.

[31] P. Rana and R. Bhargava, "Flow and heat transfer analysis of a nanofluid along a vertical flat plate with non-uniform heating using fem: effect of nanoparticle diameter," *International Journal of Applied Physics and Mathematics*, vol. 1, pp. 171–176, 2011.

[32] S. S. Motsa, "A new spectral local linearization method for nonlinear boundary layer flow problems," *Journal of Applied Mathematics*, vol. 2013, Article ID 423628, 15 pages, 2013.

[33] S. S. Motsa, Z. G. Makukula, and S. Shateyi, "Spectral local linearisation approach for natural convection boundary layer flow," *Mathematical Problems in Engineering*, vol. 2013, Article ID 765013, 7 pages, 2013.

[34] C. Canuto, M. Y. Hussaini, A. Quarteroni, and T. A. Zang, *Spectral Methods in Fluid Dynamics*, Springer Series in Computational Physics, Springer, Berlin , Germany, 1988.

[35] L. N. Trefethen, *Spectral Methods in MATLAB*, SIAM, New York, NY, USA, 2000.